IMPROVEMENTS IN THE USE OF METEOROLOGICAL SATELLITE DATA:

SOME TECHNIQUES DEVELOPED FOR GATE

David Suchman
Brian Auvine
Raymond Lord
David Martin
Frederick Mosher
David Santek

Space Science and Engineering Center
The University of Wisconsin - Madison
Madison, Wisconsin 53706

December 1981

IMPROVEMENTS IN THE USE OF METEOROLOGICAL SATELLITE DATA:

SOME TECHNIQUES DEVELOPED FOR GATE

David Suchman
Brian Auvine
Raymond Lord
David Martin
Frederick Mosher
David Santek

Space Science and Engineering Center
The University of Wisconsin - Madison
Madison, Wisconsin 53706

December 1981

ERRATA

pages 90-91 (references) should appear at the end of chapter 4 (page 102).

Section	Title	Page
	ACKNOWLEDGMENTS	
	CONTENTS	
1.	INTRODUCTION	1
2.	CLOUD HEIGHTS & CLOUD THICKNESS DETERMINATION	2
2.A	Cloud Heights From Geostationary Meteorological Satellites	2
2.A.1	Introduction	2
2.A.2	GOES Data Source	3
2.A.3	Sensed Cloud Temperatures	5
2.A.4	Temperature to Height Conversion	12
2.A.5	Cloud Thickness Determination	13
2.A.6	Cloud Height Observations	18
2.B	Improvements to Cloud Height & Thickness Determination	25
2.B.1	Adding Local Soundings	25
	a. Comparisons of Climatology vs. Local Soundings Without Moisture	25
	b. Use of Moisture in Determining Cloud Heights	29
	c. Use of Wind Information to Edit Cloud Heights	31
2.B.2	Real Stereo Images	31
2.B.3	False Stereo Images	32
3.	CLOUD TRACKING FOR GATE WIND FIELDS	38
3.A	Introduction	38
3.B	Delineating Mid and High Level Tracers	40
3.C	Cloud Tracking Techniques	45
3.D	Editing Procedures	46
3.D.1	Dynamic Vector Analysis	51

ACKNOWLEDGMENTS

Most of the research work in addition to the writing of this report was supported by NSF Grant ATM-7809716. Because this report has pulled together work from a variety of sources, a more detailed acknowledgment is needed:

- Chapter 2 - Developmental work was performed by Fred Mosher, David Santek, Brian Auvine, Dick Daly and Bill Hibbard. Additional funding came from NASA Contracts NAS8-33799, NAS5-23296, NAS5-23462 and NASW-3476, and NOAA Contract NA-80-SAC-00742.

- Chapter 3 - Developmental work was performed by David Suchman, Brian Auvine, David Martin, David Santek, Raymond Lord and Thomas Whittaker.

- Chapter 4 - Developmental work was performed by Brian Auvine, David Suchman, David Martin, and Martin Barrett.

- Chapter 5 - Developmental work was performed by David Martin and Brian Auvine with support from NSF Grant ATM-7805951.

This report was edited by John Stremikis, and typed by Angela Crowell.

1. INTRODUCTION

This is a report on a variety of techniques developed over the past few years at SSEC for extracting information from geostationary satellite images. Much of this work falls under the umbrella of an NSF program entitled "Development of Methods for Improved Use of Satellite Images and Synthesis with Other GATE Data Sets," but not all. Because the technique development does not exist in a vacuum, we have chosen to include work from other projects, most notably on Cloud Height and Cloud Mapping (see acknowledgments for details) to help make our discussion more complete.

We have chosen four general subject areas to address: Cloud Height Determination, Cloud Wind Determination, Analysis Techniques Applied to Brightness Data and Cloud Mapping. Although our techniques are primarily satellite-based, we include data from all available sources to enable us to work from the most complete data base as possible. Each section is intended to be semi-independent; each is written by a different scientist, and tries to present the state of the art as it exists at SSEC. We acknowledge and refer to similar work elsewhere when relevant, but have chosen not to discuss such work in detail.

Because this report is intended for a general audience, we have tried to limit our references to McIDAS (Man Computer Interactive Data Access System). For those wishing more details on the work performed here, please contact any of the researchers referred to in the acknowledgments section.

2. CLOUD HEIGHTS & THICKNESS DETERMINATION

2.A Cloud Heights From Geostationary Meteorological Satellites*

2.A.1 Introduction

Determination of cloud heights is fundamental for many quantitative uses of meteorological satellite data. Cloud-tracked wind derivations require a knowledge of cloud altitude, as do climatological measurements of cloud cover. Forecasters need to know cloud heights in monitoring severe storm development and in preparing guidance for the aviation community. This report reviews how cloud heights can be obtained from geostationary satellite data and discusses limitations of the methods used.

The primary method of determining cloud heights uses air temperature as the vertical coordinate. Since the troposphere, where clouds are located, generally has a temperature profile of decreasing temperature with height, the cloud top temperature can be used to determine the cloud top height. The implicit assumptions in this are that the clouds are at equilibrium with the temperature of the surrounding air and that the air temperature is a known, monotonically decreasing function with height. Problems with the temperature-to-height method include violations of the implicit assumptions such as temperature inversions, unknown profiles, and the actual measurement of the cloud top temperature. A cloud size smaller than the field of view of the sensor and a cloud emissivity

* Additional support provided by contracts NAS5-23462 & NAS5-23296.

less than unity present problems in the determination of cloud top temperature.

The most widely used method of obtaining cloud heights is the infrared temperature method. It has been used in its basic form by Fritz and Winston (1962), Rao and Winston (1963) and Kaffler, Decotiis, and Rao (1973). The technique was expanded by Mosher (1975) and Reynolds and Vonder Haar (1977) to use both the visible and infrared channels. This method forms a basis for height determination of the operational cloud-tracked winds at NESS (Young, 1975) and the FGGE cloud-tracked winds (Kahuajy and Mosher, 1981). This is the only cloud height technique used operationally and is the only technique which can be used anywhere without restrictions. The primary limitations of this technique include erroneous temperature measurements caused by thin or small clouds, unknown temperature profiles and multi-valued answers caused by temperature inversions.

2.A.2 GOES Data Source

The satellite data used in the temperature-to-height determination come primarily from the window infrared channel, with a secondary data source from the visible channel. The Geostationary Operational Environmental Satellite (GOES) is the main source of geostationary satellite data over the United States and adjacent ocean areas. It has a Visible and Infrared Spin-Scan Radiometer (VISSR) consisting of a 16-inch telescope connected through fiber optics to eight visible photomultiplier tubes in the 0.55 to 0.75 micron range and two Hg-Cd-Te infrared detectors (one primary and the

other backup) in the 10.5 to 12.6 micron range. The visible sensors have a field of view of about 1 km, while the infrared detector has a view of about 8 km at the subsatellite point. An image is composed of data gathered as the satellite-mounted telescope sweeps west to east across the face of the earth. The telescope scans an 8 km strip, and is then mechanically stepped down for the next scan. The whole earth is scanned in about 18.2 minutes. Routine operations have whole earth images completed every 30 minutes, though more frequent scanning of only part of the earth is done during severe weather situations.

The eight visible sensors are arranged in a north-south line, so as the satellite scans west to east, eight lines of visible data are produced. Because of slight differences in the photomultiplier tubes, there is a minor amount of stripping produced by the different visible sensors. Every 1 km the visible sensors are digitized into six-bit words which are proportional to the square root of the light intensity. The square root digitization allows for an expanded dynamic range without contamination from the photomultiplier noise which is proportional to the square of the light intensity. The visible sensors are not operationally calibrated.

The infrared sensor has a field of view of 8 km, so the single sensor fills up an entire scan line width. The infrared data is digitized every 4 km, making an overdigitized 4 km x 8 km sample. Most processing systems divide the infrared sample in half, making two 4 km x 4 km samples, even though the inherent resolution of the sensor is 8 km x 8 km. The infrared data is digitized into eight-bit words proportional to temperature. The infrared data is calibrated

and put into a NESS standard temperature table which is a two-part linear curve of temperature. The conversion between infrared counts (c) and temperature (T) is as follows:

for $c \leq 176$,

$$T = 330 - c/2 \qquad (1)$$

for c > than 176

$$T = 418 - c \ .$$

2.A.3 Sensed Cloud Temperatures

The infrared sensor of the GOES can be used to determine the cloud top temperature from which the height can then be determined. However, the sensed cloud top temperature is not always the true temperature. The radiation (I) reaching the infrared sensor is a function of the radiation from the cloud top (I_c), the fraction of the sensor covered by cloud (N), the cloud emissivity (ε) and the radiation from the underlying ground (I_g):

$$I = \varepsilon N I_c + (1-N) I_g \quad (1-\varepsilon) N I_g \ . \qquad (2)$$

The radiation from the cloud top (I_c) and the ground (I_g) is determined by Planck's Law:

$$I_c = \frac{c_1}{\lambda_5} \frac{1}{\exp\left(\frac{c_2}{\lambda T_c} - 1\right)} \qquad (3)$$

$c_1 = 3.740 \times 10^5$ erg cm^2 s^{-1}

$c_2 = 1.4385$ cm °K

λ = wavelength of light .

In equation (2), the first term is the radiation coming from the cloud, the second term is the radiation coming around the cloud and the third term is the radiation coming through the cloud. If the cloud is a black body with an emissivity of one and the cloud completely fills the field of view of the sensor (N=1), then the other terms in equation (2) are zero and the sensed temperature is the true temperature.

If the cloud is smaller than 8 km across, then the field of view of the sensor is not filled entirely by cloud. Some of the radiation from the ground or underlying cloud field goes around the cloud to contaminate the sensed cloud top temperature. If the cloud is larger than 24 km or three fields of view, then it is certain that the center pixel of the cloud image is not contaminated by ground radiation. If the cloud is between 8 and 24 km across, there is a chance that the infrared sensor's field of view is overlapping an edge of the cloud and allowing some ground radiation to contaminate the measurement. Hence, any cloud smaller than 24 km across has the potential for erroneous temperature determination. Any cloud smaller than 8 km definitely does have sensed temperature contamination.

The emissivity of the cloud is determined by the number and size of the particles within a cloud. The radiation is sensitive to the optical thickness (τ) of the cloud. The optical thickness of a homogeneous cloud is determined by the scattering cross section (σ)

of the cloud particles (which is wavelength dependent), the number density (ρ) of the particles, and the physical thickness (z) of the cloud.

$$\tau = \sigma \rho z \tag{4}$$

Hence, if the number density of cloud droplets in a given volume were doubled, it would have the same effect as doubling the cloud thickness. Figure 2.A.1 from Liou (1974) shows the emissivity of

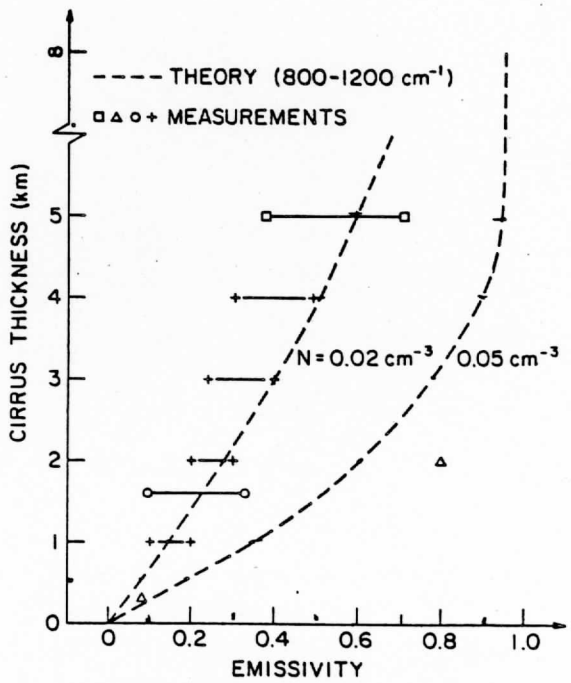

FIG. 6. Comparisons of the emissivity between theory (dashed lines) and observations. The symbols for the measured data are as follows: □ (Fritz and Rao, 1967), + (Kuhn and Weickmann, 1969), △ (Brewer and Houghton, 1956), and ○ (Platt and Gambling, 1971).

FIG. 2.A.1 (from Liou [1974])

cirrus clouds as a function of cloud thickness. As the clouds get very thick or as the number density gets very high, the cirrus emissivity tends toward unity. Figure 2.A.2 from Liou (1974) shows

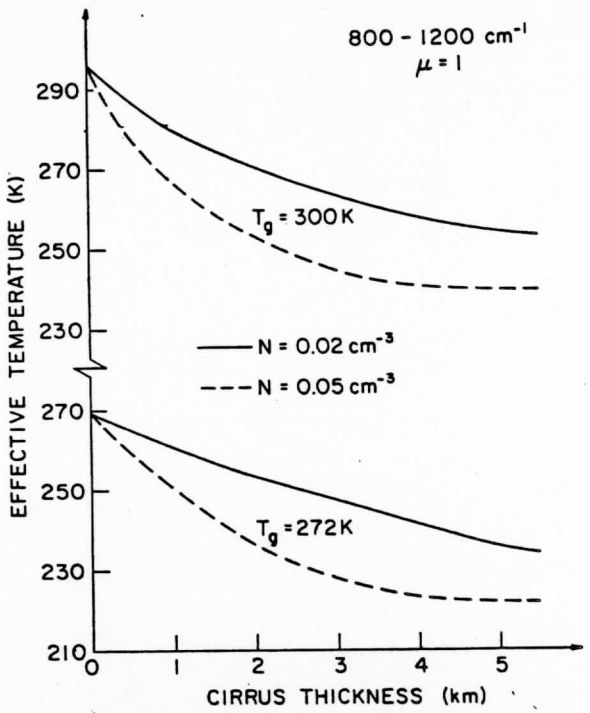

FIG. 7. Effective temperatures calculated from the upwelling intensity at the top of the atmosphere as functions of the cirrus thickness for two model atmospheres.

FIG. 2.A.2 (from Liou [1974])

the effect of the cirrus emissivity on the sensed temperature as a function of cloud thickness. These figures demonstrate that sensed temperature errors of 0 to 60°K are possible because of emissivity problems.

The number density of cumulus clouds is much higher than cirrus clouds. Average droplet concentrations of over 100 cm^{-3} are common in fair weather cumulus and cumulus congestus (Byers, 1965) with liquid water content of 0.2 to 2 g m^{-3}. The cirrus clouds used in the calculations of Liou (1974) of Figure 2.A.1 had number densities of 0.05 cm^{-3} and ice water content of 0.007 g m^{-3}. The larger number of drops make the emissivity of cumulus clouds closer to 1. Figure 2.A.3 from Yamamoto et al. (1970) shows the computed emissivity curve

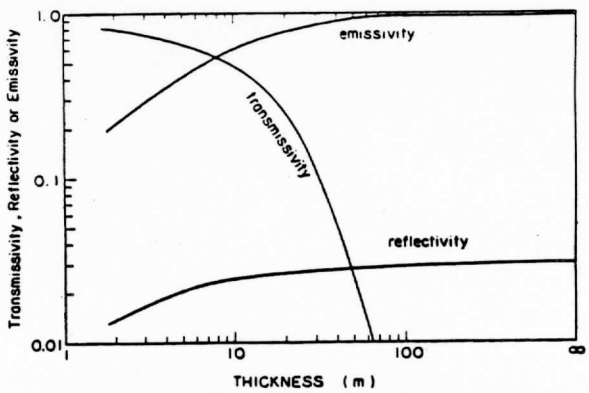

FIG. 12. Emissivity, reflectivity and transmissivity of clouds for the infrared region from 5–50 μ vs cloud thickness in meters.

FIG. 2.A.3 (from Yamamoto [1970])

for a cumulus cloud with a number density of 450 cm^{-3} and a liquid water content of 0.28 g cm^{-3}. Figure 2.A.3 shows that for cumulus clouds thicker than 50 m, the emissivity is essentially unity. Hence, cumulus clouds do not present an emissivity problem, while thin cirrus do present an emissivity problem.

Measurements of cirrus emissivity show a large variability, even within the same region of cirrus. Figure 2.A.4 from Platt (1975) shows a band of cirrus over Australia and the measured emissivity. While most of the cirrus had very low emissivity, there were regions within the cirrus which had emissivities close to 1. This fact has been used by interactive cloud-wind tracking groups to define "fleets" of cloud wind vectors. The operator views the cloud images in time lapse and mentally determines which cloud features are related with similar motions. The operator then searches the cloud band for the coldest cirrus which should have an emissivity close to 1. The temperature of this particular cloud is then manually assigned to all the clouds within the band being tracked, thus forming a "fleet" of vectors with the same temperature and height.

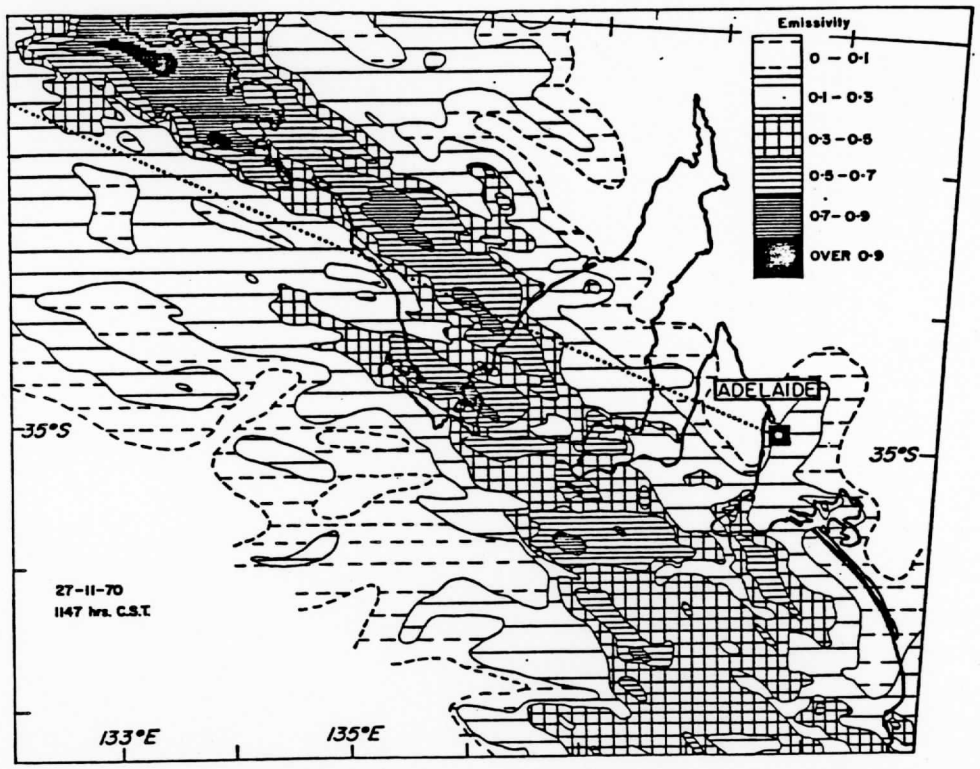

Figure 2. Map of cirrus emissivity ε (10·5–12·5μm) over the Adelaide region from Nimbus 4 THIR data. Scan time: 1147hr. Central Standard Time on 27 November. Dotted line indicates direction of wind drift.

FIG. 2.A.4 (from Platt [1975])

This fleet technique is used operationally by NESS and the University of Wisconsin for determining cirrus tracer heights.

Several attempts have been made to eliminate the problems of sensing correct cloud temperatures. Mosher (1975) and Reynolds and Vonder Haar (1977) have developed bispectral techniques which use the visible channel to help determine the fractional cloud cover and the infrared emissivity. The sensed temperature is then corrected to the true temperature. These techniques have not found wide acceptance in operations, primarily because of difficulties in cases which violate some of the basic assumptions of the models used. The bispectral techniques assume that a single layer of cloud is being viewed. However, with cirrus clouds there are frequently lower clouds

underlaying the cirrus. The visible light reflected from the cirrus is contaminated by the brighter light reflected from the cumulus below, resulting in erroneous correction factors for the infrared. Another problem with the bispectral techniques is that the correction factors require determination of both the fractional cloud coverage of the infrared field of view and the emissivity. Equation (2) can be rewritten as:

$$I = (\ )N(I_c - I_g) + I_g \ . \qquad (5)$$

The sensed radiation is dependent on the "effective emissivity" which is the product of the emissivity and the fractional cloud cover. The visible radiation is linearly dependent on the fractional cloud cover and approximately quadratically dependent on emissivity (Reynolds, 1977). If a bispectral technique is tuned to measure the fractional cloud cover of small cumulus correctly, thin cirrus corrections can be in error, and vice versa. At the beginning of the FGGE cloud-tracking operations, the bispectral technique of Mosher (1975) was used for the cloud-tracked winds produced at the University of Wisconsin. It was removed from use because of the erratic results it sometimes produced when used operationally. The "fleet" technique was then used for the remainder of FGGE.

2.A.4 Temperature to Height Conversion

Conversion of measured cloud top temperature to height requires a knowledge of the temperature structure of the atmosphere. The main problems come from obtaining a temperature sounding in the vicinity of the cloud and dealing with inversions which give multiple solutions of height. Over the United States, radiosonde data is available for the conversion of temperature to cloud height. The oceans present a problem because of lack of soundings. During FGGE operations, organizations such as NESS and the European Space Agency used NMC's global analysis of temperature. The University of Wisconsin's McIDAS does not have access to the global analysis in real time, so a climatological sounding was used. Inversions were made almost isothermal with the temperature of the top of the inversion preserved. The sounding was terminated at the tropopause. In order to arrive at a sounding for any given location, the January and July soundings were interpolated to the date using a cosine interpolation. The soundings from north and south of the point were then interpolated using a linear interpolation. There was no correction made for longitudinal temperature dependence or synoptic variability. The standard atmospheres used are shown in Table 2.A.1.

Inversions present a problem in the height determination based on cloud top temperature. Most clouds have their tops in an inversion layer which caps the convective activity forming the cloud. The actual height cannot be determined with certainty. Errors of 10 to 30 mb are possible because of inversions within the troposphere.

Overshooting towers which penetrate the tropopause present the most severe problem of height determination. The towers are small compared to the field of view of the satellite infrared sensor. As the towers first rise, they cool adiabatically and are frequently colder than the tropopause. They then warm to the environmental temperatures of the stratosphere. The temperature lapse rate is weak so small changes in temperature translate into large height changes.

2.A.5 Cloud Thickness Determination

Cloud thickness is important in many applications of satellite-determined cloud height. Hasler et al. (1977) determined from in situ aircraft measurements that low-level cumulus clouds move with the wind at the cloud base, so low-level cloud-tracked winds should ideally be put at the cloud base height. Likewise, radiative divergence calculations used for energy balance studies of the atmosphere require specification of the cloud base, as well as the cloud top. However, the cloud base is not a parameter which can be accurately determined.

The visible brightness of a cloud is influenced by its thickness, so several attempts have been made to determine cloud thickness from the visible satellite data. Griffith and Woodley (1973) showed an empirical relationship between cloud brightness and cloud height (thickness) for precipitating clouds. Kaveney et al. (1977) showed a statistical relationship between cloud brightness and

thickness. The statistical relationship differed for different cloud types.

An understanding of the theoretical relationship of visible light scattering to cloud properties is helpful in giving insight into the cloud thickness problem. Most of the theoretical work dealing with scattering of light by clouds has dealt with plane-parallel homogeneous clouds. These theoretical clouds are flat on the top and bottom and extend out to infinity in the horizontal direction. Results of Hansen (1971b), Twomey et al. (1967), and others have shown that the scattered light is related to the cloud thickness. As the cloud gets thicker, the reflected brightness increases toward an asymptotic limit. When the cloud is a kilometer or so thick, the cloud has very nearly reached its full brightness limit. From these theoretical plane-parallel results one would expect clouds thicker than a kilometer to be very bright and to have a uniform brightness. Digital satellite visible images show a large variability of brightness with any given cloud. Griffith and Woodley (1973) and Reynold and Vonder Haar (1973) showed a relationship between cloud height (thickness) and satellite-observed brightness for convective clouds in the range of 3 to 15 km. Plane-parallel theory will not explain this observed relationship.

The theoretical treatment of clouds with finite horizontal domain has been done using Monte Carlo techniques by Busygin et al. (1973) for cylinder, paraboloid, and sphere clouds, and by McKee and Cox (1974) for cubic clouds. They showed that light is scattered out the sides of the clouds, resulting in a decrease in brightness of the top surface as compared to plane-parallel results. McKee and Cox

(1976) have argued that the brightness-height (thickness) relationship observed by Griffith and Woodley (1973) could be due to increased cloud width rather than increased cloud thickness. Davies (1976, 1978) has shown that the height-to-width ratio of cuboidal clouds is important in determining the amount of light scattered in a given direction. Reynolds et al. (1978) have shown from satellite data that the height-to-width ratio effect predicted by cuboidal cloud models agrees with observed cloud brightnesses. As the clouds of a given thickness got wider, they became brighter. Aida (1977) has shown that the spacing between finite cubes in an array can also influence the reflected brightness of the cloud. Mosher (1979) has shown that finite cubic clouds have brightness variations across the cloud top and that liquid water inhomogeneities within a cloud can cause brightness variations.

These theoretical studies have shown that while there is a relationship between cloud brightness and cloud thickness, other factors such as cloud shape which cannot be determined from the satellite data alone make the cloud thickness determination prone to error.

As part of the cloud height package on the McIDAS, Mosher (1976) used a cloud thickness determination based on the observed visible brightness of the cloud. A data base of theoretical cloud brightness as a function of cloud optical thickness and sun-cloud-satellite geometry was generated using the plane-parallel doubling model of Hansen (1971a). The cloud brightness can be converted to cloud optical thickness using this table. The physical thickness of the cloud can be determined from the optical thickness using equation (4)

and an assumed cloud droplet size distribution. The C1 cumulus cloud model of Deirmendjian (1969) was assumed in relating the cloud optical thickness to physical thickness. Cirrus clouds have fewer cloud particles than cumulus clouds, resulting in a larger physical thickness for a given optical thickness. Mosher (1976) has attempted to account for this by using an empirically derived stretching factor for the cloud thickness derived assuming cumulus cloud parameters. For clouds colder than 273°K, the thickness (z) was increased by:

$$z' = z + [(T_c - 273)/40.5]z \qquad (6)$$

with T_c being the cloud top temperature.

The cloud thickness program on the McIDAS assumes plane-parallel clouds. Mosher (1979) investigated the relationship of the theoretical plane-parallel brightness to finite cloud brightness. Figure 2.A.5 (Mosher, 1979) shows the ratio of the plane-parallel brightness to the finite cubic cloud brightness as a function of sun angle and cube size. This figure shows that there is no simple correction factor that can be used to account for the finite cloud characteristics. The figure also shows finite clouds can be 20 to 50% darker than the plane-parallel clouds when the sun is high in the sky, and 10 to 30% brighter when the sun is near the horizon. The relationship of brightness to thickness is approximately a logarithmic function, so an error or uncertainty of brightness can translate into a large thickness error. For instance, a 20% uncertainty in cloud brightness for a cloud with an 0.5 albedo and

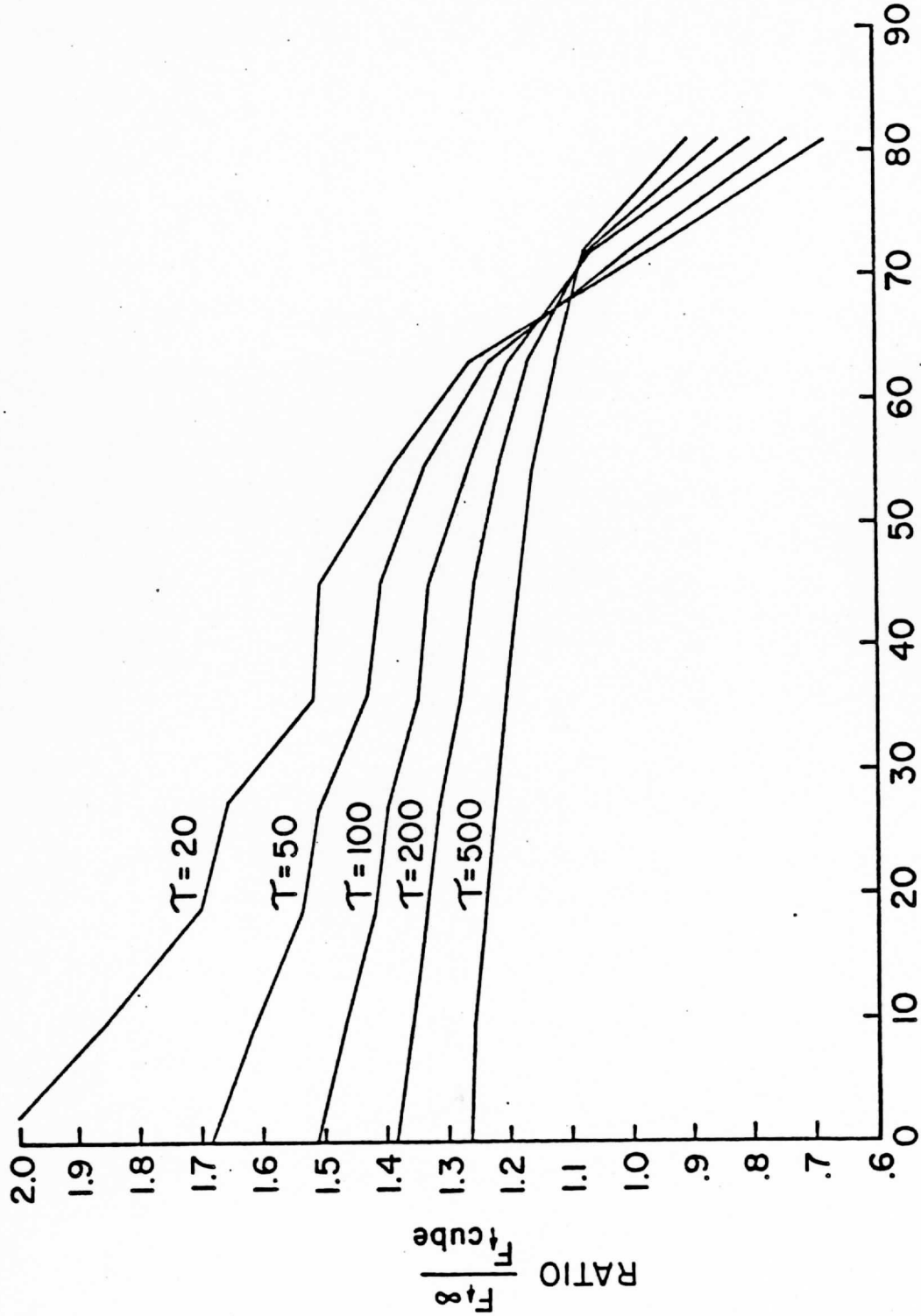

Fig. 18. Ratio of the plane-parallel flux to the average flux from the top of cubic clouds as a function of solar zenith angle for cubes of optical dimension 20, 50, 100, 200, and 500.

FIG. 2.A.5 (from Mosher [1979])

overhead sun translates into over a 50% uncertainty in cloud thickness. Consequently, the cloud thickness computation available on the McIDAS can be used as a guide to distinguish between thick and thin clouds, but the actual cloud thickness cannot be determined to better than a factor of two of the correct thickness.

2.A.6 Cloud Height Observations

The previous sections showed that accurate cloud height determinations can be made for water clouds larger than 24 km and ice clouds thicker than 5 km. The clouds where height errors can be expected are small cumulus, thin cirrus, and overshooting towers.

This section illustrates typical cloud situations and the heights derived by stereographic observations from two geostationary satellites, and the heights derived from the cloud top temperature. The stereo observations were derived by Hasler (1981) for the 2-3 May 1979 severe storm case in central Oklahoma. Table 2.A.2 shows the measured cloud height for different cases of clouds using the techniques of stereo, cloud top temperature with standard atmospheres, and cloud top temperature with a nearby radiosonde sounding. The height accuracy of the stereo measurements is in the range of 0.1 to 0.5 km. As Table 2.A.2 shows, the heights derived by the standard atmosphere and the radiosonde differed slightly, with the radiosonde height generally being slightly lower. The table shows that the heights derived from cloud top temperature for the thick anvil cirrus and the mid-level clouds agree quite well with the stereo height measurements. The penetrating towers were measured 1

to 2 km too low by the temperature techniques. This is because the towers are small compared to the size of the infrared sensor and the tower temperature at the tropopause does not vary much with height. The thin cirrus had height errors of over 5 km based on sensed temperature. This illustrates the emissivity problem discussed in Section (2.A.3).

Table 2.A.1. Standard atmospheres used for height determination

Sounding	Temp(°K)	Pressure(mb)	Height(km)	Sounding	Temp(°K)	Pressure(mb)	Height(Km)
Tropical	299.7	1013	0				
	287.1	780	2.3				
	287.0	757	2.5				
	193.2	103	16.5				
Jan 30°N	287.2	1013	0	July 30°N	301.2	1013	0
	281.2	804	2.0		293.7	905	1.0
	216.2	203	12.0		266.2	493	60
	203.2	145	14.0		203.2	133	15.0
Jan 45°N	272.2	1018	0	July 45°N	294.2	1013	0
	261.7	694	3.0		285.2	802	2.0
	219.7	257	10.0		261.2	487	6.0
	208.2	171	12.6		215.7	179	13.0
Jan 60°N	259.3	1013	0	July 60°N	287.2	1010	0
	259.2	888	1.0		260.2	541	5.0
	251.2	636	3.5		225.2	268	10.0
	217.2	307	8.5		225.1	269	10.1
Jan 75°N	253.8	1013	0	July 75°N	278.2	1012	0
	253.7	828	1.5		271.7	742	2.5
	215.2	299	8.5		226.2	284	9.5
	213.7	185	11.5		226.1	280	9.6

Table 2.A.2. Cloud heights measured by stereo, cloud top temperature with modified standard atmospheres, and cloud top temperature with radiosonde soundings.

	Stereo Height (km)	Temp. + Stand Atmos Height (km)	Temp. + Radiosonde Sounding Height (km)	Cloud Top Temp. (°K)
I. Anvil Cirrus				
	14.0	14.2	13.3	209
	14.0	13.7	12.8	212
	13.0	12.8	11.6	218
	13.5	14.2	13.3	209
II. Penetrating Towers				
	15.6	13.5	12.8	211
	15.4	13.5	12.8	211
	14.5	13.3	12.2	212
	15.4	14.0	13.2	208
	15.9	14.0	13.2	208
	16.1	15.1	14.5	200
	15.7	14.5	13.6	205
	16.1	15.1	14.5	200
III. Cirrus Around Subtropical Jet (thin)				
	12.2	6.7	6.4	257
	10.3	6.1	5.6	262
	10.4	2.9	3.1	280

IV. Mid-Level Clouds

4.9	4.1	3.8	271
4.5	4.0	3.6	272
7.6	7.2	6.8	252
9.2	8.9	8.3	240
7.8	8.8	8.2	241

References

Aida, M., 1977: Reflection of solar radiation from an array of cumuli. J. Meteor. Society Japan, 55, 174-181.

Busygin, V. P., N. A. Yevstratov, and Ye. M. Feygel'son, 1973: Optical properties of cumulus clouds and radiant fluxes from cumulus cloud cover, Atmos. Oceanic Phys., 9, 1142-1151.

Byers, H. R.; 1965: Elements of Cloud Physics, University of Chicago Press, Chicago and London, pp. 144-146.

Davies, R., 1976: The Three-Dimensional Transfer of Solar Radiation in Clouds. Ph.D. Thesis, University of Wisconsin-Madison.

_____, 1978: The effect of finite geometry on the three-dimensional transfer of solar irradiance in clouds. J. Atmos. Sci., 35, 1712-1725.

Deirmendjian, D., 1969: Electromagnetic Scattering on Spherical Polydispersions. American Elsevier Publishing Company, Inc., New York, 290 pp.

Fritz, S., and J. S. Winston, 1962: Syonptic use of radiation measurements from TIROS II. Mon. Wea. Rev., 90, 1-9.

Griffith, C. G., and W. L. Woodley, 1973: On the variation with height of the top brightness of precipitating convective clouds. J. Appl. Meteor., 12, 1086-1089.

Hansen, J. E., 1971a: Multiple scattering of polarized light in planetary atmospheres, Part I. The doubling method. J. Atmos. Sci., 28, 120-125.

_____, 1971b: Multiple scattering of polarized light in planetary atmospheres, Part II. Sunlight reflected by terrestrial water clouds. J. Atmos. Sci., 28, 1400-1426.

Hasler, A. F.; 1981: Stereographic observations from geosychronous satellites: An important new tool for the atmospheric sciences. Bull. Amer. Meteor. Soc., 62, 194-212.

_____, W. E. Shenk, and W. C. Skillmen, 1977: Wind estimates from cloud motions: Results of Phase I, II, and III of an in situ aircraft verification experiement. J. Appl. Meteor., 16, 812-815.

Kehnajy, F., and F. Mosher, 1981: GOES, Indian Ocean. The Global Weather Experiment - Final Report of the U.S. Operations. U.S. Dept. of Commerce, NOAA Office of Research and Development, FGGE Project Office, Rockville, MD, pp. 29-40.

Kaveney, W. J., F. G. Feddes, and K. N. Liou, 1977: Statistical inference of cloud thickness from NOAA-4 scanning radiometer data. Mon. Wea. Rev., 105, 99-109.

Koffler, R., A. G. DeCotiis, and P. K. Rao, 1973: A procedure for estimating cloud amount and height from satellite infrared radiation data. Mon. Wea. Rev., 101, 240-243.

Liou, K.-N.; 1974: On the radiative properties of cirrus in the window region and their influence on remote sensing of the atmosphere, J. Atmos. Sci., 31, 522-532.

McKee, T. B., and S. K. Cox, 1974: Scattering of visible radiation by finite clouds. J. Atmos. Sci., 31, 1885-1892.

_____, and J. T. Klehr, 1978: Effects of cloud shape on scattered solar radiation. Mon. Wea. Rev., 106, 399-404.

Mosher, F. R., 1975: SMS Cloud Heights. Final Report on Contract NAS 5-23296, V. E. Suomi, P.I., SSEC, University of Wisconsin-Madison, pp 301-338.

_____, 1976: Cloud Height Determination. Proceedings of the Symposium on Meteorological Observations from Space: Their contribution to the First GARP Global Experiment, 19th meeting of COSPAR at Philadelphia, Penn., printed at NCAR, Boulder, Colo., pp. 201-204.

_____, 1979: Visible Flux Variations Across Finite Clouds. Ph.D. Thesis, University of Wisconsin-Madison.

Platt, C. M. R.; 1975: Infrared emissivity of cirrus--simultaneous satellite, lidar, and radiometric observations. Quart. J. Roy. Meteor. Soc., 101, 119-126.

Rao, P. K., and J. S. Winston, 1963: An investigation of some synoptic capabilities of atmospheric 'window' measurements from satellite TIROS II, J. Appl. Meteor., 2, 12-23.

Reynolds, D. W., and T. H. Vonder Haar, 1977: A bispectral method for cloud parameter determination. Mon. Wea. Rev., 105, 446-457.

Reynolds, D., T. B. McKee, and K. S. Danielson, 1978. Effects of cloud size and cloud particles on satellite-observed reflected brightness. J. Atmos. Sci., 35, 160-164.

Young, M. T.; 1975: The GOES Wind Operation. NOAA Technical Memorandum NESS 64, NOAA/NESS, Washington D. C. pp. 111-121.

2.B Improvements to Cloud Height & Thickness Determination

The previously described cloud height algorithm needed IR data, an assumed cloud emissivity and extent, and climatological soundings to estimate cloud tops. This scheme requires only one data source, the IR temperature; therefore, heights can be calculated anywhere the IR sensor is directed. To improve this method, the number of assumptions has to be reduced or an additional independent data source has to be used in conjunction with the current algorithm.

2.B.1 Adding Local Soundings*

a. Comparisons of Climatology vs. Local Soundings Without Moisture

Replacing the Standard Atmosphere with a radiosonde-derived vertical profile near the cloud is one possibility in data rich areas such as over the United States or over the GATE region. The standard sounding is an average in both time and space (4 vertical levels, 20 degree latitude bands, twice per year), while the local sounding is a "snapshot" through the atmosphere at a particular location. Limiting factors include spatial and temporal radiosonde coverage and atmospheric variability relative to the cloud and the sounding.

Thus far, the most accurate remote measurements of cloud heights involve use of parallax information gained from viewing the same cloud from two different satellites. However, the technique is limited. Precise navigation (errors of one pixel or less) of both satellites is a prerequisite for applying this method, as small horizontal differences affect the computation of the height (Hasler,

---

* Additional support was furnished by contract NAS8-33799.

1981). Stereo images can be generated by remapping one of the satellite images into the projection of the other. When data from only one satellite are available, false stereo images can be made by offsetting the visible image based on the IR temperature to introduce parallax. To view stereo from the image pairs, one image is enhanced with green and the other red and a pixel-to-pixel interlace is done. The resulting image is then viewed with red-green glasses to produce a three-dimensional effect.

Conventional radiosonde data possess features useful in determining cloud height and thickness:

i) Radiosondes are routinely launched over most land areas twice every day;

ii) Temperature, moisture, and wind data are available;

iii) Each sounding presents a detailed vertical resolution of the atmosphere.

During meteorological experiments such as GATE or SESAME, the number of radiosondes tracked is increased to eight or more each day over a small, sub-synoptic region. To test the effectiveness of adding a local sounding, these high density data sets were used to minimize temporal and spatial differences between the cloud and the sounding. In an operational mode, the data density and resolution over the United States should aid markedly in determining cloud

heights, especially in areas that deviate significantly from the Standard Atmosphere.

The cloud height algorithm described in Section 2.A is altered only to allow an operator or an objective computer program to select a representative sounding. If the sounding is objectively chosen by the computer software, the one closest in time and space replaces the Standard Atmosphere. The same procedure is followed to convert IR and visible satellite data to height (as in Section 2.A), using a nearby sounding to interpolate the temperature between two pressure levels. Additional information converning cloud height and thickness can be obtained from the sounding's moisture profile. Also, multiple cloud layers may become evident from a display of relative humidity with height (Fig. 2.B.1). In this case two levels are noted, one from 1000 mb to 850 mb and another from 590 mb to 560 mb. Other information that may be used is the wind profile if a cloud motion has been determined (See Section 3, Cloud Tracking). Here, the cloud wind vector is compared interactively with a vertical profile of the wind and a subjective decision regarding which level the wind represents is made by the operator (See Section 3 on other techniques and wind editing). Radiosonde and cloud wind comparisons have shown ± 5 m s^{-1} discrepencies as have rawinsonde versus rawinsonde wind comparisons (Mosher and Sawyer, 1975; Bauer, 1976).

Table 2.B.1 summarizes the reliability of various parameters to determine heights, based on sensor accuracy and performance for different cloud types. This exemplifies the need for independent data to determine cloud height and distinguish between thick clouds and/or multiple cloud decks.

Three comparisons of climatology versus local soundings from ships were done using data from GATE. First, aircraft data (Warner, 1979) was chosen as ground truth to calculate differences between the two methods described above. There was no improvement in using local soundings over climatology (Table 2.B.2) mainly due to the lack of baroclinic zones in the tropics which would account for deviations of the local sounding from the mean. The standard deviation of the local sounding measurements and the standard error does indicate a tendency to be closer to the ground truth, but it is only on the order of 100 m. The cloud tops were underestimated most tops measured from the aircraft were at or below the IR sensor resolution. Time differences between the soundings and aircraft were only about 5-10 min, but parallax which would have shifted the data a few kilometers was not removed.

The second comparison used Quadra radar RHI scans as ground truth. This was done for Day 261 (18 September 1974). Table 2.B.3 shows there was improvement, reducing the error by one-third (0.4 km) and estimating closer to the ground truth 67% of the time. This data set had a mixture of high and low level echoes, whereas the aircraft data was mainly at the mid-levels. The improvement was mostly at the lower and higher levels where the temperature is more variable (Reed and Recker, 1971). The third comparison using variability between the estimates with no ground truth is shown in Table 2.B.4. Cloud tops were calculated from about 10°N to 8°N each minute of latitude along 23°W longitude for Day 245 (2 September 1974). The two methods showed about a 200 m difference in both the mean and standard deviation, but again most measurements were in the middle troposphere

(4000 m) where the variability in the tropics is a minimum. In all of the above comparisons the operator selected the most representative sounding and no adjustments were made based on moisture or wind information.

b. Use of Moisture in Determining Cloud Heights

The use of moisture in determining cloud heights and thickness and for multi-level situations is subjective in our scheme. Fig. 2.B.2 is an example of what can be done combining information from the cloud height program and the moist layers derived from the ship soundings. A number of clouds were sampled within an 80 km radius of the ship Vanguard during GATE (Day 261). Three thresholds were chosen for the relative humidity (90, 83, and 70%) to be compared with the cloud height and thickness. Relative humidity greater than 83% correlated best with a visual determination of cloud location from a Stüve plot and is the reason for choosing that particular threshold. The data presented in Fig. 2.B.2 indicate that the mid-level cloud (#4) was estimated well, clouds #1 and #2 are probably too thin based on the moisture and would most likely extend to the top of the boundary layer (960 mb, from ship surface reports). The existence of cloud #3 in the middle of the two layers is suspect and could be the result of a thin mid-level cloud over a lower deck of clouds.

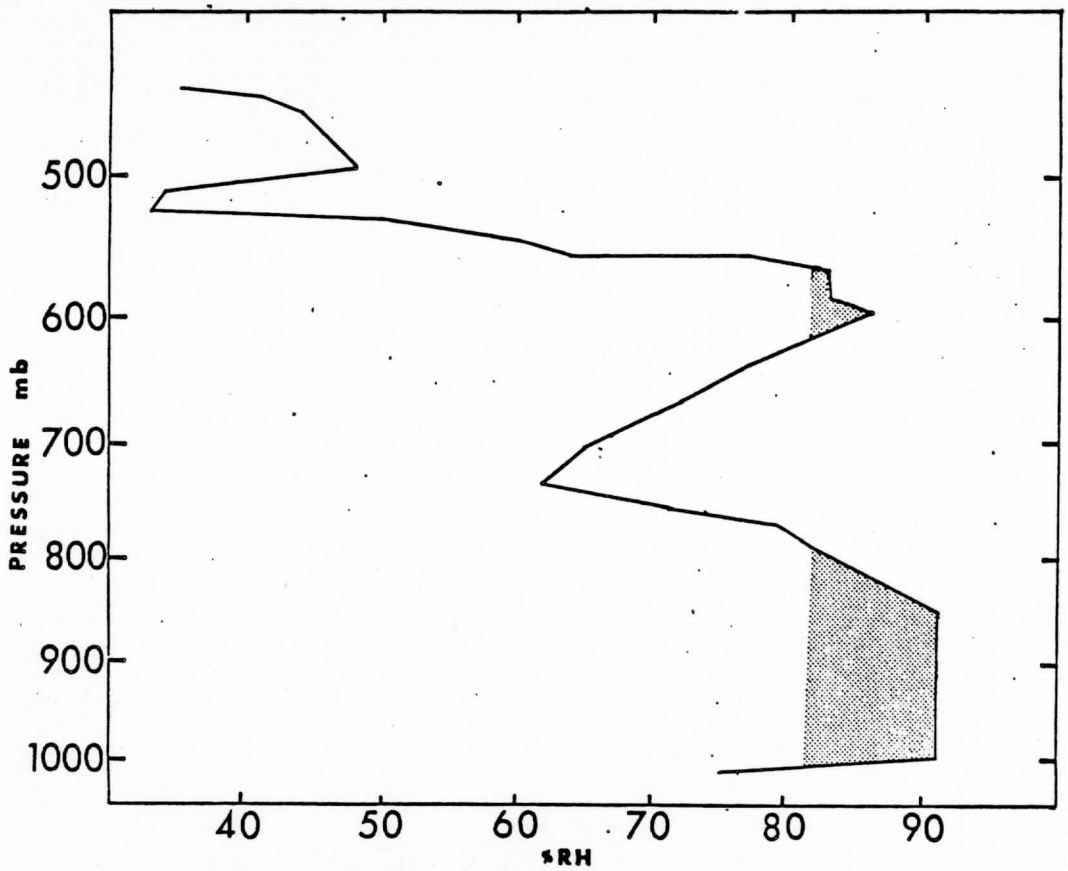

Fig. 2.B.1 Relative humidity profile from the ship Vanguard during GATE, 1500 GMT 18 September 1974. Shaded areas indicate possible cloud layers.

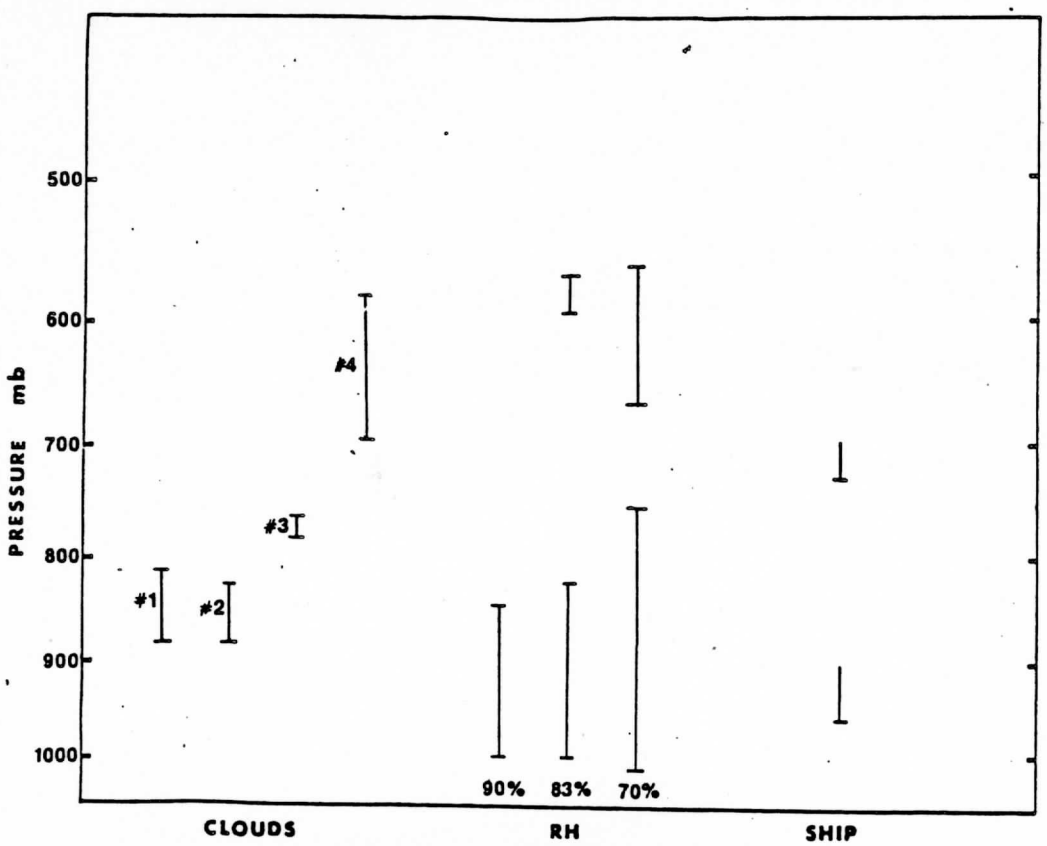

Fig. 2.B.2 A composite of local sounding derived cloud tops and bases, regions where the relative humidity exceeds a threshold (from Fig. 2.B.1), and cloud base as reported by the Vanguard.

c. Use of Wind Information to Edit Cloud Heights

Wind information was used to edit cloud heights for an extensive set of cloud motion vectors during SESAME 1979 (Goodman et al., 1982). Local soundings (operator selected) were used in calculating cloud heights and were adjusted based on the cloud motion's agreement with radiosonde-derived winds. This resulted in wind fields every 100 mb over the central United States. In the past, cloud vectors were assigned as either high and low level, with middle level vectors comprising a large nebulous region in between (Suchman and Martin, 1976). No statistics have been gathered to determine if there was improvement, but 1-2 km differences in cloud height were noted in using the local sounding over climatology (Auvine, personal communication).

2.B.2 Real Stereo Images*

The technique of using stereo images to calculate cloud height includes no assumptions about cloud emissivity and is not restricted by IR sensor resolution as is the method described in Sec. 1. Its limitations are much more basic. Data is not as abundant as two satellites in different locations must be viewing the same feature simultaneously from different locations. Navigation must be precise because a one pixel shift in the horizontal can result in a 500 m error in the vertical. Also, a recognizable cloud feature must be visible in both images. Textured clouds or regularly defined small

* Additional support was furnished by contract NASW-3476.

clouds make the best targets. In the following discussion, all mention of satellites is in reference to the geostationary satellites GOES-E and GOES-W.

Hasler (1981) developed a system to measure cloud height from the parallax difference in the cloud as it is viewed from the two satellites. Our method is similar, but is designed along the lines of cloud tracking (see Section 3). Two digital images coincident in time and space are retrieved, one from each satellite. One of the images is remapped into the satellite projection of the other. The images are visually juxtaposed, and alternately displayed on the screen. The locations of cloud elements common to both images are indicated by an operator controlled cursor. This information is entered into a computer program which converts the locations and the distance between them into an altitude. Comparison of parallax-derived heights with those from using a local sounding was not done because of the differing spatial (mesoscale versus synoptic) scales.

2.B.3 False Stereo Images

True stereo described above can be both quantitative (deriving cloud heights) or qualitative (red-green stereo display), but the latter can only apply to false stereo. An advantage of false stereo is that data from only one satellite is needed; the parallax offset is calculated artificially from the IR temperature. See Hasler et al. (1981) for a complete description of generating false stereo images. Comparing both forms of stereo display for a number of cases

indicate that the real stereo image does not improve on discerning cloud levels. This makes false stereo a good candidate over real stereo to determine relative cloud heights because of the better coverage and simpler computation.

This technique is not unique to the geostationary satellites. Hasler et al. (1981) have used the false stereo display with Tiros-N IR data and contours of humidity fields. Martin (personal communication) has used polarization differences in the microwave channel of NIMBUS-7 to create false stereo images to aid in locating rain/no rain areas. The visual impact of three dimensions is striking to the viewer, and provides an additional qualitative tool for data analysis. The technique is being enhanced to aid in delineating cloud layers and to aid in assigning relative heights to cloud motion vectors.

REFERENCES

Bauer, K.E., 1976: A comparison of cloud motion winds with coinciding radiosonde winds. Mon. Wea. Rev., 104, 922-931.

Goodman, H.M., B.A. Auvine, and D.A. Santek, 1982: The relationship of satellite and radar storm signatures to the subsynoptic wind field. Preprints, 12th Conference on Severe Local Storms.

Hasler,A.F., 1981: Stereographic observations from geosynchronous satellite: An important new tool for the atmospheric sciences. Bull. Amer. Meteor. Soc., 62, 194-212.

_____, M. desJardins, and A.J. Negri, 1981: Artificial stereo presentation of meteorological data fields. Bull. Amer. Meteor. Soc., 62, 970-973.

Mosher, F.R., and B. Sawyer, 1975: Comparison of wind measurement systems: Cloud tracked winds versus rawinsonde wind and rawinsonde winds versus rawinsonde winds. Preliminary assessment of the cloud tracking system developed at the University of Wisconsin, SSEC, University of Wisconsin-Madison.

Reed, R.J., and E.E. Recker, 1971: Structure and properties of synoptic-scale wave disturbances in the Equatorial Western Pacific. J. Atmos. Sci., 28, 1117-1133.

Suchman, D., and D.W. Martin, 1976: Wind sets from SMS images: An assessment of quality for GATE. J. Appl. Meteor., 15, 1265-1278.

Warner, C., 1979: Cloud measurements on Day 245 of GATE. Cloud populations and their interaction with the boundary layer. Tech. Rep. No. 5, Univ. of Virginia, Charlottesville. 24 pp.

Table 2.B.1. Reliability of measured parameters in determining cloud height, for different cloud types.

Parameter	Reliable	Unreliable
IR Temp.	Large uniform cloud decks (stratus) where accurate IR temperatures can be determined. Cumulonimbus.	Small, thin clouds (low level Cu, Ci) or multi-level clouds due to averaging by IR sensor.
Moisture	Layer, non-cumuloform clouds in low or mid levels.	Large cumulo-form clouds where moisture is injected to upper levels from the boundary layer. (Sounding in ambient air.) Ice clouds (Ci).
Wind	Clouds of small vertical extent in a sheared flow (low level Cu, alto-form). Cirrus.	Cumulo-form where the steering level is not the the cloud top. Regions of minimum vertical shear or large horizontal shear (fronts, cyclones).

Table 2.B.2 Determining cloud heights using aircraft, climatology, and local soundings.

	Aircraft	Climatology	Local Sounding
Mean Ht.	7.08	5.91	5.91
Standard Dev.	3.46	1.96	2.12
Mean Error	--	-1.17	-1.17
Standard Err.	--	2.27	2.17

Note: All measurements are in kilometers. Mean error and standard error are based on aircraft as ground truth. 45 observations.

Table 2.B.3 Determining cloud heights using Quadra RHI, climatology, and local soundings.

	RHI	Climatology	Local Sounding
Mean Ht.	10.75	11.64	11.41
Standard Dev.	2.23	1.49	1.19
Mean Error	--	.89	.66
Standard Err.	--	2.25	2.20

Note: All values are in kilometers. Mean and standard error are based on RHI as ground truth.

Table 2.B.4 Variability in cloud heights using climatology and local soundings.

	Climatology	Local Sounding
Mean	4.28	4.08
Standard Dev.	2.30	2.50
Observations	101	101

3. CLOUD TRACKING FOR GATE WIND FIELDS

3.A Introduction

Satellite-based cloud motion winds offer a wide spectrum of wind data for various meteorological purposes. They can provide coverage from global scales down to motions within the anvil of a cumulonimbus. The finished product varies according to the needs of the researcher. Consequently, the techniques developed to meet these needs will vary also. The cloud tracking for GATE has been concerned with high density mesoscale wind fields with a high degree of accuracy as a means of obtaining wind fields on a variety of scales of motion. These fields differ both qualitatively and quantitatively from those produced for FGGE (which deals with larger scale flow), for example.

Because we are concerned with extracting as much information as possible from the cloud field, the production of these wind sets is quite laborious. Over the past few years, we have improved our methods of cloud height determination, delineating mid- and high-level cloud tracers, combining satellite-derived cloud winds with those obtained from other platforms, and editing. Many of the techniques to be discussed will not be applicable to those interested in coarse, large scale wind fields, or in real-time information. As the GATE wind fields are intended to support the scientific study of the structure and dynamics of tropical systems, accuracy and completeness are our primary goals.

Our main objectives have been to 1) expand satellite wind coverage in middle and high levels, 2) develop objective means for editing these

winds, and 3) integrate all of the satellite winds with those available from rawinsonde and aircraft observations.

In general, our data come from the following sources:

1) Full resolution SMS-I visible and infrared data at 15 or 30 min intervals. A three image sequence is generally the basis for cloud tracking, with a picture on either side for reference.

2) Ship winds. These are radar winds, nationally processed and validated.

3) 12-h filtered VLF/Omega winds. Provided by Ooyama and Chu, these winds have been subjected to an iterative editing and two-dimensional time-height filtering.

4) Aircraft winds. These were obtained during GATE from flights of the DC-6 and Electra aircraft.

Background information on cloud tracking at SSEC can be obtained from Suchman and Martin (1976), and Johnson and Suchman (1980). The Suchman and Martin paper, "Wind Sets from SMS Images: An Assessment of Quality for GATE", explores the accuracy, representativeness and reproducibility of tracer winds in the area of the 1974 GATE region. Two questions are addressed: 1) How accurately can the cloud displacements be measured? and 2) To what extent do the cloud displacements represent the wind field? Accuracy is evaluated in terms of data characteristics, McIDAS

precision and consistency. The Johnson and Suchman paper, "Intercomparisons of SMS Wind Sets: A Study Using Rapid-Scan Imagery", examines the effect of variations in the time and space resolutions of satellite images on satellite-derived drift winds. Rapid-scan satellite data are used as a basis for computing cloud-tracked wind fields over the south central United States on three synoptically different days in 1978. Winds from 30, 15, 6 and 3 min intervals are produced, discussed and compared. Also, we acknowledge the cloud tracking work at other institutions, e.g., Goddard Space Flight Center (Hasler, 1981), Colorado State University (Negri & Vonder Haar, 1980), and NESS,(Hayden, et al., 1979) and at the University of Wisconsin (Wilson & Houghton, 1979), but have chosen not to discuss them here, because of their publication elsewhere.

3.B Delineating Mid- and High-Level Tracers

For most of the GATE systems studied, it was relatively easy to identify and track the low-level clouds (i.e., those below 850 mb). On the other hand, there were occasionally several layers of clouds at middle levels (400-700 mb), and the cirrus level often contained blow-off from convective systems as well as ambient cirrus. The first objective is to identify and represent the various levels of flow.

Clouds typically move with the wind at their level. Once it is determined which cloud feature moves with the wind, the motion of this feature can be used to represent the wind field.

In order to begin, we initially assume that clouds exist in fields, with each field having the same motion characteristics and sharing a common level.

Loops of the satellite images(see Fig. 3.B.1, 3.B.2a-d) are set up, with an individual loop containing a minimum of five images [see 1 above]. These loops are then viewed at varying speeds, to help the scientist separate the various fields of motion. These fields are then roughly sketched out on paper or a clear overlay analogous to the production of cloud maps. The procedure is repeated for the infrared data only, and the results compared to the visible data fields. Up to this point, no actual cloud tracking has been performed.

Next, individual clouds are identified within these cloud fields and their heights are determined (see Section 2.A on cloud height determination). If all the clouds within a cloud field have similar heights, then the next cloud field is examined. If inconsistencies are found, then the scientist returns to viewing the cloud loops to try and resolve them.

When the heights of the individual fields are determined, they are overlayed on the satellite images. These fields are then compared with the image loops for consistency with the observed physical changes in the cloud systems. For example, diffluent flow would be expected at upper levels in the vicinity of a growing convective system. Finally, the individual clouds are identified, tracked and edited using the techniques described below.

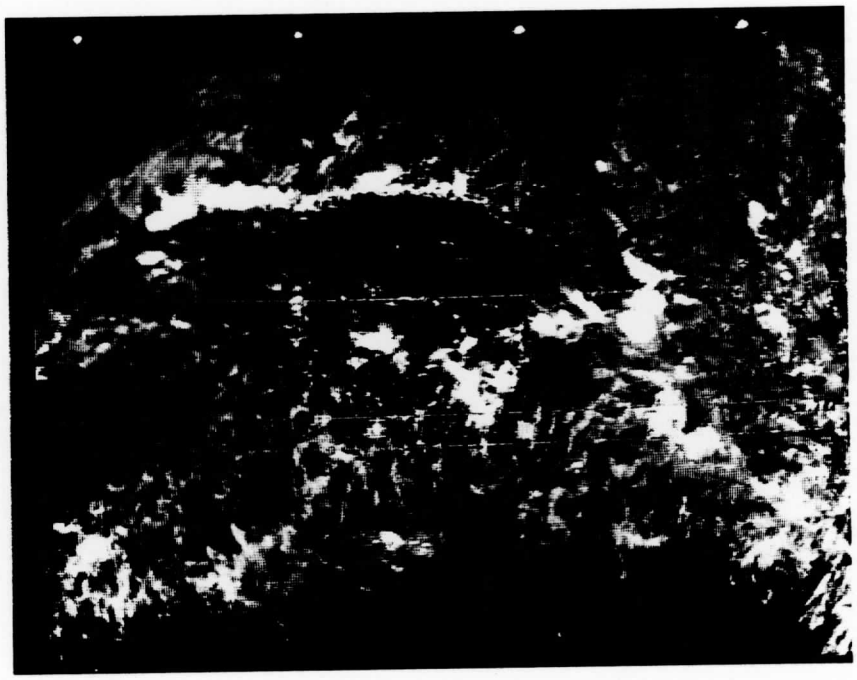

Fig. 3.B.1 SMS-I Visible photograph (with deep convection enhanced) of GATE area, 18 September 1974, 1500 GMt, 4 mi resolution.

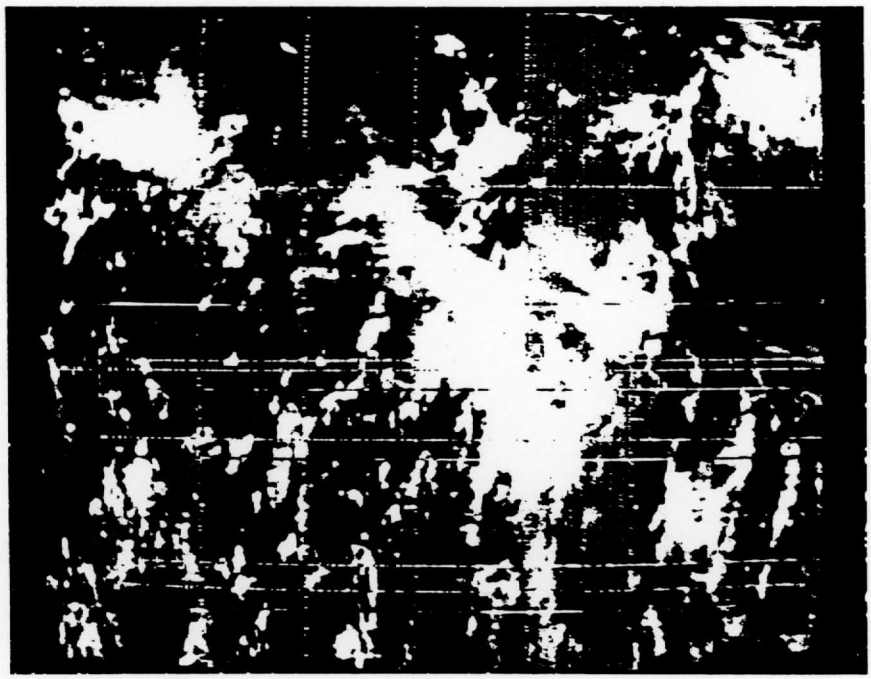

Fig. 3.B.2a SMS-I Visible photograph of GATE area, 18 September 1974, 1500 GMT, 1 mi resolution.

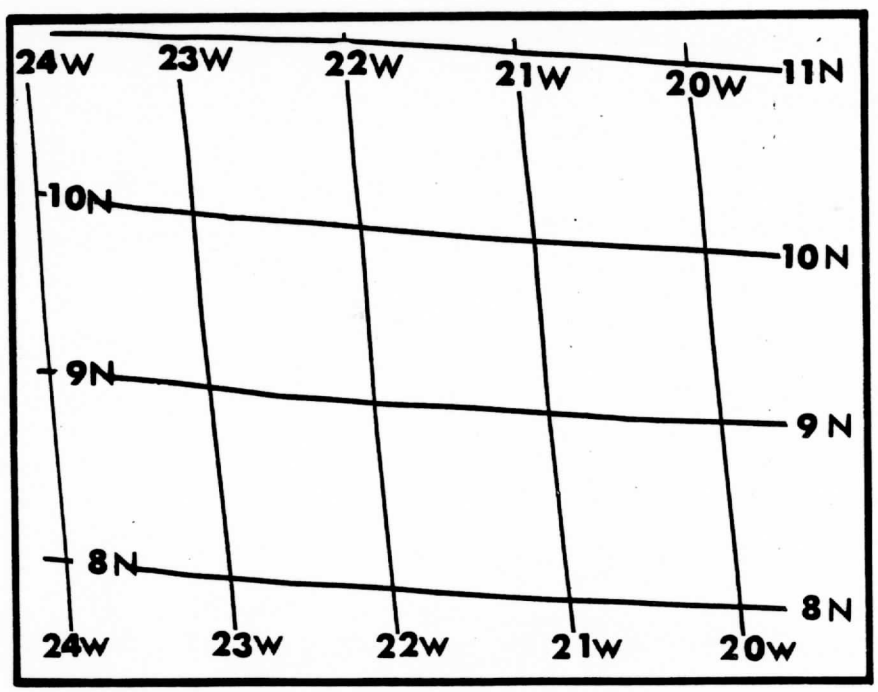

Fig. 3.B.2b Grid for figures 3.B.2.a,c,d.

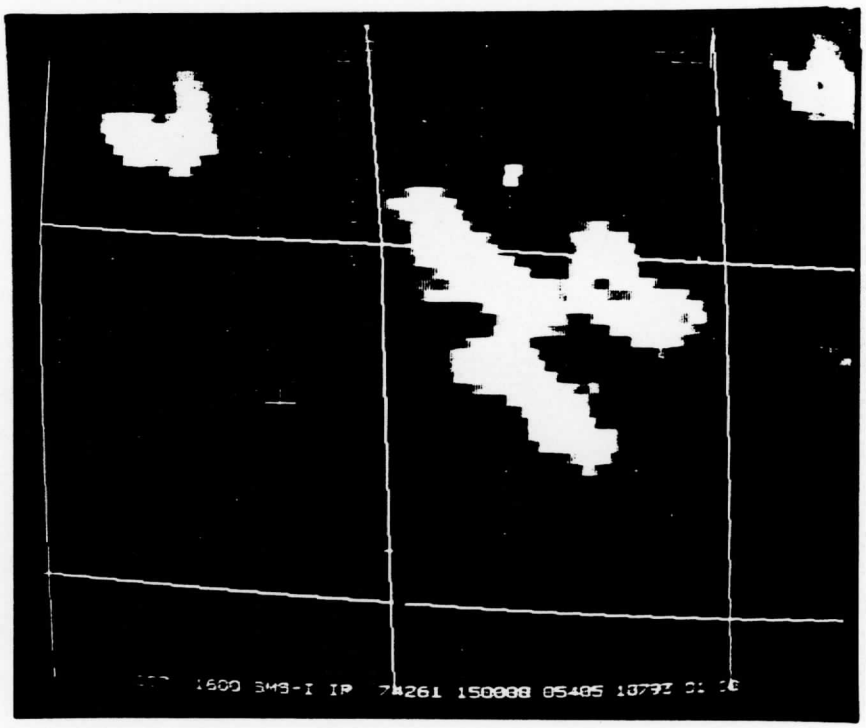

Fig. 3.B.2c same as fig. 3B2a, except infrared photograph.

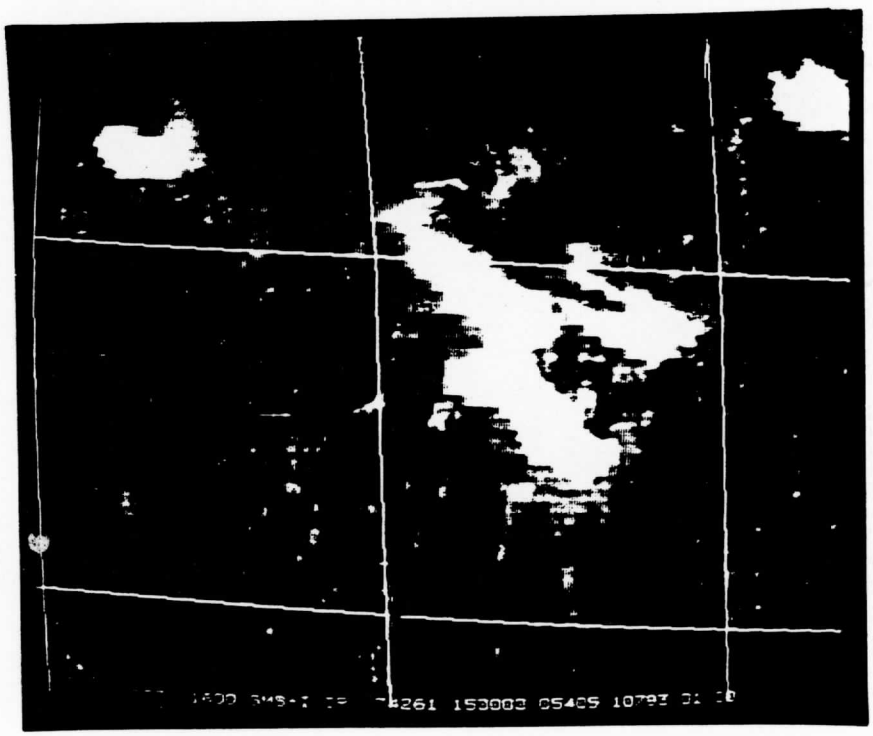

Fig. 3.B.2d same as fig. 3.B.2a, except infrared superimposed on visible image.

3.C Cloud tracking techniques

Our problems are twofold: determining which cloud feature to track, and tracking it accurately. The problem of wind set reproducibility, i.e., making sure that a wind set is not scientist-dependent, has been dealt with in a previous paper (Suchman and Martin, 1976).

Once the general cloud fields are identified and their height established, it is most efficient to track all the clouds within one field at the same time. Hence, the first step is to identify which cloud tracers to track. These tracers should, if possible, be observable in the entire five image viewing sequence, though actual tracking usually occurs only on the middle three pictures. In addition, the cloud features should not be growing or dissipating, and should roughly maintain their size and shape. We initially attempt to track all possible cloud features that meet these criteria.

There are two types of cloud tracking methods available on McIDAS, single picture element (pixel) and correlation (for details see Johnson and Suchman, 1980). The single pixel method seems to meet the needs of GATE better by giving a scientist more complete control over what is tracked and how it is tracked. In this mode of cloud tracking, the scientist and not the computer determines which cloud feature to track, and also does the actual tracking.

The results using the single pixel metric improved markedly when the tracking sequence images are enlarged (blown up) by a factor of two. For example, for images 15 min apart, one would normally use full resolution (1 km) pictures. However, for this method the images are enlarged. This method is especially useful for trade cumulus winds, because the

displacement of tracer clouds is typically small compared to the resolution of the images. If blow ups are made, the centers should be picked to provide overlap at the edges.

During the actual tracking of cloud fields, it is very useful to check for internal consistency. Because we are assuming that clouds at the same level act as fields, it would be unusual for clouds within that field to have radically different motion vectors. When clouds vary significantly from the streamlines of that field, we assume that they are either at a different height, that they reflect local influences, or that they were incorrectly tracked. Plotting the motion vectors on an overlay of the satellite images as they are being tracked usually simplifies this process. It also helps to take a break between the time of the vectors are initially plotted, and when they are edited for internal consistency.

3.D Editing Procedures

The next step in the generation of a wind data set(see Fig. 3.D.1a-c) is comparing that wind set with ground truth, usually rawinds. There is a variety of causes of errors found in wind sets; some of these (errors due to navigation, resolution, and operator) are discussed in Suchman and Martin (1976). Some other problems are encountered when comparing satellite winds and rawinds. Satellite winds tend to be clumped; they often represent different scales of motion than ship or aircraft winds; and they sometimes reflect local effects or movements resulting from changes in convective intensity. There is uncertainty in the determination in the height of cloud winds, especially from

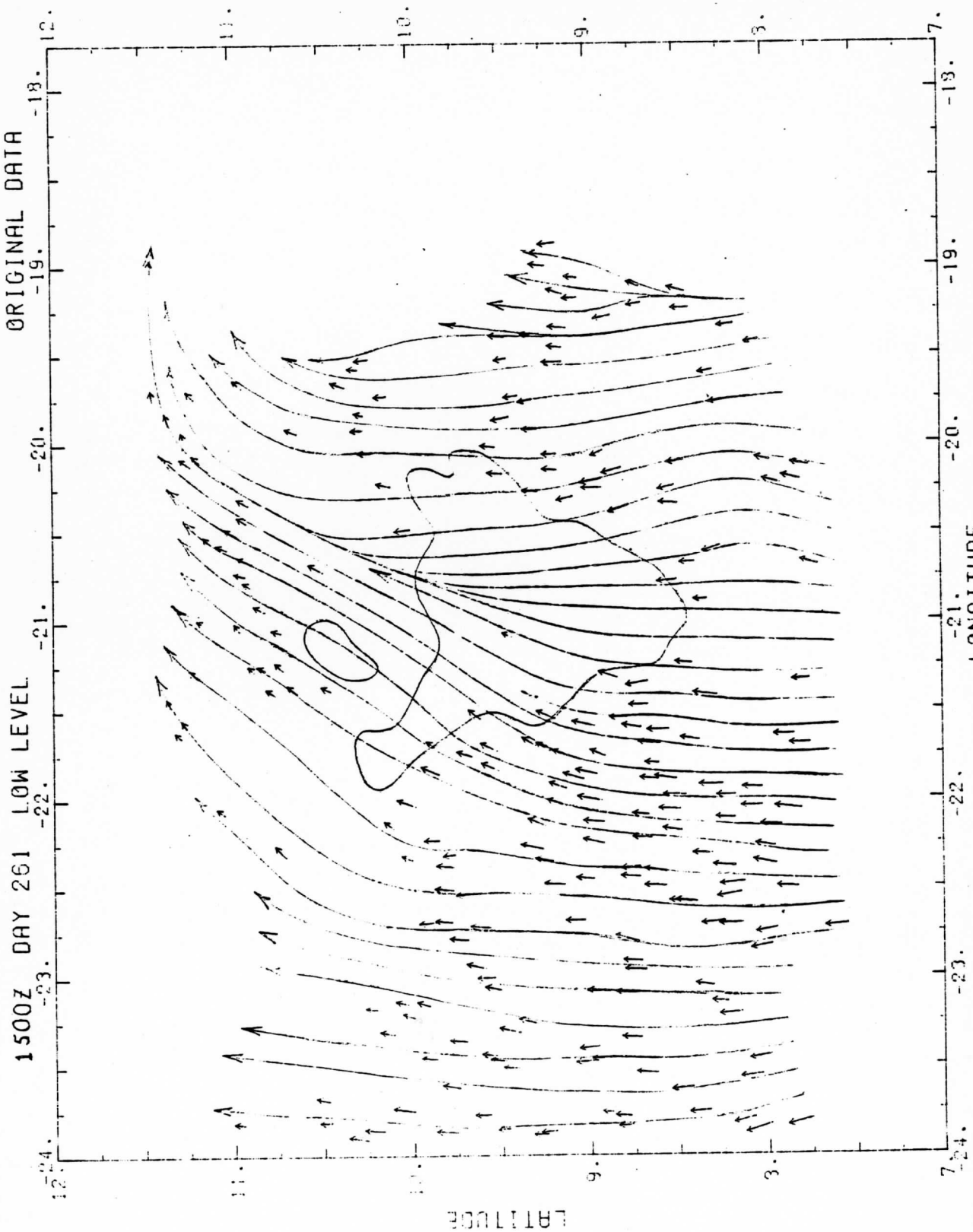

Fig. 3.D.1a "Original" winds and streamlines, 18 September 1974, 1500 GMT, low level.

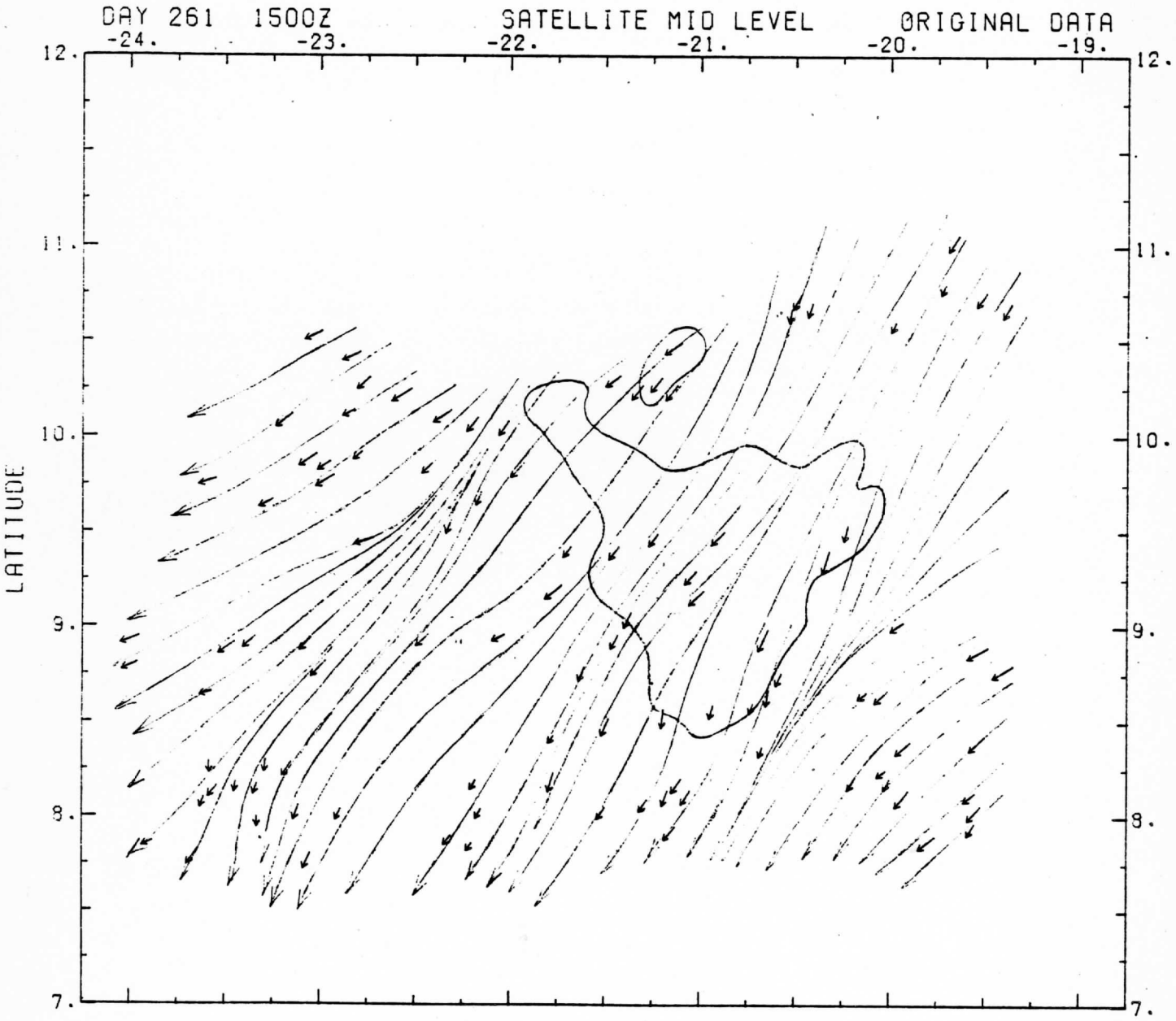

Fig. 3.D.Ib same as fig. 3.D.Ia, except middle level.

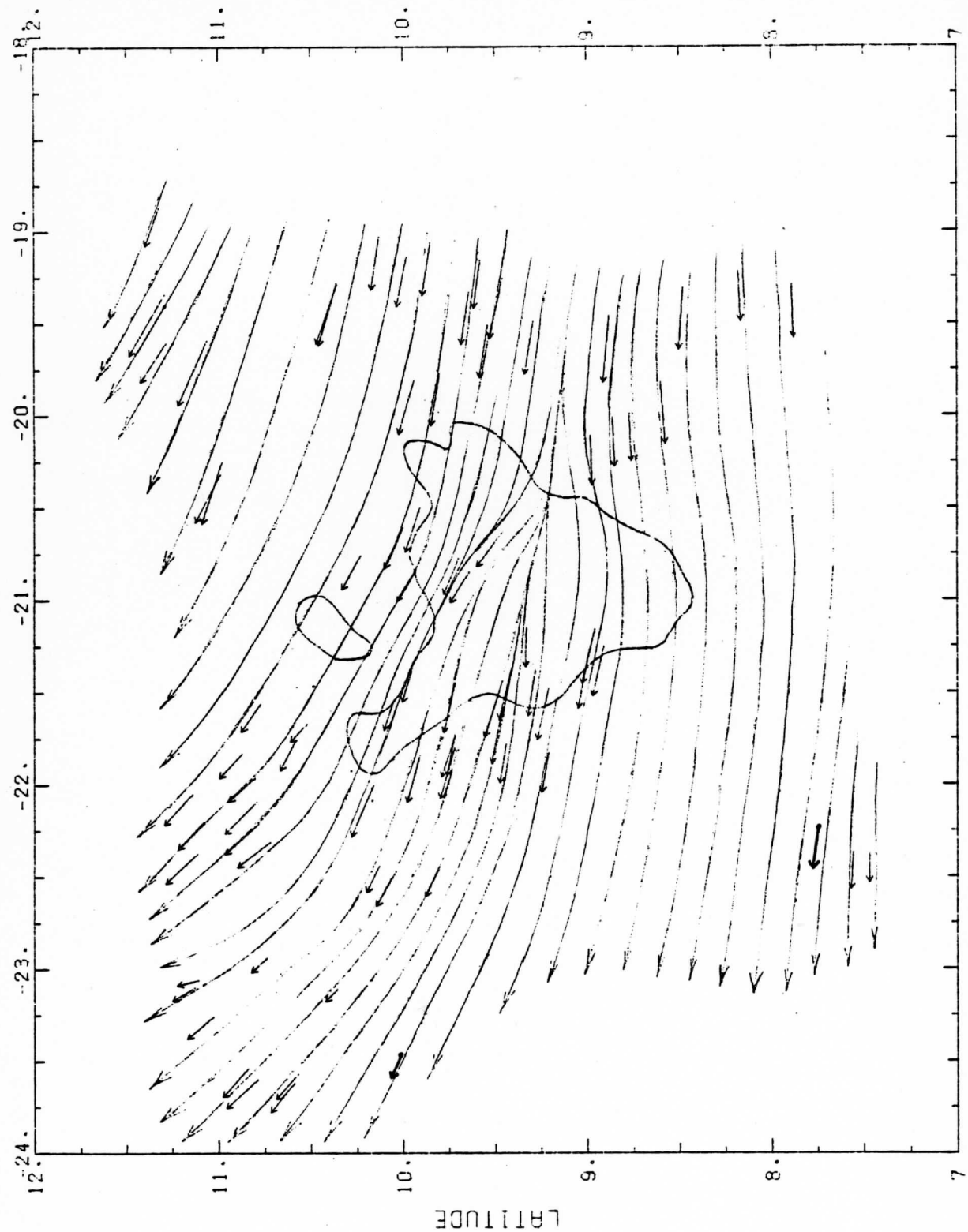

Fig. 3 D.Ic same as fig. 3.D. Ia., except high level.

multiple-layered clouds; there are often time/space differences between cloud winds and the nearest rawinds; and there are sometimes uncertainties in the tracking of clouds and whether the clouds are representative of the wind field in which they are imbedded.

The easiest comparisons for the cloud wind sets are with the 12-h filtered VLF/Omega winds. These two wind sets can be overlayed and the height and range of the various rawind cloud fields can be viewed. This is also an appropriate time to check mid-tropospheric cloud winds against radiosonde and rawind moisture profiles, if this has not been previously done on McIDAS. Cloud winds should occur in moist layers, and the moist layer wind speed and direction should match cloud wind speed and direction. If there is no match, the quality of the rawind, the radiosonde, and the satellite wind should be evaluated, and the suspect measurement eliminated.

Some other possible solutions to be above problems include: 1) instead of tracking every suitable cloud, avoid redendancy by tracking according to a grid (real or imagined) across the image; 2) apply suitable averaging to ship and aircraft winds; ship winds may easily be averaged vertically and in time; 3) when in the single pixel metric, track each cloud individually; if displacements are small, enlarge the image sequence.

In general, there are three main rules for cloud tracking:

1) For cloud heights, make spot measurements of heights where individual clouds of each field are likely to give the best results. These are in regions of high emissivity, with no clouds above or below, and the clouds are large compared with data resolution. Compare height with ambient moisture soundings.

2) Keep each level of cloud winds separate.

3) By comparing with measured radiosonde wind soundings, find the level of best fit.

The problem still arises when satellite and conventional winds still disagree. Often, the scientist uses his own judgment by choosing to retain the wind which is more consistent with the wind field in general, or with the evolution of the cloud system.

3.D.1 Dynamic Vector Analysis

One of the major problems of satellite- derived cloud drift wind analysis is assigning the proper level for a cloud tracer. This is especially true for mid-level clouds and multiple levels of clouds. This also true for cumuloform clouds where the steering level is not necessarily the cloud top and in regions of minimum shear. [See Sections 2 and 3 and Suchman and Martin(1976) for further discussion.]

The dynamic vector interactive analysis program was developed as an aid in assigning the proper level to satellite- derived cloud winds. Using this program, the scientist can compare a cloud drift vector's speed and direction interactively with different rawinsonde wind levels to find the level of best fit.

A specified satellite cloud drift wind vector is plotted on the graphics display. From computer files, the scientist selects a sounding which is close both temporally and spatially to the wind vector. A pressure scale (in millibars) is located on the left-hand side of the

screen. The cursor is moved vertically along this pressure scale and the rawinsonde wind is plotted for that pressure level similar to a wind flag (see Fig. 3.D.2).

Visual comparison can be accomplished rapidly by the superposition of the rawin-wind vectors with the cloud drift vector in the center portion of the screen. As the cursor is moved vertically, the previous wind is erased and the new wind is drawn. In the upper right-hand portion to the screen, the pressure (mb) and wind direction and speed (DDDFF) in degrees and knots are displayed. After careful comparison, the scientist subjectively chooses the rawin level that best fits the cloud wind vector.

3.E Combining Cloud, Ship and Aircraft Winds

One of the major goals of this project was to find ways of efficiently assembling the most complete data sets possible, including one wind set containing winds from satellite cloud motion vectors, rawinds, aircraft winds, etc. The major problems are the potential incompatibility in time or space of the various winds (i.e., satellite winds are often 30 min averages, while those from aircraft may be 2 min averages), and the uncertainty of the height of the cloud tracer winds. The following is the procedure for obtaining a <u>complete</u> wind set:

1) First, examine the ship and aircraft data alone to determine how reliable and internally consistent they are. It is assumed that this has already been done with the satellite winds.

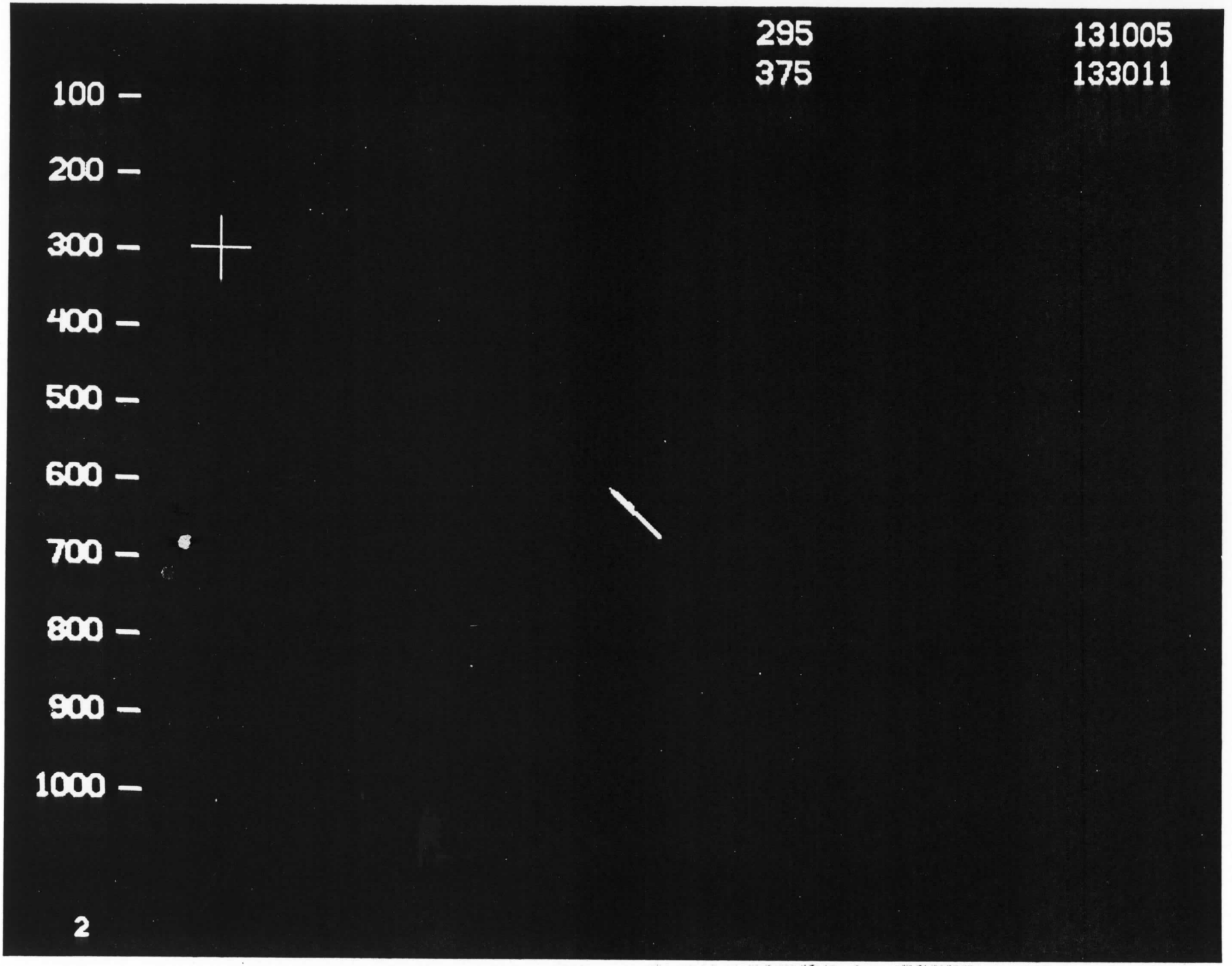

Fig. 3.D.2 Dynamic vector graphic at 1315 G.M.T. 18 September, 1974. Quadra raob used for comparison to cloud drift wind vector. A cloud height of ~375 mb was obtained from the IR data.

2) If the time difference between the ship and the satellite data is significant, then determine how much the situation has changed during this time interval (e.g., has a front moved through, are the systems moving quickly, etc.). If changes are large, decide whether rawinds can be used to only give a general idea of speed and direction or whether they can be used more quantitatively.

3) If spatial differences are large between the location of the satellite tracers and the rawinds, determine how far away the satellite wind and rawind can be compared without causing additional errors. This will depend on the meteorological situation and on the possibilities of reliable interpolation.

4) Assess the reliability of the satellite vectors. Some tracers are unmistakable, while others may be either ambiguous or misleading. Likewise, assess the reliability of winds from other platforms; e.g., what are their limits of reliability? A check for internal consistency within each type of wind set is a good place to start. A good assessment of the reliability of each wind is the basis for a good total wind set.

5) It should be noted that editing and combining is an iterative process. One goes back and forth between the various wind sets trying to resolve differences. The scientist often must resort to educated judgment for the final decision. Once these winds are selected, then

6) Replot edited satellite wind set in combination with ship and/or aircraft winds and re-edit.

7) Perform a preliminary u + v and streamline-isotach analysis and hand correct this.

8) In areas where hand corrections have been made, determine new u's and v's and add to grid point u's and v's calculated in step 3).

9) Use the revised u's and v's to replot a new streamline-isotach analysis and calculate divergences and vorticities.

Final wind sets are shown in Figs. 3.E.1a-c.

3.F Objective Analysis of Cloud Wind Fields Including Moisture Field Analysis

3.F.1 Introduction

One of the major thrusts of GATE has been quantitative use of SMS (Synchronous Meteorological Satellite) data. Subsequent efforts have focussed on improving these developments, including the addition of information from other measurement platforms. In these regards, previously developed objective analysis techniques for cloud wind fields have been examined, compared, and combined to produce a hybrid analysis scheme.

3.F.2 Background

In order to analyze the composite wind sets of GATE, the capabilities and flexibility of the objective analysis scheme had to be expanded. There

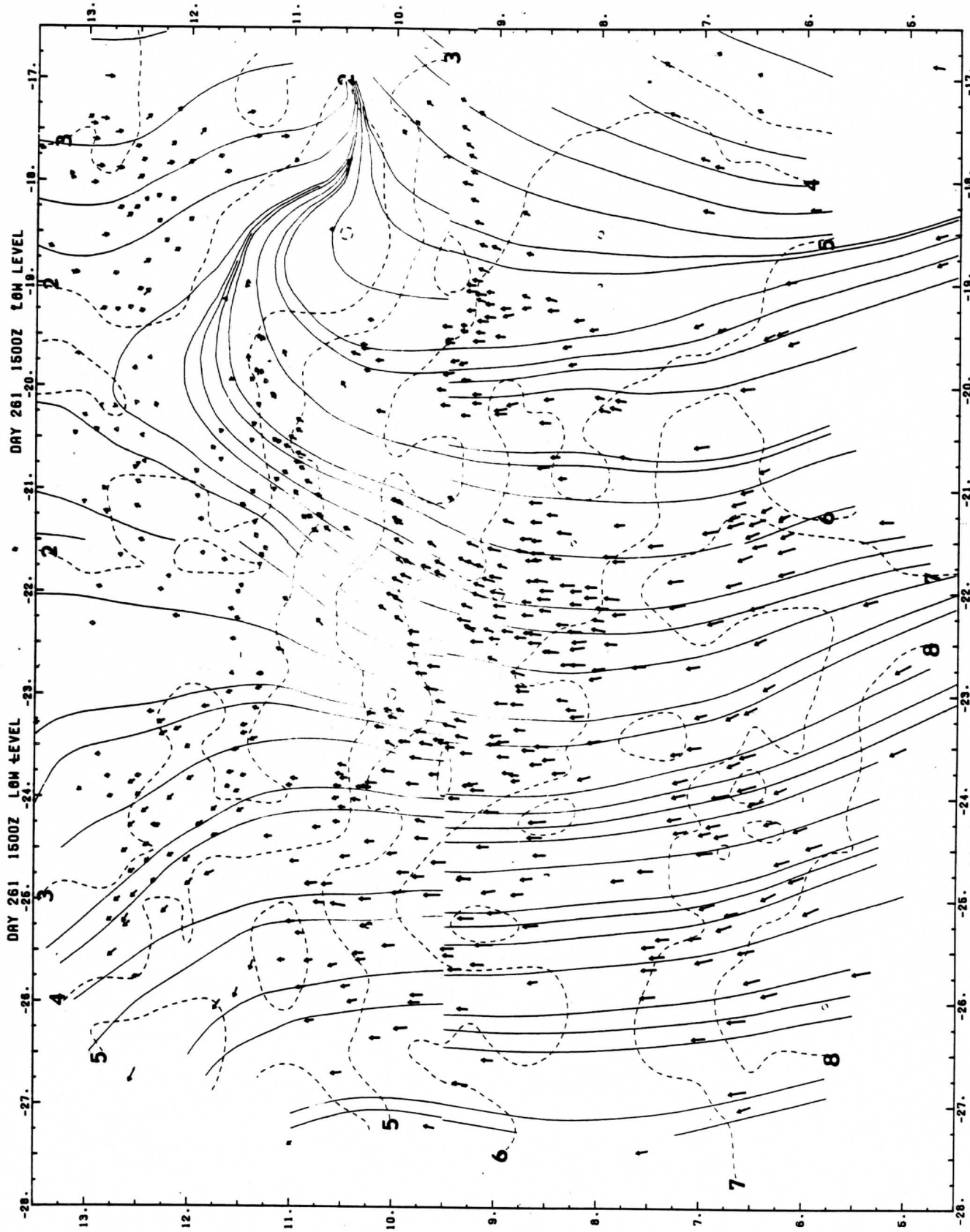

Fig. 3.E.Ia "Final" streamlines and isotachs, 18 September 1974, 1500 GMT, low level.

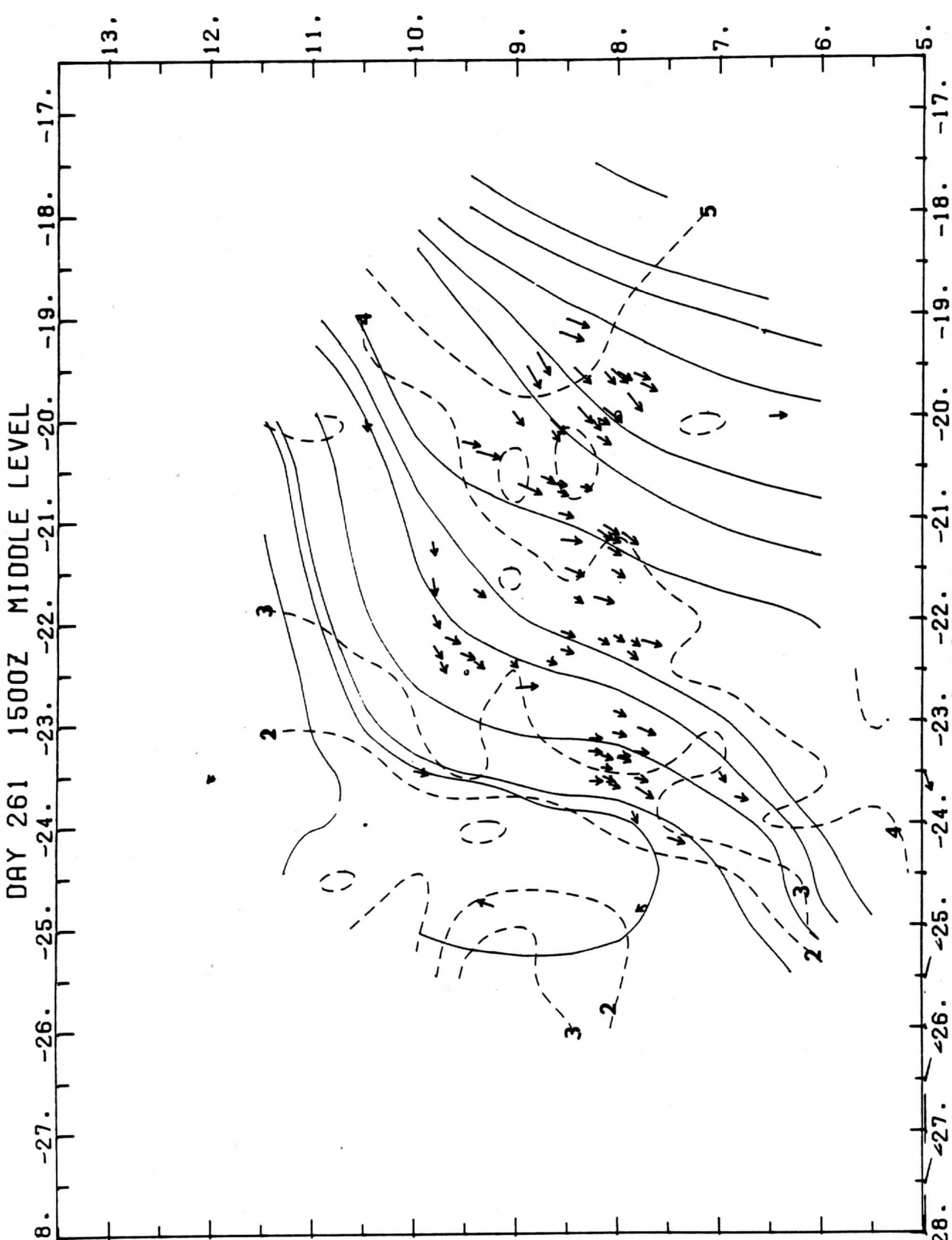

Fig. 3.E.1b same as fig. 3.E.1a, except mid level.

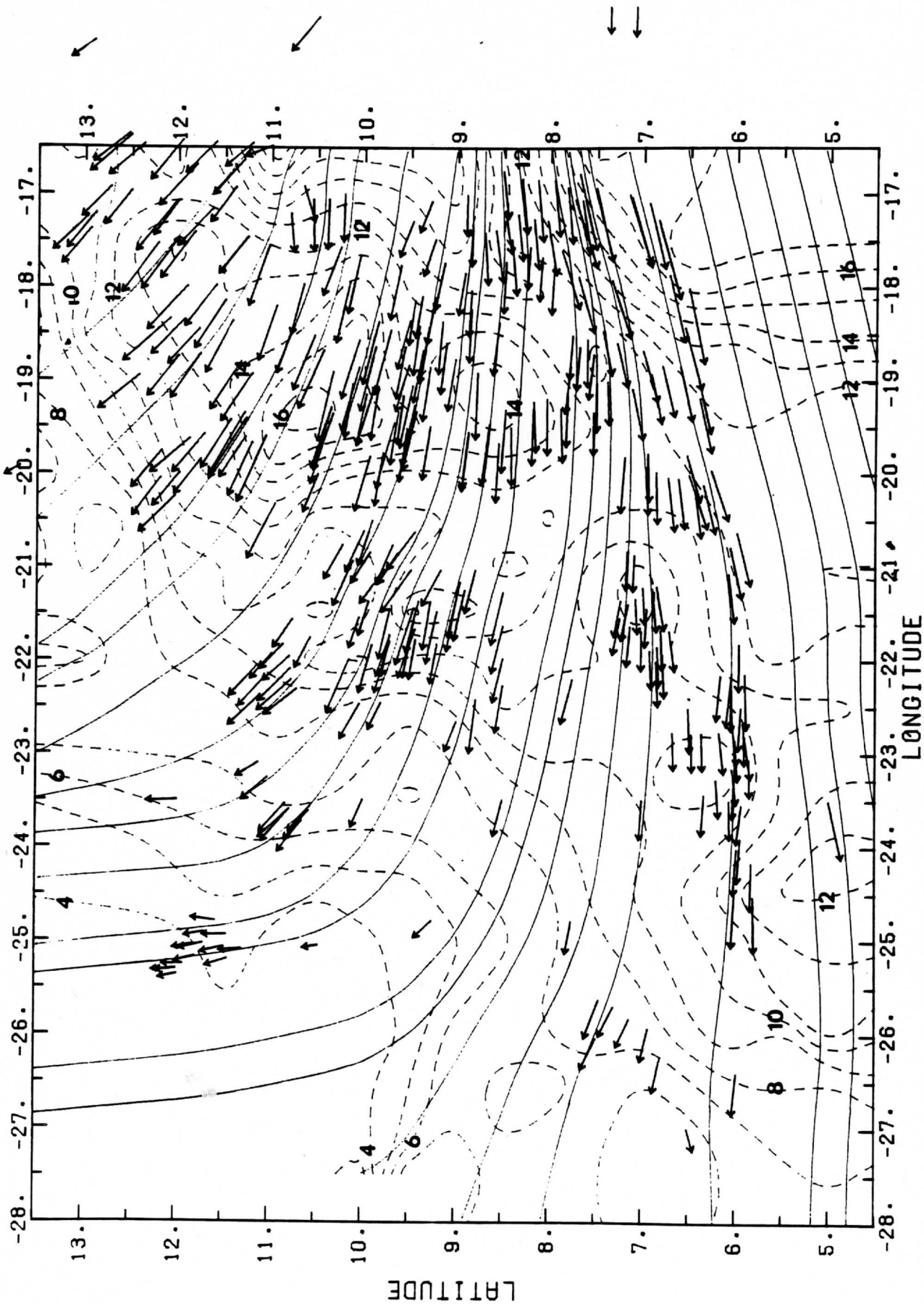

Fig. 3.E.1c same as fig. 3.E.1a, except high level.

were three objectives. First, the scheme needed the capability to utilize wind data from a number of sources (e.g., cloud tracer, rawinsonde, aircraft) to produce reasonable gridpoint analyses of u, v, divergence and vorticity. Next, the scheme needed the flexibility to be simple to use and manipulate (in terms of the parameters needing adjustment) for different scales and locations; third, it needed to be computationally economical. To meet these objectives, two main analysis schemes were examined and compared.

a. Wind Editing and Analysis Program (WIND*SRI)

The first scheme examined was the Wind Editing and Analysis Program of the Stanford Research Institute (Mancuso and Endlich, 1973), hereafter referred to as WIND*SRI. Certain awkward constraints of WIND*SRI became evident. Namely, the search radius of the grid and the number of winds per grid point need to be set for each analysis. Weighting of the data is also set according to the inverse square of the distance of the data observation from the grid point. For a rather uniform field of data, these set parameters perform quite adequately. However, for a non-uniform field or areas where there is an absence of data, the quality of the analysis varies depending upon data density, distribution, and the proper manipulation of the search radius and number of winds per grid point.

b. The Barnes Scheme

The Barnes scheme (Barnes, 1973) was then examined and compared with WIND*SRI. As with WIND*SRI, the Barnes scheme incorporates space weighting of simultaneous observations to obtain interpolated grid values on a square mesh (WIND*SRI uses a spherical grid). In addition, an arbitrary weight function parameter (scale factor) is used in conjunction with a low-pass filter to fit the data density and scale of the analysis. The data is weighted by the exponential of the distance to the grid point divided by the weight function parameter. In this way, the arbitrary parameter wavelength dependent) allows for greater flexibility in fitting the analysis to the data.

After extensive comparisons between the two schemes under varying conditions, the Barnes scheme proved to be superior to WIND*SRI in a number of respects. These were:

i) the presence of a low pass filter in the Barnes scheme which could easily be adjusted to preserve more or less small scale detail depending on the nature of the data and the purpose of the analysis,

ii) the ability to interpolate easily into data poor areas, thus connecting together regions of higher data density for a more thorough analysis (in

WIND*SRI there is no analysis in data blank areas).

iii) slightly cheaper computing costs.

c. Hybrid Analysis Scheme

The ability of the Barnes scheme to interpolate or extrapolate into data poor areas has one serious disadvantage: particularly on the edges of the analysis region, there is often no data on which to base the extrapolation. Rather than fill in such areas with a completely hypothetical analysis, it often would be better to leave them out of the analysis altogether. To accomplish this, a hybrid analysis scheme combining some of the features of WIND*SRI with the Barnes scheme is used to confine the analysis to areas with or adjacent to data. The rectangular analysis area containing the data is divided into boxes with dimensions equal to the x and y grid spacing. If wind vectors are found in a box, they are averaged as in WIND*SRI (weighted approximately by the inverse square of their distance from the center of the box) and this grid value stored for later analysis using the Barnes scheme. If no winds are found in a box, it is flagged for possible later deletion from the analysis. During the Barnes analysis, all flagged boxes are examined. If boxes on all sides and diagonally are also flagged, the newly calculated Barnes grid value is replaced by a zero.

Using the initial input of mesoscale to synoptic scale cloud tracer winds (it is also possible to include aircraft and sounding

winds), the final analysis package was modified to allow plotting of the original data, gridpoint winds, and streamlines and isotachs alone or in combination (Fig. 3.F.1). U and v components, divergence and vorticity are also calculated and can be saved on file for other applications.

3.F.3 An Application of the Scheme to Predict Clouds and Precipitation

One useful application is the incorporation of moisture information along with the derived windfield to predict locations favorable clouds and precipitation (Negri and Vonder Haar, 1980). Using a simple two-layer model, one first produces a low level (950 mb) u and v analysis (gridpoint field using Barnes scheme). From this u and v analysis, a grid field of divergence is calculated. These values, when combined with gridpoint fields of mixing ratio (obtained from soundings) are processed at two levels (e.g., 950 and 850 mb). The following equations are solved, both representing the equation of moisture in two different forms:

$$\frac{\partial q}{\partial t} + u\frac{\partial q}{\partial x} + v\frac{\partial q}{\partial y} + w\frac{\partial q}{\partial p} = 0$$

$$\frac{\partial q}{\partial t} + \frac{\partial (uq)}{\partial x} + \frac{\partial (vq)}{\partial y} + \frac{\partial (wq)}{\partial p} = 0$$

The second, third and fourth terms of each equation are computed and summed. The fourth term is solved by taking the differences in

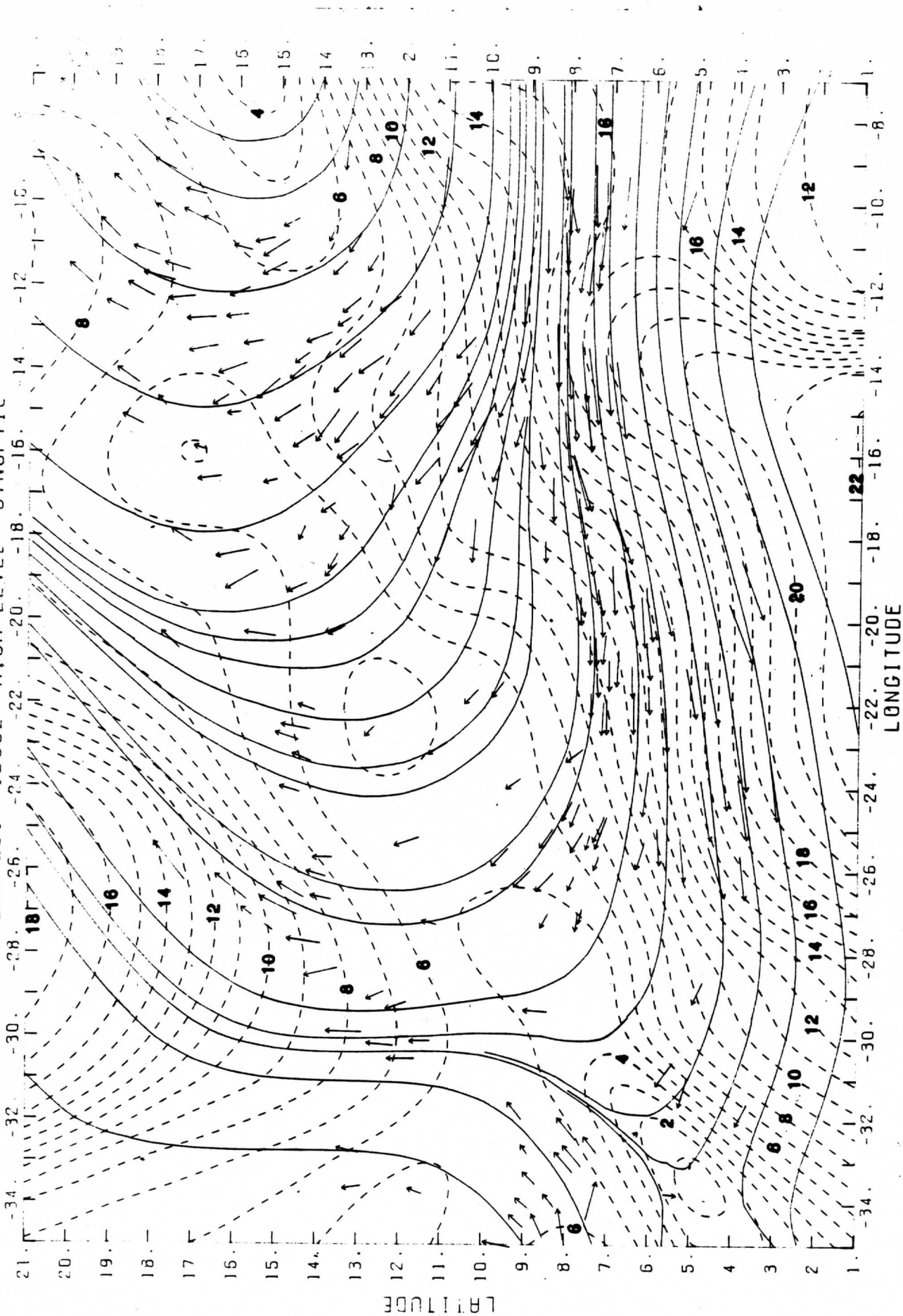

Fig. 3.F.1 Streamlines (solid) and isotachs (dashed) in m/sec over GATE area at 1200 G.M.T. 18 September, 1974.

mixing ratio between the two layers and computing w from the equation:

$$-\text{Div} = \frac{\partial w}{\partial p} \text{ where } w = 0 \text{ at the surface.}$$

The values of each term and their total (q/ t)are printed out at each grid point.

References

Barnes, Stanley L., Mesoscale objective map analysis using weighted time series observations, NOAA Technical Memorandum SRL-NSSL-62, 60 pp.

Hasler, A. F. 1981: Sterographic observations from geosynchronous satellites: An important new tool for the atmospheric sciences. Bull. Amer. Meteor. Soc., 62, 194-212.

Hayden, C. M., L. Hubert, E. McClain and R. Seaman, 1979: Quantitative meteorological data from satellites. WMO Technical Note No. 166.

Johnson, G. L. and D. Suchman, 1980: Intercomparisons of SMS wind sets: A study using rapid-scan imagery. Mon. Wea. Rev., 108, 1672-1688.

Mancuso, R. L. and R. M. Endlich, Wind editing and analysis program--spherical grid. Users Manual., Stanford Research Institute, Feb., 1973, 51 pp.

Negri, A. J. and T. Vonder Haar, 1980: Moisture convergence using satellite-derived wind fields: A severe local storm case study. Mon. Wea. Rev., 108, 1170-1182.

Suchman, D. and D. Martin, 1976: Wind sets from SMS images: an assessment of quality for GATE. J. Appl. Meteor., 15, 1265-1278.

Wilson, T. A. and D. D. Houghton, 1979: Mesoscale wind fields for a Severe storm situation determined from SMS cloud observations. Mon. Wea. Rev., 107, 1198-1209.

4. ANALYSIS TECHNIQUES APPLIED TO SATELLITE & RADAR BRIGHTNESS DATA

4.A Introduction

The use of digital satellite information has become increasingly sophisticated in recent years. While there is much useful meteorological information to be gained by simple inspection of an image or image sequence, the trend has been to use the numerical cloud brightness as direct input into models, prediction schemes, and statistical analyses. This chapter presents three techniques that have successfully utilized visible and infrared digital satellite data, sometimes in combination with digitized radar, to describe and measure some physical attributes of individual clouds and cloud systems (Sections 4.B, 4.C, and 4.D). In addition, one section has been included (Section 4.E.) which describes a general method of generating areal measurements of clouds and statistical summaries of satellite and radar brightnesses.

4.B Illustrating Cloud Cores

Cloud cores are those portions of convectively generated cloud that have the coldest tops and the greatest thicknesses. Depending on the criteria chosen, one may delineate approximately those areas covered by significant precipitation, cumulonimbi and/or the deep central portions of large cumulonimbi.

Which of these areas is depicted depends to an extent on the thresholds chosen for the visible and the infrared images. The visible brightness is related to the thickness of a cloud, and there is a direct correspondence between infrared brightness and cloud top blackbody temperature. By selecting and displaying those areas of the satellite image which exceed both a visible and an infrared threshold, one can locate the cloud cores.

Unfortunately, there is not a known precise relationship between cloud cores and the physical features mentioned previously. There are several reasons for this ambiguity. In the range of large cloud thicknesses, the visible brightness changes relatively little for added increments of thickness (Kondrat'yev et al., 1964); other extraneous factors such as cloud geometry and water droplet size distribution can affect the visible brightness in complicated ways, thus obscuring actual thickness changes. Second, the infrared channel is at best capable of resolving areas no smaller than 4 km on a side. This averaging considerably reduces the amount of detail that can be brought out in a cloud core display. Finally, the relationships between satellite brightness and features such as updrafts, rainfall, and active convection are only roughly understood.

4.B.1 Digital Stretching

Despite these problems, it is still possible to obtain useful information out of a visible and/or infrared image. There are two methods of doing so. One of these, digital stretching, uses the visible channel only and is primarily of qualitative use. This

method relies on the fact that the visible channel contains most of the useful information relating to cloud cores. Because the visible data has a higher resolution and because thickness has a clearer relationship to convective variables than does cloud-top temperature, one can essentially enhance the contrast in regions of highest visible brightness to bring out features of the deepest convection. One first examines an area of interest (usually including extensive cumulonimbus anvils) to determine the range of visible brightness for the convective areas. One then uses a computer routine to proportionally stretch this limited brightness interval over a much larger interval and display the recalculated digital data. An example of such an effort is shown in Figures 4.B.1 and 4.B.2. The first figure, representing Day 261, 1300 GMT, is the original visible image of a growing cloud cluster in the GATE area. It is difficult to differentiate the deeper cloud from low-level cumulus and thin cirrus. The second figure shows the effect of the digital stretching. Various regions of deeper cloud can now be easily located, giving valuable information about the structure of the cluster.

4.B.2 Visible and Infrared Thresholding

A more quantitative method using both visible and infrared data involves first selecting appropriate thresholds in each channel. Some work has been done in relating such thresholds to precipitation (see the following section). Using this research as a guide suggests that a useful infrared boundary lies around 160 digital counts (d.c.), or a

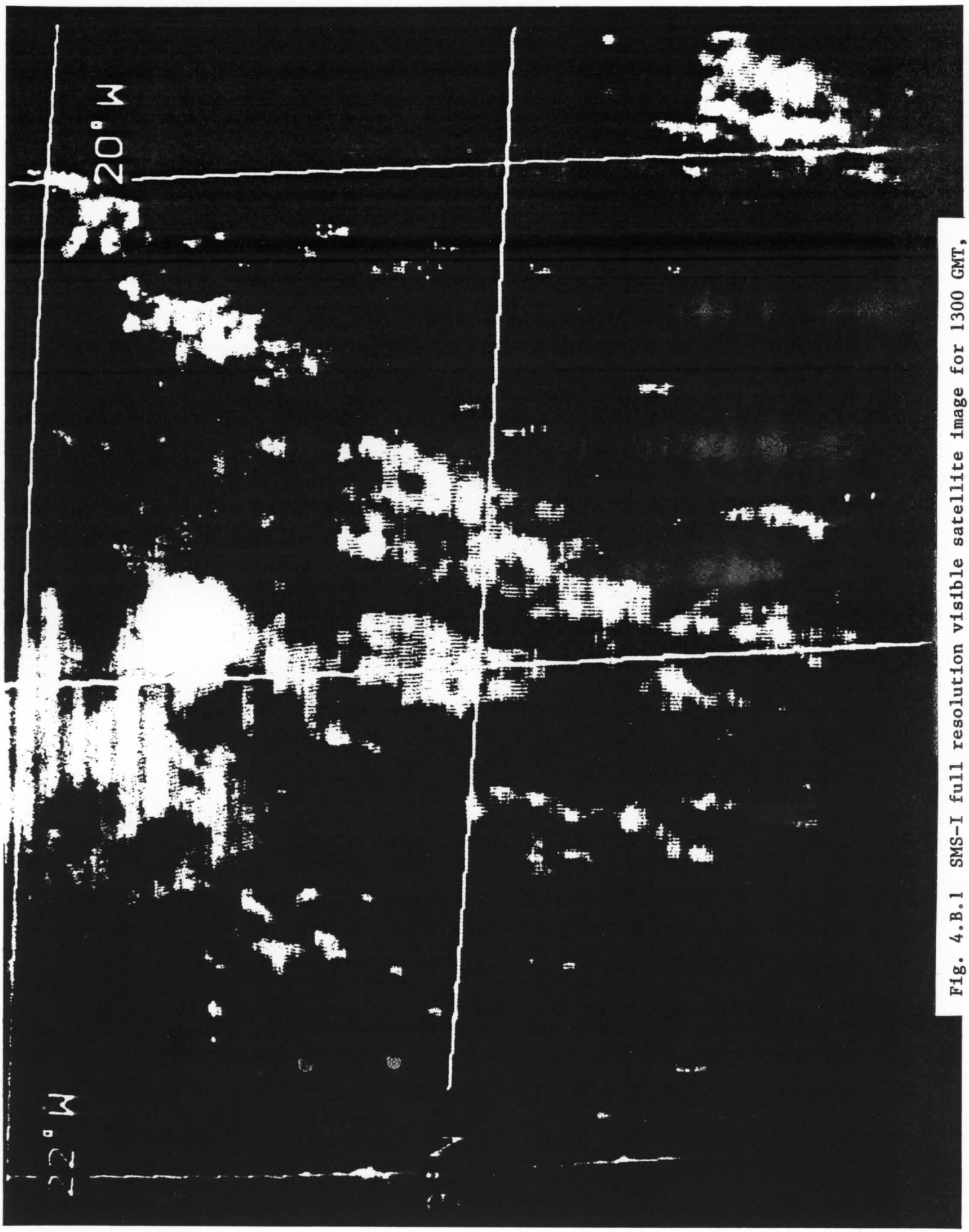

Fig. 4.B.1 SMS-I full resolution visible satellite image for 1300 GMT, September 18, 1974.

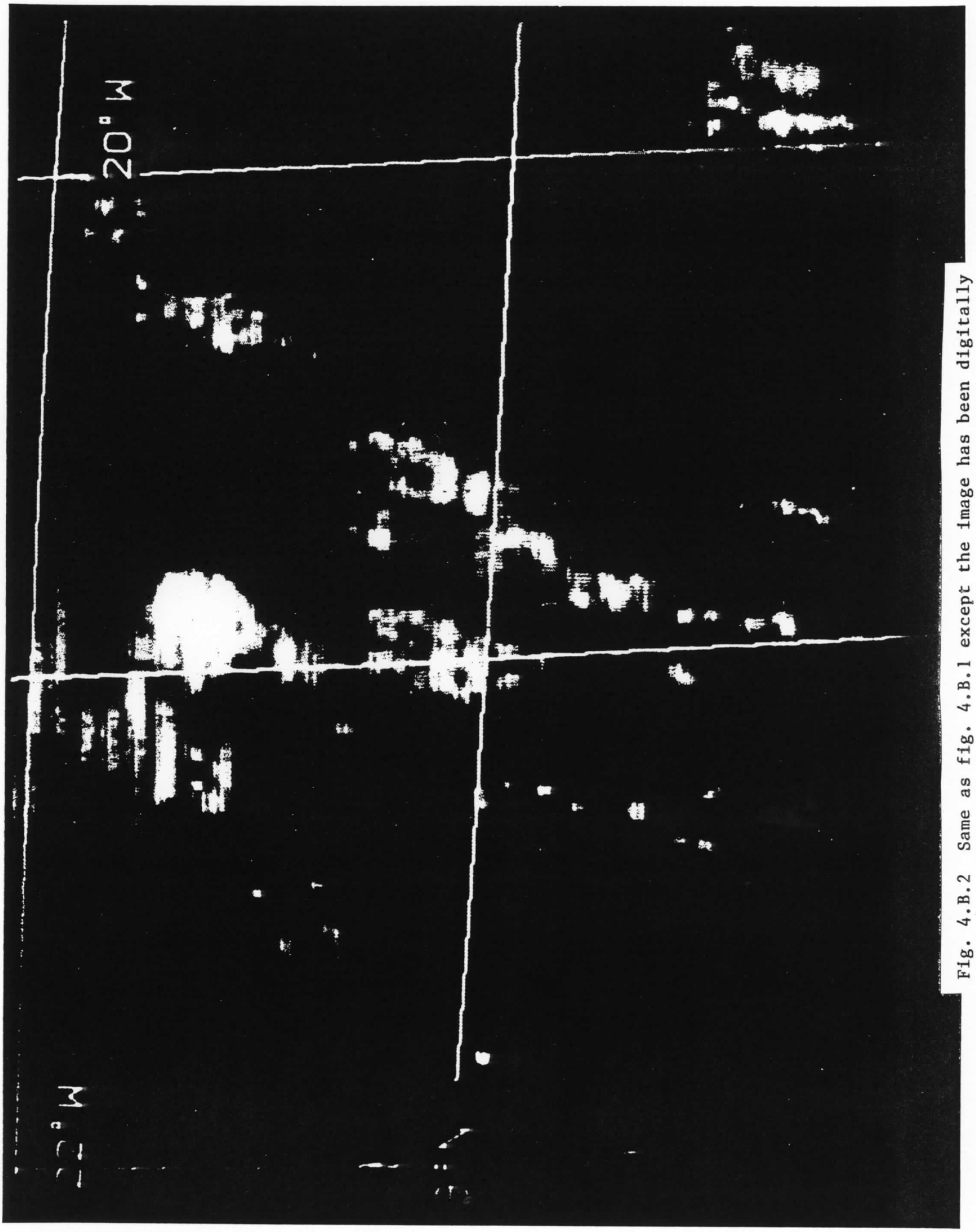

Fig. 4.B.2 Same as fig. 4.B.1 except the image has been digitally stretched.

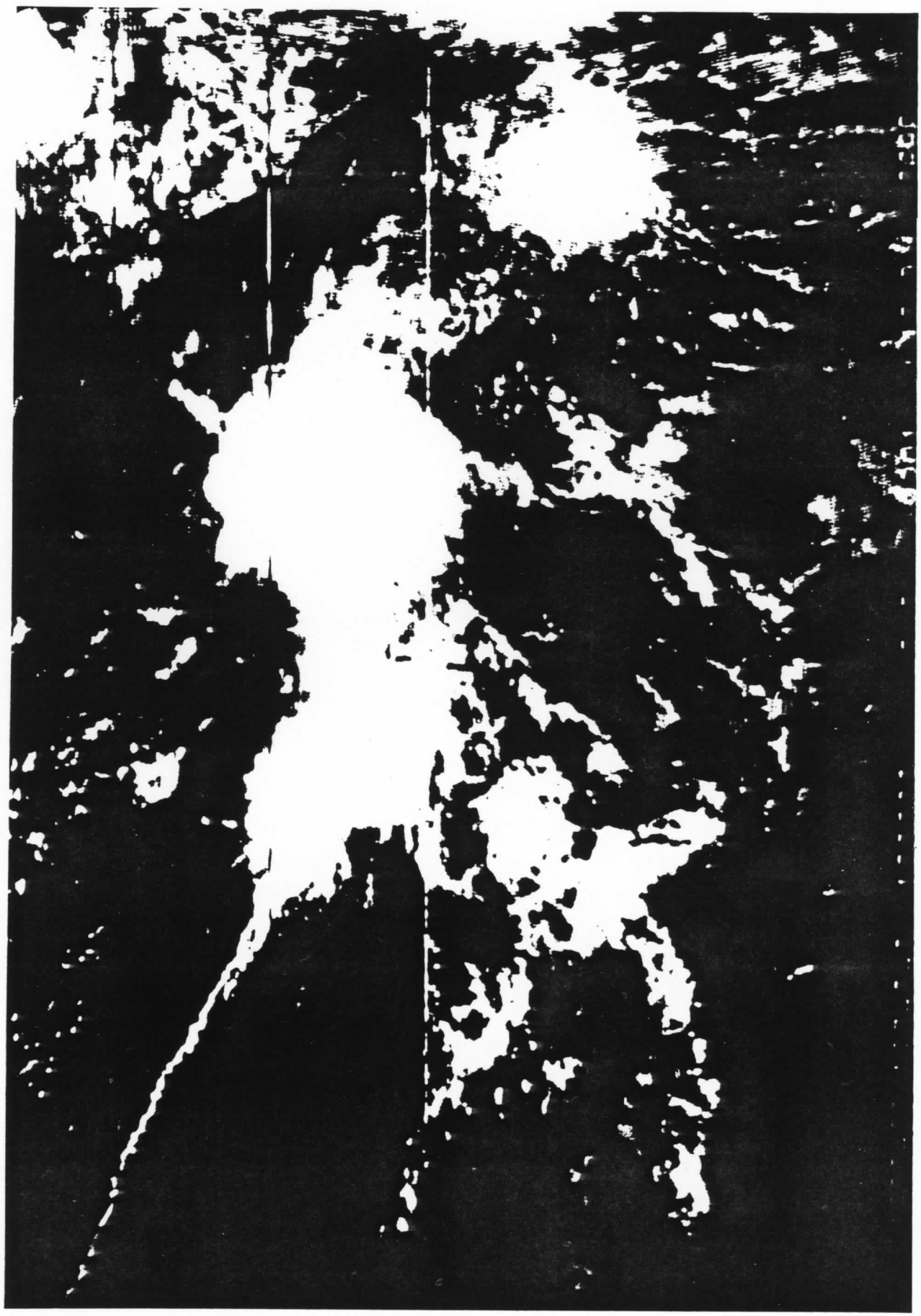

Fig. 4.B.3 SMS-I 4 km visible satellite image for 1330 GMT, September 5, 1974.

Fig. 4.B.4 Same as fig. 4.B.3 but for infrared.

Fig. 4.B.5 Cloud cores using thresholds of 220 d.c. in the visible and 160 d.c. in the infrared.

blackbody temperature of 247°K, a value which separates cirrus from non-cirrus clouds.

The visible threshold is more problematic. Digital count 120 (equivalent to an albedo of about 0.23) eliminates shallow clouds and some cumulus congestus; 180 d.c. is a useful boundary to separate the deeper cumulonimbi clusters (albedo of approximately 0.51). Whatever the final choice, the two thresholds are applied to the data in such a way that areas exceeding both the visible and infrared thresholds are coded with one color or number (e.g., white, d.c. 255) while areas falling below either threshold are colored/numbered black (d.c. 0).

An example of this technique is shown in Figures 4.B.3, 4.B.4, and 4.B.5. Figures 4.B.3 and 4.B.4 show the original visible and infrared images for Day 248, 1330 GMT. These pictures feature a double cloud cluster in the middle with small centers of activity to the southwest and southeast. Also, over Africa in the northeast corner, a squall line arc cloud is visible.

In Figure 4.B.5, using thresholds of 225 in the visible and 160 in the infrared, some well defined cloud cores in the centers of the convective activity are evident. Such displays can be used to determine cloud structure and evolution (if a time series is available) and to relate this structure to other parameters (e.g., vertical velocities, divergence). It is also possible to calculate the cloud core areas either as a measure of precipitation coverage (if the proper thresholds have been chosen) or as an index of convective activity. Changes in area over time can also help monitor fluctuations in cumulonimbi growth. Finally, sequences of core

locations have been used to give better estimates of storm motion than would have been available from unchanged satellite images (Sikdar and Hentz, 1980).

Hopefully, these applications can be expanded in the future through studies of the relationships between satellite brightness and storm variables such as updraft intensity, heavy precipitation, and cumulonimbus growth.

4.B.3 Remapping and Display of Radar in a Satellite Projection

Satellite images are often more useful when they can be directly compared with other forms of data. In particular, overlays that show various conventional variables superimposed on visible or infrared cloud patterns have proven popular. Pictorially this technique allows immediate cross-reference to satellite and conventionally observed features. There is also the possibility of quantitatively correlating the two data sources if both the satellite and conventional data exist in a digital format.

Digital radar has proved to be one of the most commonly used data sources in conjunction with the satellite. The relationship between precipitation, satellite cloud brightness, growth and other cloud characteristics has been studied intensively (e.g., Stout et al. 1979; Griffith et al., 1978; Lovejoy, 1978; see Section 4.C for more details). These techniques rely extensively on digital radar for verification.

Generally, transposition of radar echoes on satellite imagery gives the viewer an idea of where the most active areas of convection

lie (see Section 4.B), whether cumulonimbi hidden under extensive anvils are in growth or decay, and how mesoscale phenomena observed by radar (e.g., hook echoes, echo merging or separation) relate to the clouds themselves.

Remapping of radar images into satellite coordinates is relatively simple using a computer, but depending on the amount of data being processed can be expensive. This processing cost can be controlled, however, if one is willing to either lower the resolution through data averaging or limit the area of remapping. The satellite image itself must first be adequately navigated (Young, 1976). This means that there is a known correspondence between every line and element of the satellite image and a latitude and longitude. With a digital PPI or CAPPI display in which the earth coordinates are also known for every point, it is a simple matter for the computer to calculate a correspondence between the radar and satellite and to remap these radar points into the satellite line and element system. Correlation between the two data sets can then be easily displayed pictorially or processed digitally (see Section 4.E, Area Statistics--Two or Three Channel Histograms). Figure 4.B.6 is an example of such a remap for the GATE area, 1300 GMT 18 September 1974. The white areas are 4 km radar data from the Quadra centered at 9°N, 22°W, transposed on the darker visible SMS-I 1 km satellite data.

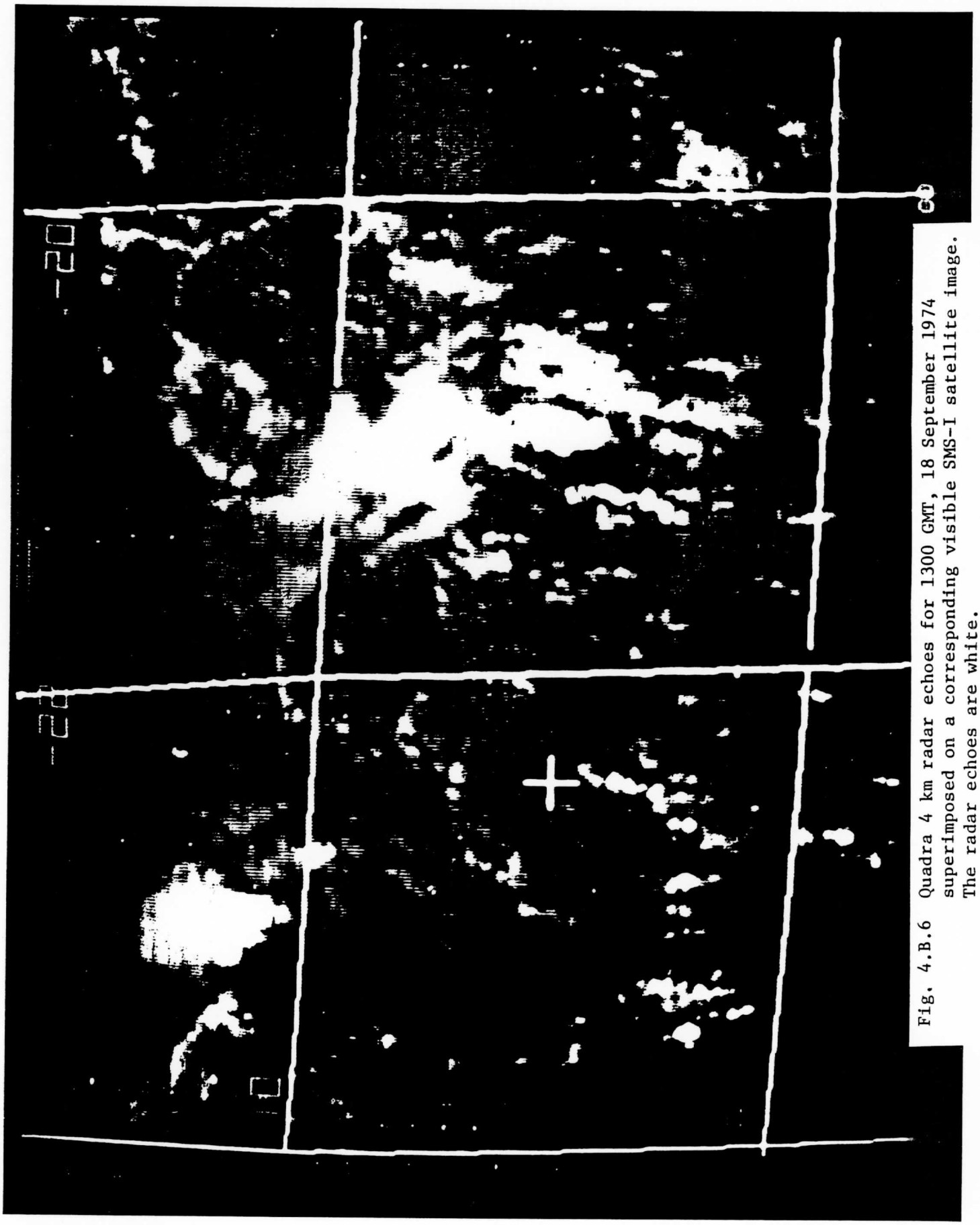

Fig. 4.B.6 Quadra 4 km radar echoes for 1300 GMT, 18 September 1974 superimposed on a corresponding visible SMS-I satellite image. The radar echoes are white.

4.C Using Satellite Data for Depiction of Rainfall Coverage

Satellite images, both visible and infrared, have been used by many researchers as a tool in rainfall depiction and measurement. Their exact usage has varied widely, ranging from qualitative use of the image (Scofield and Oliver, 1977) to predominately quantitative use based on anvil expansion and cloud brightness (Stout et al., 1979). These techniques have been extensively reviewed in Barrett and Martin (1981).

Our major concern here is rainfall depiction methods relying primarily on the visible and infrared brightness. These methods do not attempt to measure the rainfall, but simply predict rain/no rain. Two methods are compared here, a single visible threshold method (Lovejoy and Austin, 1978) and another featuring a dual visible threshold recently developed from our own experimentation.

Both methods rely on the fact that the visible satellite brightness locates areas of deep convection where most precipitation falls. In the tropics these areas may be either cumulus congestus or thicker cumulonimbi with cirrus tops. The dual threshold method, however, recognizes that the critical threshold in a visible image at which rain appears is lower for cumulus congestus than for clusters of cumulonimbi; this result may be the effect of decaying cells which have ceased producing significant rainfall but which still have a fairly high thickness. The infrared brightnesses are useful primarily because they identify cold clouds including cumulonimbi cirrus.

Combined, the two satellite sources allow the cloud classifications, shown schematically using typical brightness thresholds in Chart 4.C.

4.C.1 Single Threshold Method

Applying the single visible threshold method to a set of data is straightforward. The method is essentially the same as that presented in Section 4.B for finding cloud cores. Choosing a good visible threshold, however, is difficult because one tends to either miss varying amounts of Type II rain or include too many Type III clouds. The best solution is to calibrate the thresholds by using a radar scan to make the initial choice.

4.C.2 Dual Threshold Method

For the dual threshold method, one first selects an infrared threshold which distinguishes between cirrus and non-cirrus cloud. This value is usually near 160 digital counts (d.c.) (247°K). The visible threshold which best distinguishes well developed cumulonimbi from cumulus congestus and small isolated cumulonimbi is then found. This value lies in the vicinity of 180 d.c (albedo approximately 0.51). Finally, one finds the visible threshold which can separate vertically developed clouds from low, middle, and high thin layer clouds. Here the digital count will range from around 110 (albedo approximately 0.19) for small, scattered areas of convection in their initial stages of growth to 150 (albedo approximately 0.35) for

Chart 4.C: Typing Scheme
for clouds using a dual visible threshold.

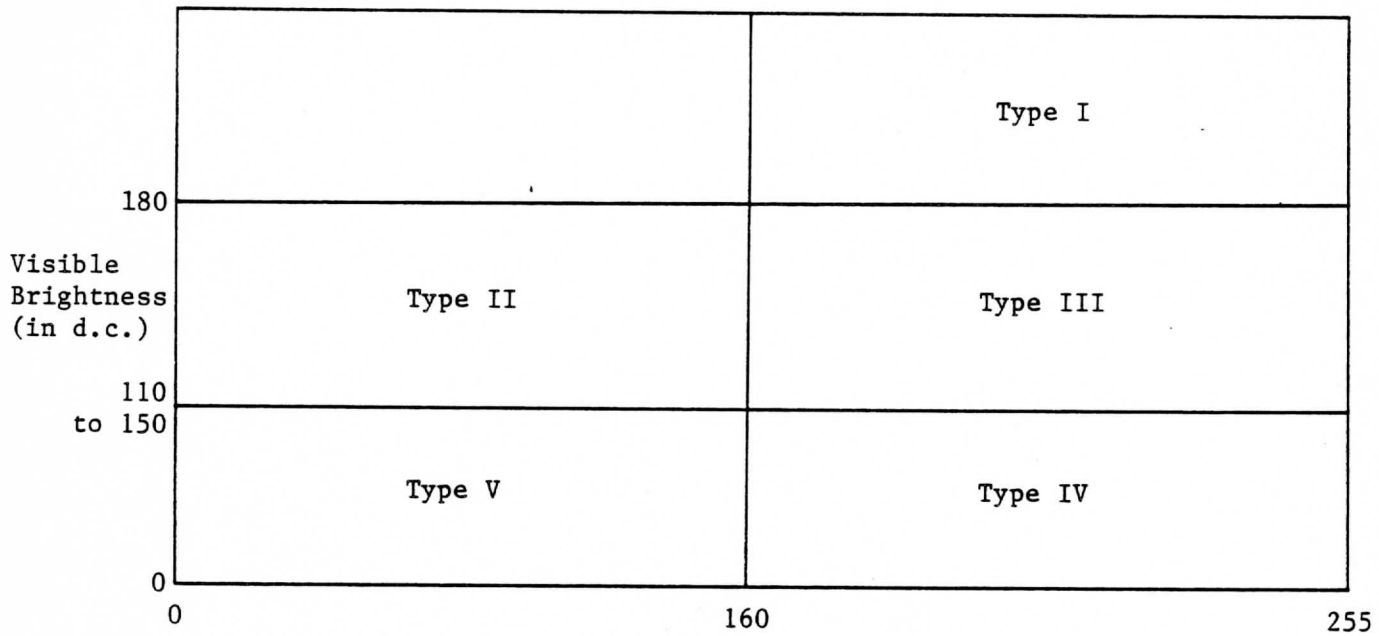

Type I -- Very thick clouds with cirrus
= high visible and IR
= rain

Type II -- Moderately thick clouds, no cirrus
= medium visible, low IR
= rain

Type III -- Moderately thick clouds with cirrus
= medium visible, high IR
= no rain

Type IV -- Thin clouds with cirrus
= low visible, high IR
= no rain

Type V -- Thin clouds, no cirrus
= low visible and IR
= no rain.

convection. Points in the area of interest are then classified according to the typing scheme above using these thresholds to indicate the bounds between the high and low infrared and the low, medium, and high visible brightnesses.

4.C.3 Examples of the Two Methods

To provide examples of the results from these two methods, data was used from six GATE days with at least three visible, infrared, and radar images each. The data were averaged over 40 km squares to simplify comparisons. The radar data came from either the Quadra or the Oceanographer. For a given square to be considered raining, the averaged reflectivity had to equal or exceed the minimum dBZ value used by that radar. Tables 4.C.1, 4.C.2, and 4.C 3 show the error statistics for each of the days and individual times. All error statistics are defined in Table 4.C.3. Tables 4.C 1 and 4.C.2 show the variation of the weighted error and the percent error for each day and time compared with different thresholds. Only the thresholds with the lowest errors are shown. Many others were tried in addition to these in even multiples of ten. Table 4.C.3 shows the grand optimal threshold results. The grand optimal threshold was selected by choosing the threshold which gave the smallest weighted error for all days and times.

In general, the weighted error stresses accurate determination of rain areas at the expense of overestimating the total areal coverage. This error is more stable over small time periods (compare Tables 4.C.1 and 4.C.2) and over small precipitation areas (as in Days 261 and 242)

Table 4.C.1. Comparison of weighted error* versus threshold.
Underlined values are those that are lowest for that time period.

		Dual Visible Threshold					Single Visible Threshold					
	IR=	160	160	160	160	160	70	70	70	70	90	100
	VIS=	110/180	120/180	130/180	140/180	150/180	110	120	130	140	150	160
Day	Time											
242	1400	.206	.317	.619	.683	.667	.190	.302	.603	.667	.667	1.00
	1430	.177	.229	.465	.400	.600	.177	.229	.465	.432	.500	.700
	1500	.294	.465	.432	.432	.500	.294	.465	.432	.400	.600	1.00
	Aver	.226	.337	.505	.505	.589	.220	.332	.500	.500	.589	.900
245	1130	.458	.521	.521	.625	.604	.396	.458	.458	.563	.563	.646
	1200	.399	.358	.380	.444	.488	.459	.418	.378	.400	.485	.592
	1215	.391	.427	.356	.377	.519	.450	.486	.416	.391	.493	.529
	Aver	.416	.435	.419	.482	.537	.435	.454	.417	.451	.514	.589
247	1300	.556	.556.	.406	.411	.344	.678	.678	.528	.428	.417	.500
	1330	.663	.505	.505	.497	.457	.875	.665	.585	.537	.497	.554
	1400	.520	.520	.520	.400	.351	.680	.680	.600	.480	.391	.383
	Aver	.580	.527	.477	.436	.384	.744	.674	.571	.482	.435	.479
248	1100	.324	.243	.190	.200	.150	.393	.311	.259	.269	.203	.170
	1200	.429	.397	.337	.274	.263	.540	.469	.409	.366	.334	.351
	1300	.456	.346	.258	.190	.216	.545	.433	.323	.255	.258	.309
	1400	.481	.452	.400	.466	.417	.509	.479	.427	.494	.445	.396
	1500	.608	.520	.500	.471	.500	.627	.559	.539	.490	.500	.471
	Aver	.460	.392	.337	.320	.309	.523	.450	.391	.375	.348	.339

249	1300	.408	.329	.291	.199	.173	.500	.395	.382	.238	.212	.319
	1330	.488	.409	.357	.292	.279	.500	.421	.342	.317	.238	.293
	1400	.506	.432	.384	.335	.262	.512	.439	.390	.341	.268	.164
	Aver	.465	.390	.344	.275	.238	.504	.418	.371	.299	.239	.259
261	1315	.085	.000	.000	.125	.500	.000	.000	.000	.125	.500	.875
	1330	.136	.200	.200	.300	.600	.200	.200	.200	.300	.600	.800
	1345	.018	.200	.300	.300	.500	.200	.200	.300	.300	.500	.700
	1400	.109	.364	.455	.455	.545	.091	.273	.455	.545	.545	.818
	1415	.212	.320	.286	.286	.429	.086	.160	.143	.286	.429	.714
	Aver	.112	.577	.248	.293	.515	.115	.167	.220	.311	.515	.781
Tot. Av.		.377	.443	.388	.385	.429	.424	.416	.412	.403	.440	.558

*See Table 4.B.3 for definition of "weighted error".

Table 4.C.2. Comparison of percent error versus threshold.

		Dual Visible Threshold					Single Visible Threshold					
	IR=	160	160	160	160	160	70	70	70	70	90	100
	VIS=	110/180	120/180	130/180	140/180	150/180	110	120	130	140	150	160
Day	Time											
242	1400	18.1	11.1	12.5	9.7	8.3	16.7	9.7	11.1	8.3	8.3	12.5
	1430	15.3	12.5	11.1	5.6	8.3	15.3	12.5	11.1	5.6	8.3	13.9
	1500	18.1	11.1	8.3	8.3	6.9	18.1	11.1	8.3	8.3	6.9	9.7
	Aver	17.2	11.6	10.6	7.9	7.8	16.7	11.1	10.2	7.4	7.8	12.0
245	1130	20.8	25.0	27.8	37.5	40.3	15.3	19.4	22.2	31.9	34.7	40.3
	1200	18.3	18.3	21.1	25.4	29.6	16.9	16.9	16.9	19.7	25.4	33.8
	1215	18.3	22.5	21.1	22.5	32.4	15.5	19.7	18.3	18.3	25.4	29.6
	Aver	19.1	21.9	23.3	28.5	34.1	15.9	18.7	19.1	23.3	28.5	34.6
247	1300	21.4	21.4	16.1	17.9	17.9	25.0	25.0	19.6	16.1	19.6	25.0
	1330	30.4	23.2	23.2	23.2	21.4	37.5	30.4	26.8	25.0	23.2	26.8
	1400	22.8	22.8	22.8	17.5	15.8	29.8	29.8	26.3	21.1	17.5	17.5
	Aver	24.9	22.5	20.7	19.5	18.4	30.8	28.4	24.2	20.7	20.1	23.1
248	1100	20.0	14.7	10.5	9.5	6.3	25.3	20.0	15.8	14.7	11.6	8.4
	1200	24.7	22.4	18.9	14.1	12.9	31.8	25.9	23.5	20.0	17.6	17.6
	1300	23.5	17.6	12.9	9.4	10.6	28.2	22.4	16.5	12.9	12.9	15.3
	1400	23.5	22.4	20.0	23.5	21.2	24.7	23.5	21.2	24.7	22.4	20.0
	1500	32.9	27.1	25.9	23.5	24.7	35.3	30.6	29.4	25.9	25.9	23.5
	Aver	24.9	20.8	17.6	16.0	15.1	29.1	24.5	21.3	19.6	18.1	17.0
249	1300	23.8	19.1	15.9	9.5	7.9	30.2	23.8	22.2	12.7	11.1	14.3
	1330	27.0	22.2	19.0	14.3	12.7	30.2	25.4	20.6	17.5	12.7	12.7
	1400	30.2	25.4	22.2	19.0	14.3	33.3	28.6	25.4	22.2	17.5	7.9
	Aver	27.0	22.2	19.0	14.3	11.6	31.2	25.9	22.7	17.5	13.8	11.6
261	1315	7.5	0.0	0.0	1.5	6.0	0.0	0.0	0.0	1.5	6.0	10.4
	1330	1.5	3.1	3.1	4.6	9.2	3.1	3.1	3.1	4.6	9.2	12.3
	1345	1.5	3.1	4.6	4.6	7.7	3.1	3.1	4.6	4.6	7.7	10.8
	1400	3.1	6.2	7.7	7.7	9.2	1.5	4.6	7.7	9.2	9.2	13.8
	1415	7.7	6.2	3.1	3.1	4.5	7.7	3.1	1.5	3.1	4.5	7.7
	Aver	4.3	3.7	3.7	4.3	6.8	3.1	2.8	3.4	4.6	7.3	11.0
Grand Av		19.6	17.1	15.8	15.1	15.6	21.1	18.6	16.8	15.5	15.9	18.2

Table 4.C.3. Grand optimal thresholds and error statistics.**

Single Visible Threshold Method: IR = 70, Visible = 140
Dual Visible Threshold Method: IR = 160, Visible = 110/180

				Single Method			Dual Method		
Day	# of images	N	R	% error	weighted error	rho	% error	weighted error	rho
242	3	62	10	7.4	.500	.500	17.2	.226	.774
245	3	23	48	23.3	.451	.549	19.1	.416	.584
247	3	23	33	20.7	.482	.518	24.9	.580	.420
248	5	49	38	19.6	.375	.541	24.9	.460	.540
249	3	39	24	17.5	.299	.701	27.0	.465	.533
261	5	56	9	4.6	.311	.689	4.3	.112	.877
Grand Average		42	27	15.5	.403	.583	19.6	.377	.621

If N = # of no rain points, and R = # of rain points, and

R_n = # of incorrectly predicted points in R

N_r = # of incorrectly predicted points in N

R_r = # of correctly predicted points in R

N_n = # of correctly predicted points in N,

then

% error = $(R_n + N_r)/(R + N)$,

weighted error = $(R_n/R) + (N_r/N)$,

rho = correlation coefficient = $(R_r * N_n - R_n * N_r)/(N * R)$

** Ref: Lovejoy and Austin(1978)

than is the percent error. Likewise, in a day-to-day comparison, the lowest weighted error is found more consistently under the same threshold for the dual threshold case than is the percent error. Using the percent error to determine the grand optimal threshold gives different results for the dual case, due to the effect of the Day 242 and the 261 statistics.

Both methods are generally insensitive to small changes in the infrared threshold. It is thus less important in determining actual rainfall. Likewise, the upper visible threshold for the dual case varies little.

Table 4.C.1 shows lower visible thresholds for days with newly forming areas of precipitation (as opposed to large, established ones). Days 242 and 261 are examples of primarily new convection, days 247, 248, 249 have well established areas of convection, while Day 245 is a hybrid case. These characteristics are reflected in the thresholding. These results suggest that perhaps a triple visible threshold approach would yield greater accuracy, although the benefits may not repay the effort.

Choosing the grand optimal thresholds to do all calculations (Table 4 C.3) can result in up to a 10 to 15% increase in percent error (a doubling of the error) and a 0.23 to 0.28 increase in the weighted error. Thus the choice of thresholds appropriate to a given situation can be important. Usually, the opposite is true: the error increase is generally on the order of a few percent.

Using daily optimal thresholds from Table 4.C.1 and 4.C.2, the percent error is about 12.5% for <u>both</u> methods. (Table 4.C.3 shows a lower percent error for the single visible method only because we were

attempting to minimize the weighted error.) A similar result is given from the weighted error (about 0.3 for both). Thus, provided one selects the right threshold, both methods give about the same accuracy. However, the dual visible method seems to offer a systematic basis on which to select the correct threshold without calibration and for this reason would be superior to the single threshold method.

Finally, for the dual method, those rain areas missed (R_n) had a consistently lower reflectivity than those areas predicted correctly. This fact suggests that there is some information on rain intensity in this scheme, although just how much is not known.

4.D Determining Anvil Expansion and Mass Fluxes

One of the most noticeable dynamic features observed in satellite imagery is the rapid expansion of cumulonimbus anvils during early and mature stages of thunderstorm growth. Recent statistical techniques (see Section E) make the measurement of this growth over time a simple matter.

4.D.1 Procedure for Measuring Anvil Area

The steps in this process are as follows. First one selects a full resolution digital satellite image sequence, preferably visible, with a maximum of 30 minutes between pictures. A corresponding infrared sequence is optional but helpful in determining the anvil edge. Since visible reflectance varies with sun angle, it is then necessary to

normalize the brightness to one time, usually by assuming that the variation in reflectance is proportional to the cosine of the sun's zenith angle. A brightness contour at the edge of the anvil is then selected and located in each picture and the area inside this contour is computed. Of course, nearby anvils may combine with one another or be obscured by non-anvil cirrus, in which case one must appropriately select or modify the contours being used for computation.

4.D.2 Horizontal Divergence and Mass Flux

Converting such measurements into physically meaningful numbers is not quite so simple, although a number or researchers have attempted to convert anvil growth to such physical parameters as horizontal divergence and mass flux. Horizontal divergence is easily calculated as $A^{-1}dA/dt$ (where A = area). The magnitude of this parameter is inversely proportional to the size of A and thus declines drastically as the anvil increases in size. These changes make comparison of divergences between different storms difficult and limit the use of such divergence as a measure of storm intensity.

A more constant and therefore representative measure of storm size and intensity is the volume or mass flux. This parameter can be calculated by multiplying the change in area over time with the estimated anvil thickness (to produce the volume flux) and the air density (to produce the mass flux). This basic method was first introduced by Sikdar (1970), applied to GATE convection by Weickmann et al. (1977) and later modified by Lo et al. (1981) to help account for entrainment. Lo et al. also present an interesting comparison of

mass flux measurements by various authors using different techniques.

4.D.3 Limitations of the Method

The factors introducing varying degrees of inaccuracy in mass flux estimates derived from anvil expansion are as follows:

1) Sun angle change. The change in visible brightness due to sun angle changes can only be adequately corrected during a period of a few hours centered on midday (Martin and Suomi, 1972). Infrared may be used instead but its resolution is coarser.

2) Evaporation along the edge of the anvil. This error is smaller for rapidly growing cumulonimbi but may be more substantial for later stages of storm growth.

3) Anvil thickness. It is hard to get a good estimate of average anvil thickness without actual aircraft measurements, although visible brightness gives some indication. Values around one kilometer have commonly been used (Sikdar, 1970), although Zipser (1977) suggests that anvil thickness as grest as 10 km are not unusual.

4) Entrainment and mesoscale fluxes. The mass flux at the base of the cloud is not the same as the flux into the anvil. Entrainment is the primary cause of this descrepancy. Lo et al. (1981) have introduced a correction for entrainment which helps lower this error. Houze et al. (1980) have pointed out that in well-developed cumulonimbus complexes,

REFERENCES

Auvine, B., and C.E. Anderson, 1972: The use of cumulonimbus anvil growth data for inferences about the circulation in thunderstorms and severe local storms. Tellus, 24, 300-311.

Barrett, E.C., and D.W. Martin, 1981: The Use of Satellite Data in Rainfall Monitoring, Academic Press, 340 pp.

Griffith, C. G., W. L. Woodley, P. G. Grube, D. W. Martin, J. Stout, and D. N. Sikdar, 1978: Rain estimation from geosynchronous satellite imagery - Visible and infrared studies. Mon. Wea. Rev., 106, 1153-1171.

Houze, R.A., C.-P. Cheng, C.A. Leary, and J.F. Gamache, 1980: Diagnonsis of cloud mass and heat fluxes from radar and synoptic data. J. Atmos. Sci., 37, 754-773.

Kondrat'yev, K., A. Minorova, and A.Otto, 1964: Spectral albedo of natural surfaces. Pure and Applied Geophys., 59, 207-216.

Lo, C.S., W.R. Barchet, and D.W. Martin, 1981: Vertical mass transport in cumulonimbus clouds on Day 261 of GATE. submitted to Mon. Wea. Rev.

Lovejoy, S., 1978: The relationship between coarse resolution satellite data and area of rain. Fourth Symposium on Meteorological Observations and Instrumentation. AMS, Boston, Mass.

_____, and G.L. Austin, 1979: The delineation of rain areas from visible and IR satellite data for GATE and mid-latitudes. Atmosphere-Ocean, 17, 77-92.

Martin, D. W., and V. E. Suomi, 1972: A satellite study of cloud clusters over the tropical North Atlantic Ocean. Bull. Amer. Meteor. Soc., 53, 135-156.

Scofield, R.A. and V.J. Oliver, 1977: A scheme for estimating convective rainfall from satellite imagery, NOAA Tech. Memo. NESS No. 86, 47 pp.

Sikdar, D.N. and S.J. Hentz, 1980: Kinematic structure of an Atlantic cloud cluster during GATE and its time variation. Tellus, 32, 439-455.

_____, V.E. Suomi, and C.E. Anderson, 1970: Convective transport of mass and energy in severe storms over the United States--an estimate from a geostationary altitude. Tellus, 22, 521-532.

Smith, E. A., 1975: The McIDAS system, IEEE Trans. on Geosci. Elec., vol. GE-13, no. 3.

Stout, J.E., D.W. Martin, and D.N. Sikdar, 1979: Estimating GATE rainfall with geosynchronous satellite images. Mon. Wea. Rev., 107, 585-598.

Weickmann, H.K., A.B. Long, and L.R. Hoxit, 1977: Some examples of rapidly growing oceanic cumulonimbus clouds. Mon. Wea. Rev., 105, 469-476.

Young, J. T., 1976: Navigation of geostationary images. In Proc. Symposium on Meteorological Observations from Space: Their Contributions to the First GARP Global Experiment, Philadelphia, PA, COSPAR Working Group 6, NCAR, Boulder, CO, 198-200.

Zipser, E. J., 1977: Mesoscale and convective-scale downdrafts as distinct components of squall-line structure. Mon. Wea. Rev., 105, 1568-1589.

mesoscale fluxes in and under the anvil can constitute a major contribution to the total fluxes of the storm, a factor which is neglected if anvil expansion alone is measured.

Despite these errors, it is possible to get estimates of mass/volume fluxes to within at least the correct order of magnitude. Even this amount of accuracy is helpful since it appears that intense storms vary by at least one order of magnitude from ordinary storms in their fluxes and divergences (Auvine and Anderson, 1972).

4.E Area Statistics

Area statistics is a set of programs on McIDAS (see Smith, 1975) designed to produce brightness or infrared temperature statistics on irregular regions of a line image. When the image is a navigated satellite image, the system is capable of making crude transformations of scale so that the areas of desired brightness/temperature in the selected regions are reported in square kilometers.

4.E.1 Methodologies

The scientist draws a contour (outline) around a selected region of an image using the joysticks, viewing it on the screen as it is being drawn. The system samples the joystick position every 100 milliseconds and connects the sampled points with straight lines. Thus the system interprets the outline as an n-sided polygon, with n being typically 40. To the scientist, the outline usually appears as a smooth curve when n is greater than 20. A square cursor (box) area

may also be used instead of the drawn outline. When the outline is completed, it is filed on disc.

The system converts the outline into an internal form which allows the desired statistics to be computed in a single pass over the data. The images are stored line by line, meaning the system must prepare a list for each line showing which pixels are inside the outline and which are not. This collection of lists is prepared automatically whenever a new outline is drawn or when an old one is recalled from the disc file.

Computer capabilities allow for the enhancement of particular portions of the digital image data. This is a visual aid to the scientist as it may accentuate certain features or distinguish boundaries between features of interest that otherwise would be difficult to accurately outline for measurement. Specific thresholds within the digital brightness scale (0 to 255) or infrared temperature scale (163°K to 330°K) may then be chosen to delineate areas of interest within an outline. After careful examinations of threshold consistency, (spatial and temporal where appropriate) statistics may then be computed.

The scientist invokes a command to compute statistics on that part of some image which lies within the outline. A pass over the image outline data produces a brightness/temperature versus pixel count histogram. Then, a navigational scale transformation is effected by computing the earth surface area corresponding to a single pixel. Finally, the desired statistics are calculated and displayed. The system can calculate the area between two brightness values, mean and standard deviation of the mean brightness, and the

integral of brightness/temperature over area.

Inaccuracies of the area statistics system begin with the nature of the outlines. These outlines are polygonal approximations to smooth curves and even the straight line edges of the polygon cannot be plotted perfectly since a plotted line cannot occupy just a part of a pixel. Within the interior of the boundary, computation of relative areas (in fractional number of pixels) is as accurate as the data, since they are computed by counting. However, the areas when computed in units of earth surface area are much less accurate due to the slowness and large memory requirements of the McIDAS navigation subsystem. All that is computed is a scale factor from the true area enclosed by the outline. This works well only if the region is nearly Euclidean, i.e., not for large regions near the earth's limb.

4.E.2 Applications

In these regards, two interactive programs have been developed and are described here:

a) Contouring of Brightness Areas, and Their Statistics

The general area statistics system (see previous discussion) provides a means of selecting individual areas by operator generated outlines and threshold determination. However, to examine brightness/temperature fields over a large area may require many outlines or averaging over the entire area. To deal with this situation, a routine was developed which approximates drawing many

outlines over a large region by use of thresholding. This objective mapping technique is quite useful in analyzing digital satellite image cloud populations (i.e., cloud cluster groups or areas of textured cloud). Digital radar data may also be analyzed (i.e., echo intensity information).

Methodology

A digital image is scanned line by line and endpoints for segments above a chosen threshold are stored. A provision allows for the connecting of segments along a line that are separated by n or less data elements. There is one back-scan attempted for each line in case the previous line contains more than one segment that overlaps the current line. Because only one back-scan is performed, very irregularly shaped areas will be divided into separate areas.

Some basic statistics can be extracted from the digital data within the regions (a minimum number of lines which defines an area may also be input). An example is shown for satellite viewed clouds (VIS channel in Fig. 4.E.1) over the GATE area on 18 September, 1974. To exclude all but the highest clouds, a threshold of 200 digital counts (219°K) was chosen. Those cloud areas at or above 200 digital counts (shaded) are shown in Fig. 4.E.2 with associated reference numbers. The criteria set for cloud determination allowed for up to a two element gap along a line to define it as continuous and for the area to be at least 20 lines long.

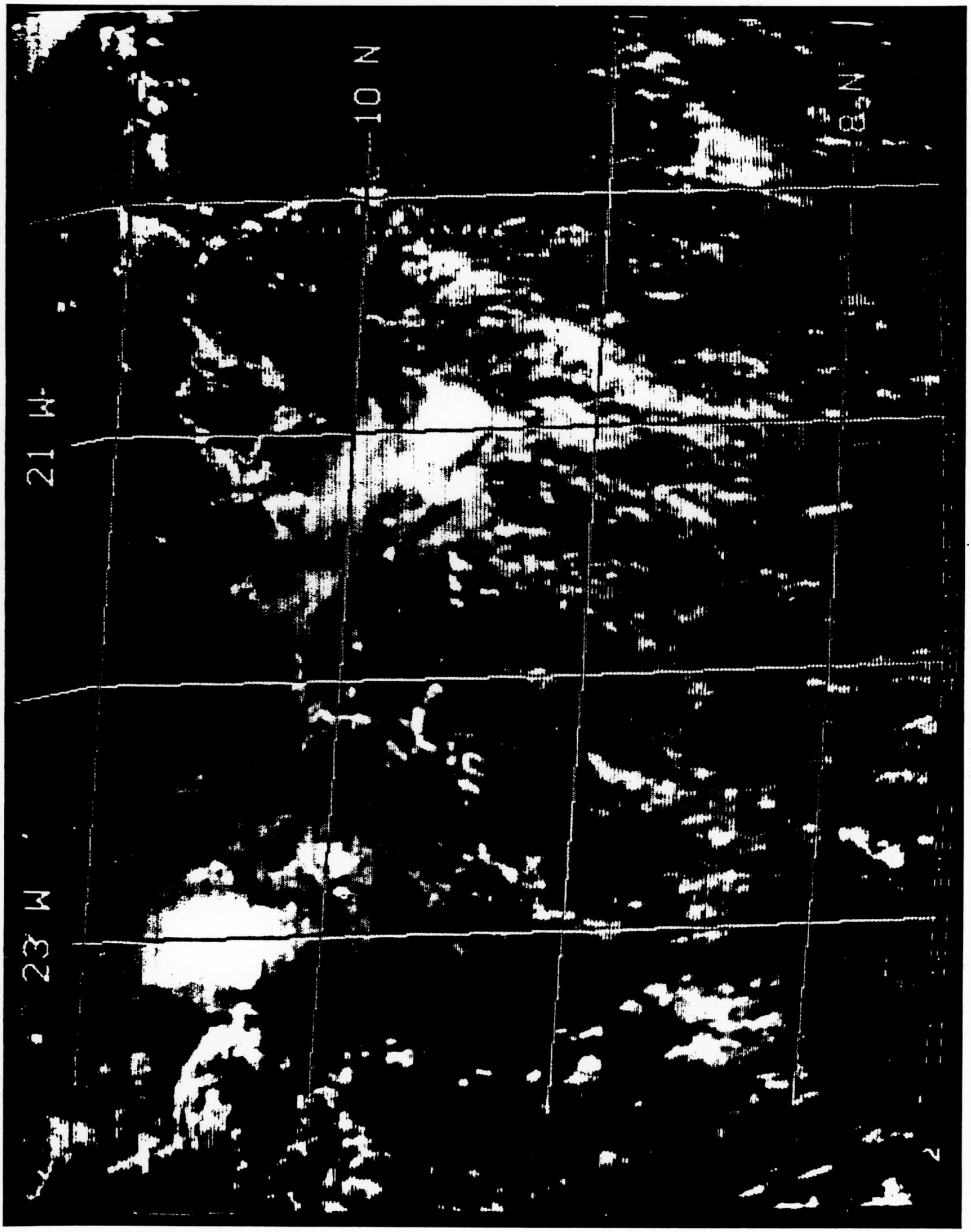

Fig. 4.E.1 SMS-I visible satellite image over GATE area at 1315 G.M.T. 18 September, 1974.

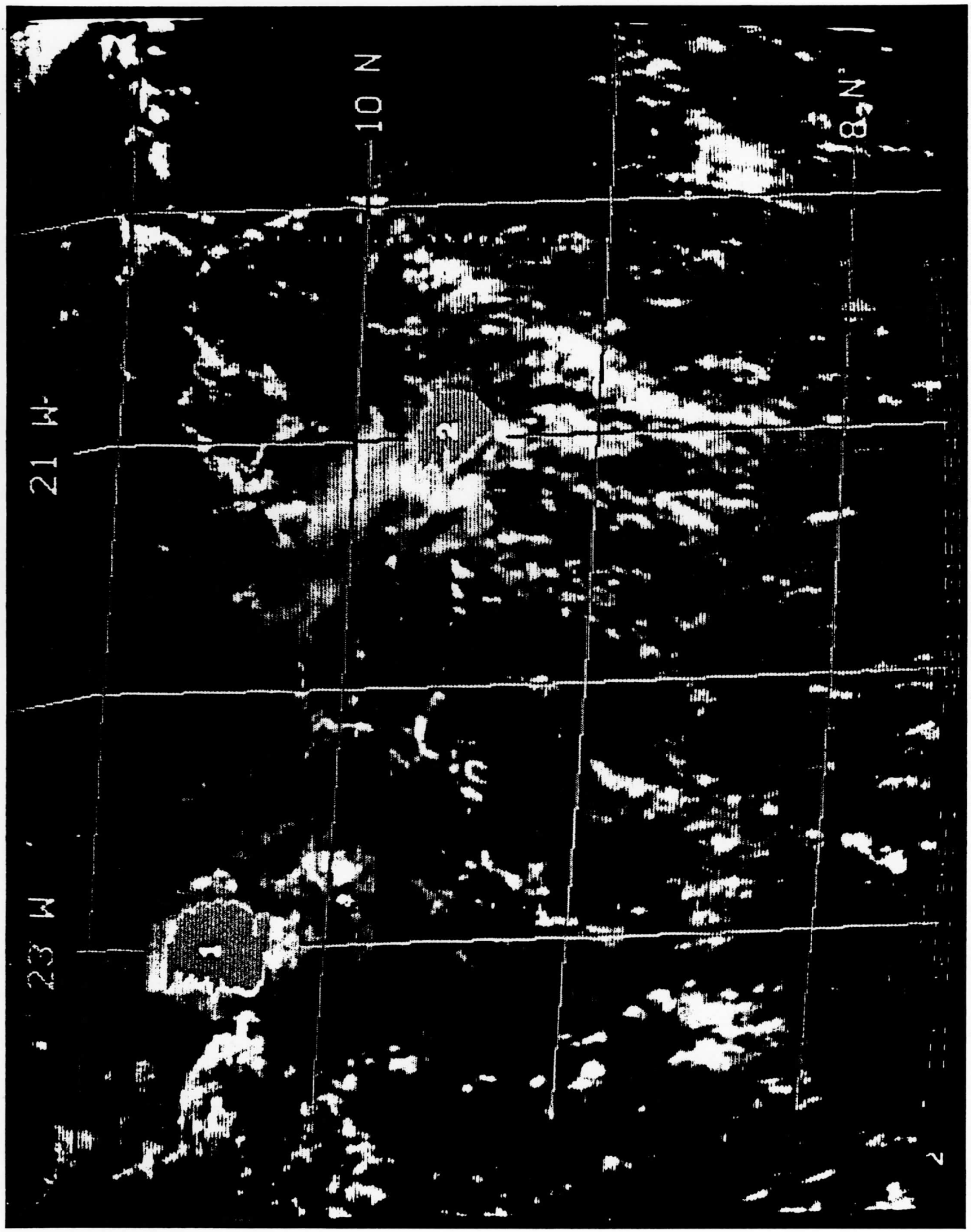

Fig. 4.E.2 Cloud population areas (shaded) at 1315 G.M.T. 18 September, 1974.

Printed statistical output may also be generated. In reference to Fig. 4.E.2:

CLD	LAT	LON	MEAN	RMS	AREA(PIX)	AREA(KM)
1	19275	-[illegible]	216.9	12.3	.168706E+04	.129836E+04
2	30630	-106529	216.1	12.6	.903006E+03	.775505E+03

Each cloud determined lists center location (latitude and longitude), mean and standard deviation of brightness, and the cloud area in both data elements (pixels) and square kilometers.

b) Two or Three Channel Histogram

One of the most useful capabilities of an interactive computer system is the ability to combine and examine data from more than one source simultaneously. Often, more information can be obtained from combining the data gathered at two or more measurement platforms than from a single data source. Secondly, information comparing two or more sets is invariably more useful when examined in a statistical manner than in a descriptive manner. By these means, the statistics act as a record of comparison and correlation between two or more data sets.

The two or three channel histogram interactive program was developed to allow an objective examination of two or three data sources (channels) simultaneously. Input may be satellite visible and infrared digital data. Radar digital data mapped into the satellite projection (see Section 4.B) may also be used.

Methodology

The two or three channel histogram program allows the operator to choose two main options. The first option involves the use of two channels (data sources). For each channel, the operator must specify three parameters (within the 0 to 255 digital brightness scale) that characterize the data analysis. These are:

i) a minimum brightness value,

ii) a brightness range -- this specified range groups the data into bins to smooth the analysis,

iii) the number of bins desired for analysis.

After the channel parameters are specified, the data are scanned over a specific area (see Section 4.E, on the Area Statistics System discussion). The value of each pixel (data value) scanned from each channel determines in which bin it is contained. This analysis procedure produces a bivariate frequency distribution. The distribution may be displayed graphically as a three-dimensional histogram with the x and y axes representing the bins for each variable and the z axis the frequency (Fig. 4.E.3).

The second option involves the use of three channels. The channel parameter specification is identical to the above mentioned

procedure. This analysis produces a tri-variate frequency distribution. In this case, the graphic display results in a series of three-dimensional histograms representing each bin specified for the third channel (Fig. 4.E.4).

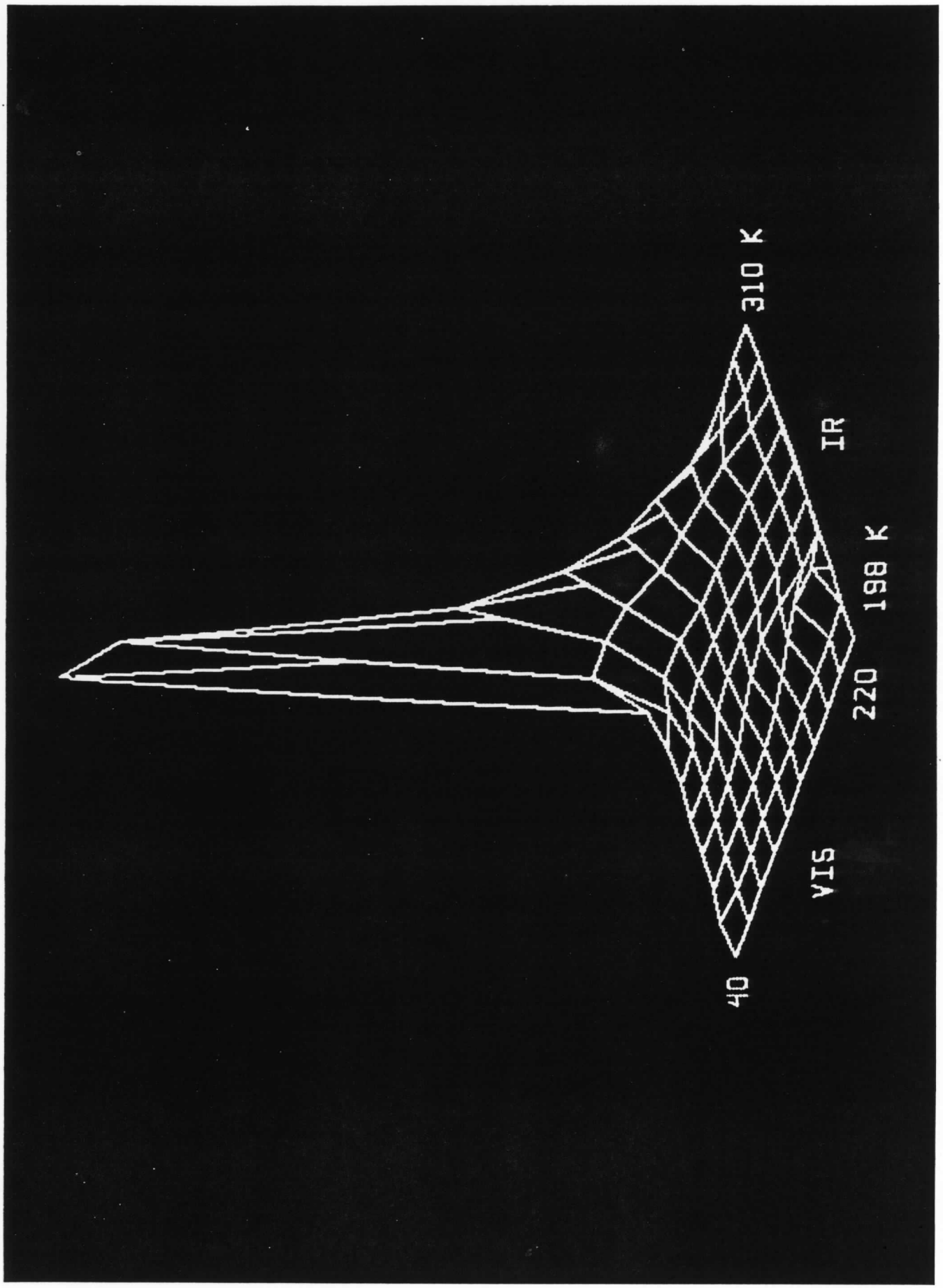

Fig. 4.E.3 SMS-I Visible VRS infrared histogram at 1315 G.M.T.
18 September, 1974
Channel 1: Visible brightness range from 40 to 220 in steps of 20.
Channel 2: Infrared temperatures range from 198°K to 310°K.

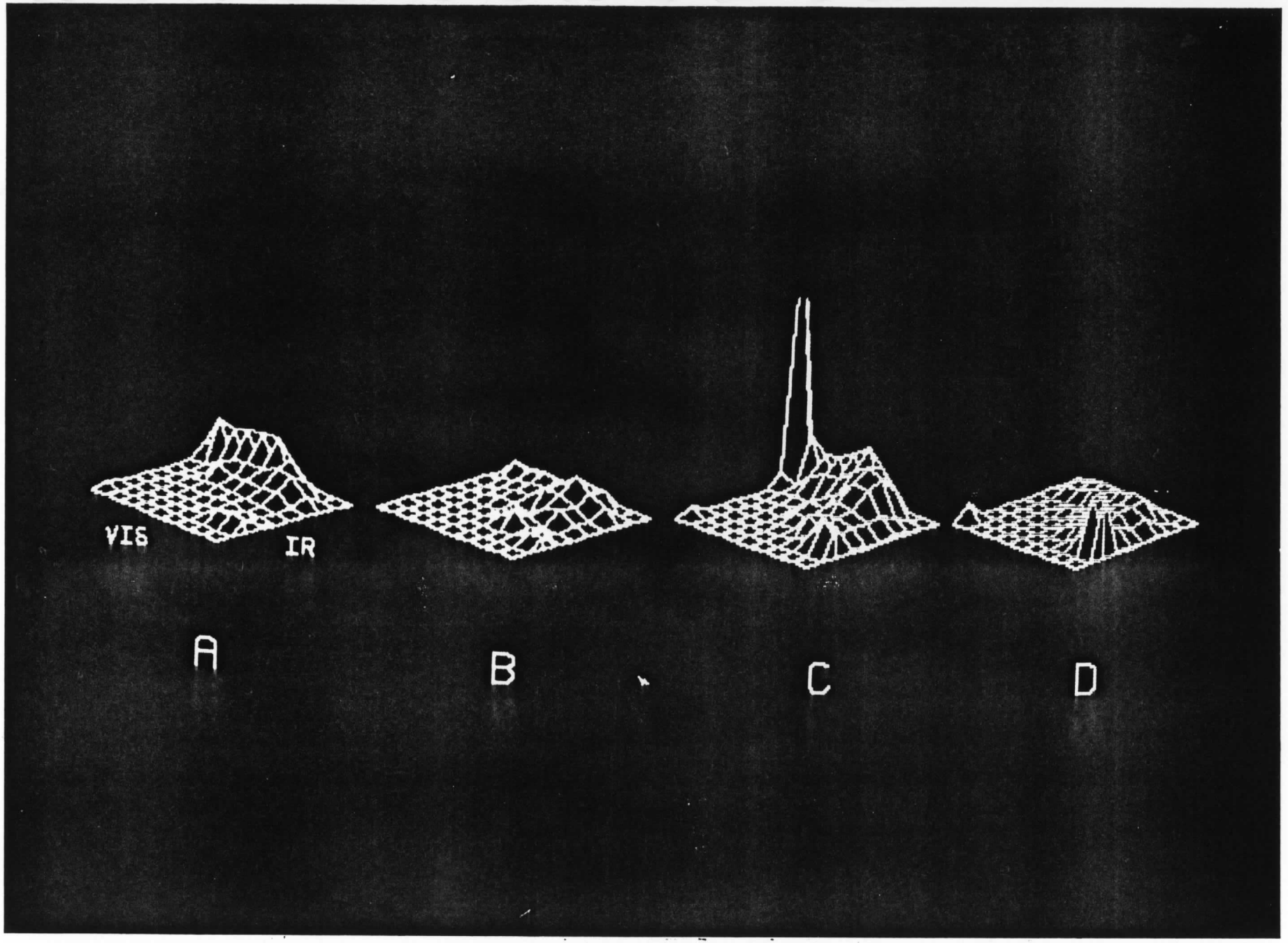

Fig. 4.E.4 SMS-I Visible and infrared VRS Quadra radar histograms at 1315 G.M.T. 18 September, 1974.
Channels 1 and 2: Same as in Fig. 4.E.3
Channel 3: Radar reflectivities range.
A) ~23.8 to ~26.1 dBz B) ~26.2 to ~28.7 dBz
C) ~28.8 to ~30.7 dBz D) ~30.8 to ~33.6 dBz

5. CLOUD MAPPING

5.A Plan & Section View Maps

Cloud mapping is a way of protraying the spatial distribution of clouds--often, particular types of cloud. Clouds represented here are cumulus, stratocumulus, altostratus and altocumulus, cirrus and cirrostratus, and cumulonimbus. The mapping takes one of two forms: horizontal (plan view, or x - y) and vertical (section view, or x - z).

Cloud maps are derived from calculations of cloud-top temperature (or equivalent altitude), thickness, and growth in size and height. In addition, determinations are made of cloud phase (ice or water) and cloud size, shape, organization, texture, and motion. Each of these characteristics is based upon information gleaned from visible and infrared wavelength geostationary satellite image sequences. Rather different procedures are followed to prepare plan and section view maps.

5.A.1 Construction Procedures for Plan View Maps

Making a plan view map begins with computer-produced maps of visible and infrared radiance (expressed as digital counts, one map per image). All visible/infrared image or map pairs and image sequences have the same scale and resolution. The resolution of the visible map determines the resolution of the cloud map.

A piece of tracing paper is overlaid on the visible map. The image pair corresponding to the contour maps is displayed on a television screen (these are the primary images). Image pairs (of the same area)

just before and just after the map image pair are also available (these are the supplementary images). A cloud of the particular type to be mapped is identified on the display, located on the visible contour map, then outlined on the overlay using both visible and infrared contours as a guide. Other clouds of the same type are similarly mapped. The analyst then may map clouds of other types, in the same fashion, until the picture is complete.

5.A.2 Construction Procedures for Section View Maps

To make a section view map of clouds one also begins with a visible/infrared image pair displayed on a television screen, with access to images immediately before and after the primary image. The section line is marked on a graphics frame overlaying one of the primary images. An electronic cursor is set to a size consistent with the image resolution and the desired map resolution (it should be at least twice the true resolution of the infrared sensor--see Section 2). The cursor is placed at one end of the section line and is moved in contiguous steps along the line by means of the joystick control. At each step the maximum height of the cloud within the cursor is calculated, together with the location (latitude and longitude) of the center of the cursor. Both are automatically saved on a disc file, which is printed on paper or written on tape when the measurements are complete. If, because of size or emissivity or multiple layering, a cloud top altitude along the section line cannot be accurately measured, the analyst may move the cursor to a nearby cloud judged (on the basis of motion and appearance) to be at the same altitude and use this cloud as a proxy for the cloud

height calculation. Shadows may also be useful in checking infrared calculations of cloud height, especially heights of cumulonimi and masses of cirrus.

Once cloud height and thickness calculations are complete the primary images are photographed, with and without section lines and a grid of latitude and longitude. Cloud top and base altitudes are plotted by hand on a worksheet scaled in distance and height, then cloud boundaries are marked, using the photographs as a guide. Other information is added to the section map--the lifting condensation level, moist layers, inversions, or the tropopause--depending on what is available from nearby soundings. Finally, mindful that

i) thin cirrus will be too warm (too low);

ii) small clouds (relative to the resolution of the satellite infrared sensor) will be too warm (too low);

iii) bases of clouds (especially cumulus) will be too variable; and

iv) tilted clouds, or clouds distant from the subpoint, may be too broad, the analyst sketches cloud outlines.

5.B Typing Clouds

The art of typing clouds in satellite pictures has been intensively studied over the years. Principles used here to make such determinations by means of an inspection of visible or infrared images or image pairs are summarized in reports and monographs beginning with Erickson and Hubert (1961) and Conover (1962, 1963), and continuing with Anderson, Ferguson and Oliver (1966), Anderson et al. (1969), Barrett

(1974), and Brandli (1979). Perhaps the single most comprehensive treatment of the topic is contained in the satellite cloud atlas edited by Anderson and Veltishchev (1973).

By comparison, cloud typing by means of radiance measurements has received much less attention. Lo and Johnson (1971) wrote an early paper on this subject. An outstanding recent example is the paper of Shenk, Holub, and Neff (1976), which includes window infrared and shortwave radiation.

In the present technique, determinations of cloud type are based primarily on the appearance of the cloud in visible and infrared wavelengths, using established criteria such as brightness, size, shape, texture, and spacing and other elements of pattern. Height and thickness are calculated selectively, for clouds which either are representative of groups or lie close to a critical threshold (for example, the -10°C isotherm). Where these tests are not sufficient to define type, the last resort is behavior, that is, growth or motion of a cloud. Cumulonimbus clouds characteristically exhibit rapid upward growth, then rapid expansion of the top. In cirrus, on the other hand, changes in size generally occur slowly; however, movement is usually rapid.

5.C Examples of Mapping Techniques

The present cloud mapping techniques are illustrated in two examples for each of the plan and section view maps, one pair of examples from 2 September 1974, the other from 18 September 1974.

5.C.1 Plan & Section Views of Widespread, Intense Convection

The first, 2 September (Julian day 245) was a day of widespread, intense convection across the GATE ship array (Fig. 5.C.1; also see Mower et al., 1979; Betts, 1978). Broken lines of cumulonimbi formed and moved south toward the center of the ship array. A solid band of deep cloud with embedded cumulonimbi was stretched across the southeast part of the B-array; this gradually moved westward. Early in the afternoon research aircraft flew a line pattern across two of the cumulonimbus lines. That track is marked on the plan view map (Fig. 5.C.2), which is based on 1200 GMT satellite images (Fig 5.C.1). The map helps to make plain the rich diversity of cloud types on this day and the organization of the convective clouds in particular.

Clouds were mapped in height along the aircraft track (Fig. 5.C.3). This figure contains several noteworthy features: first, the tendency of lines A and B to tilt toward the rear; second, the composition of these lines as a progression of discrete cells beginning on the forward (southern) edge as small cumulus and ending on the trailing edge as patches of cirrus; and third, differences in the cloud structure of the old line A (more cirrus) and the new line B (more cumulus). A radar echo scan along the same line confirms the structure deduced from the satellite observations. In addition, aircraft observations of clouds along the track are consistent with the satellite maps (personal communication, C. Warner and R. N. Mower).

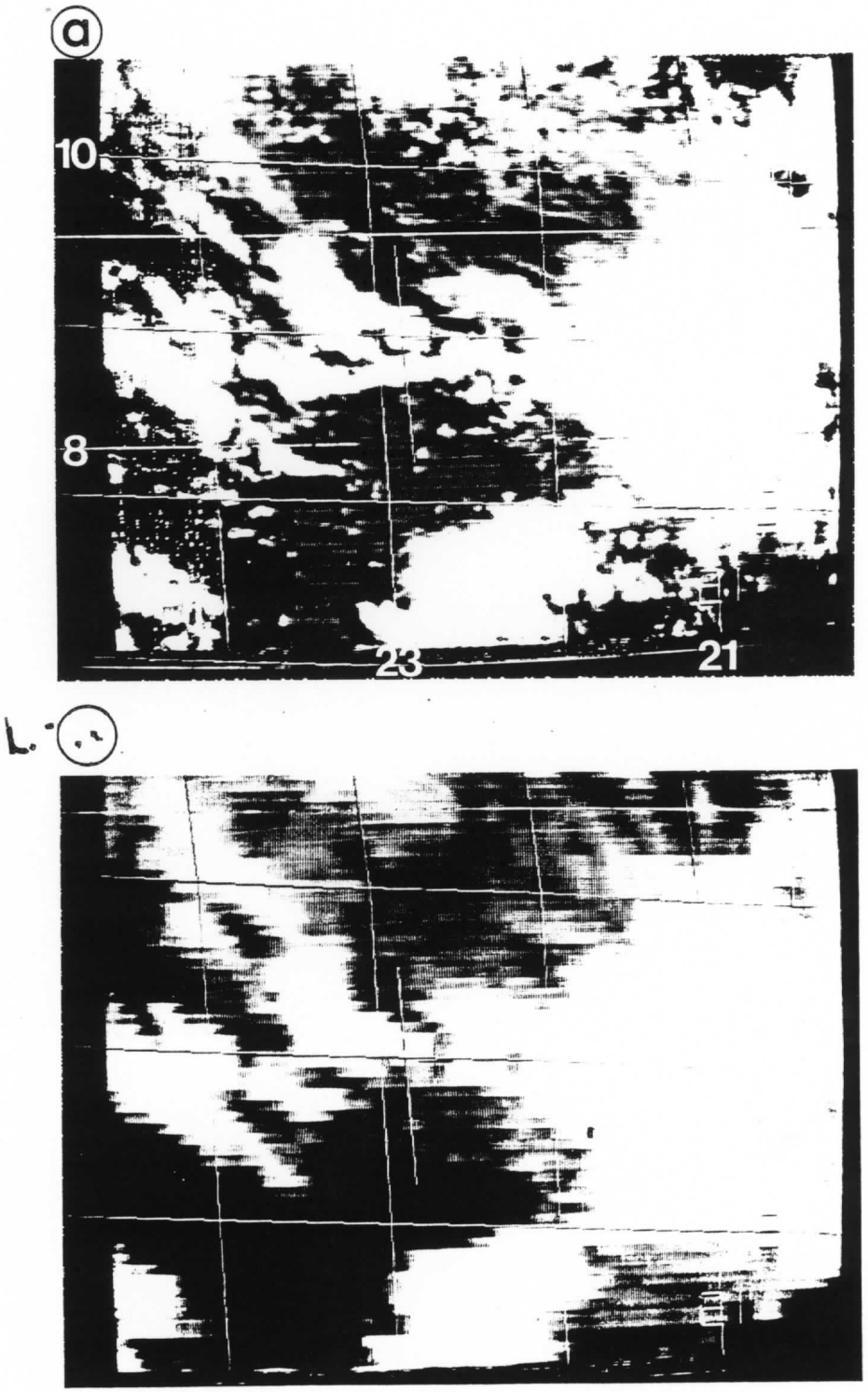

Fig. 5.C.1 SMS-I images for 1200 GMT, 2 September 1974. Grid interval is one degree of latitude and longitude. Line along 22°51'W shows the track of the research aircraft.
a. Visible.
b. Infrared.

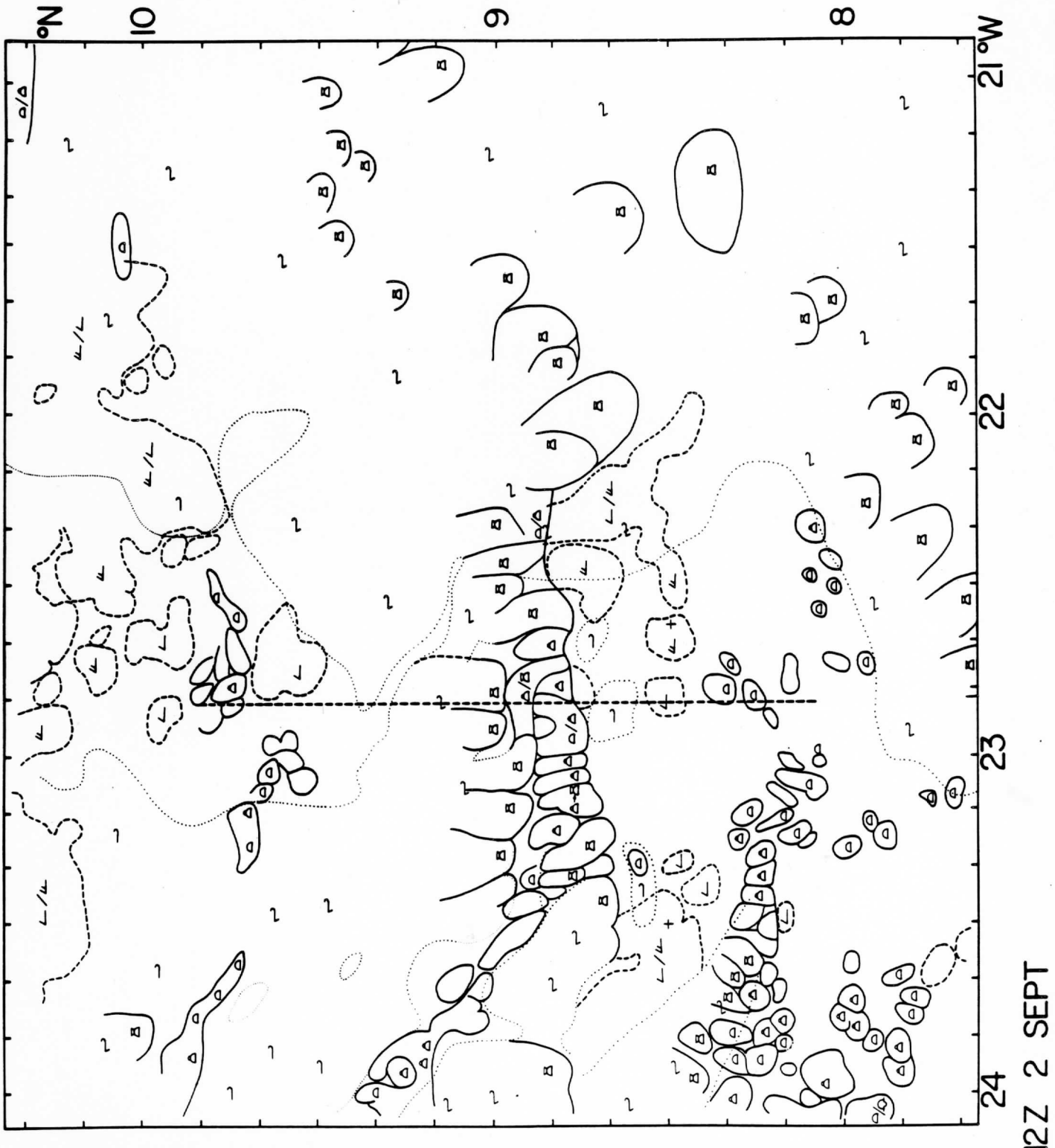

Fig. 5.C.2 Plan view map of clouds for 1200 GMT, 2 September 1974. Solid lines show cumuliform clouds, dashed lines show altostratiform clouds, and dotted lines show cirriform clouds. Thin solid, dashed, or dotted lines indicate some uncertainty in cloud boundary. Dash line at 22°51'W shows the track of the research aircraft.

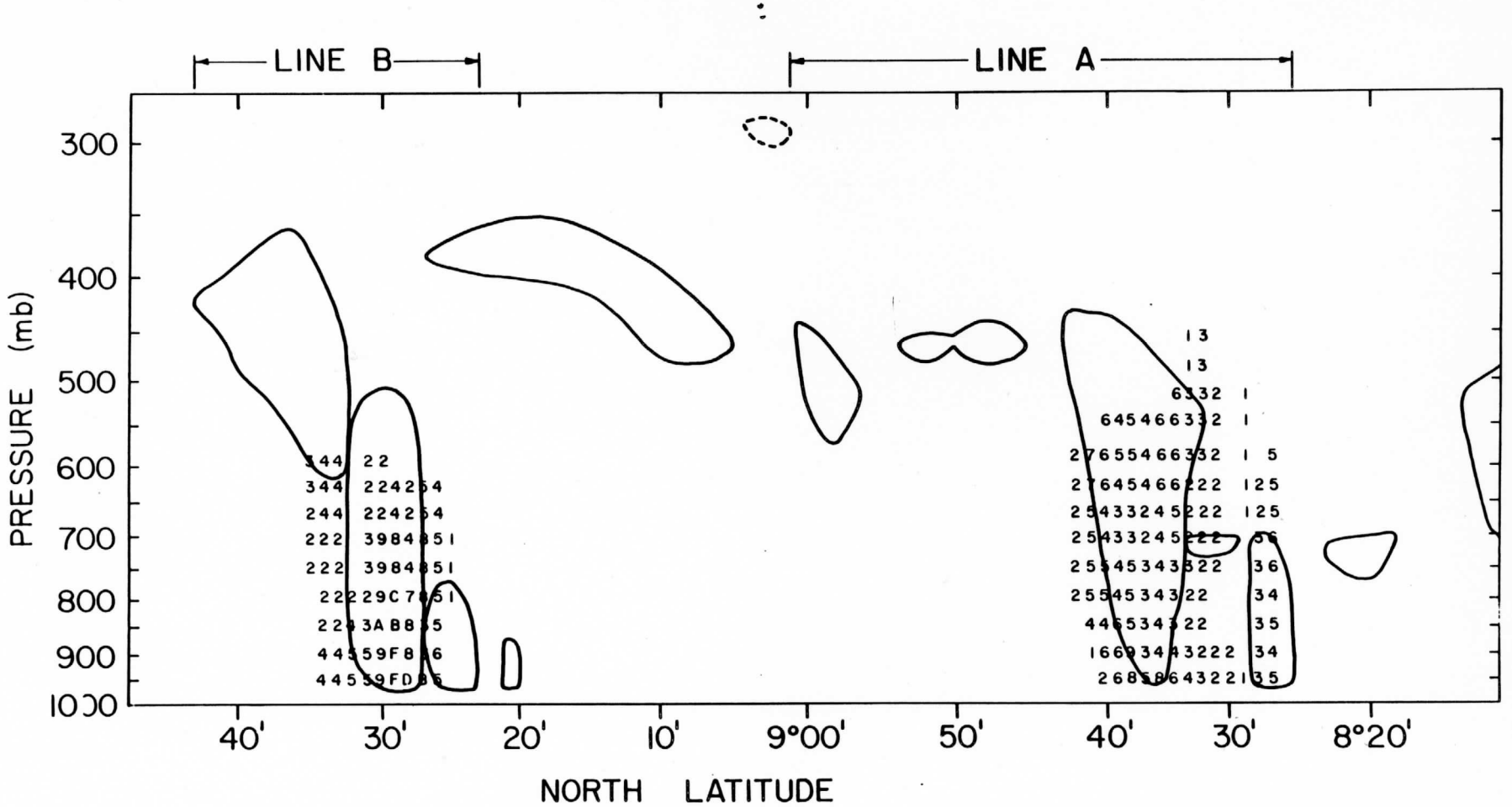

Fig. 5.C.3 Section view map of clouds for 1330 GMT, 2 September 1974, along the meridian of 22°51'W. Overplotted numbers and letters indicate radar echo in the plane of the section.

5.C.2 Plan & Section Views of Isolated, Deep Convection

The second example, 18 September (Julian day 261) was quite a different case (see Warner et al., 1979, 1980). Deep convection was isolated and concentrated in three relatively small clusters, all in the northeast quadrant of the ship array (Fig 5.C.4). Research aircraft flew a box pattern intercepting the largest of the clusters. Clouds were mapped for this box and its near vicinity from satellite images centered on 1345 GMT (Fig. 5.C.5). Although several types of clouds are present the map shows a preponderance of cumulus and cumulus congestus. Cumulonimbus appear only in the northeast corner. The cumulus tend to be aligned in arcs concave to the north and northeast; the congestus (especially toward the south and east) tend to be organized in lines toward the north-northeast. Warner et al. (1980) report somewhat larger cloud coverage in the satellite map than in an aircraft map for the same approximate time, otherwise good agreement in type and location.

The section view on this day (Fig. 5.C.6) is intended to show the distribution of clouds of the Intertropical Convergence Zone along a line of (relatively) dense ship soundings. Thus it was taken through the center of the array along the 23°30' meridian, for a synoptic time, 1200 GMT. The tilt of small cumulus south of 10°N is based mainly on aircraft photographs (see Warner et al., 1980); otherwise this map is based entirely on satellite observations. Clouds appear in two bands. The narrow northern band (which resembles the lines of Fig. 5.C.3) is dominated by cumulonimbus; the southern band is dominated by cumulus and congestus. The cumulus of the southern band deepen--in almost a stepwise fashion--toward the north, culminating (off the section line) in

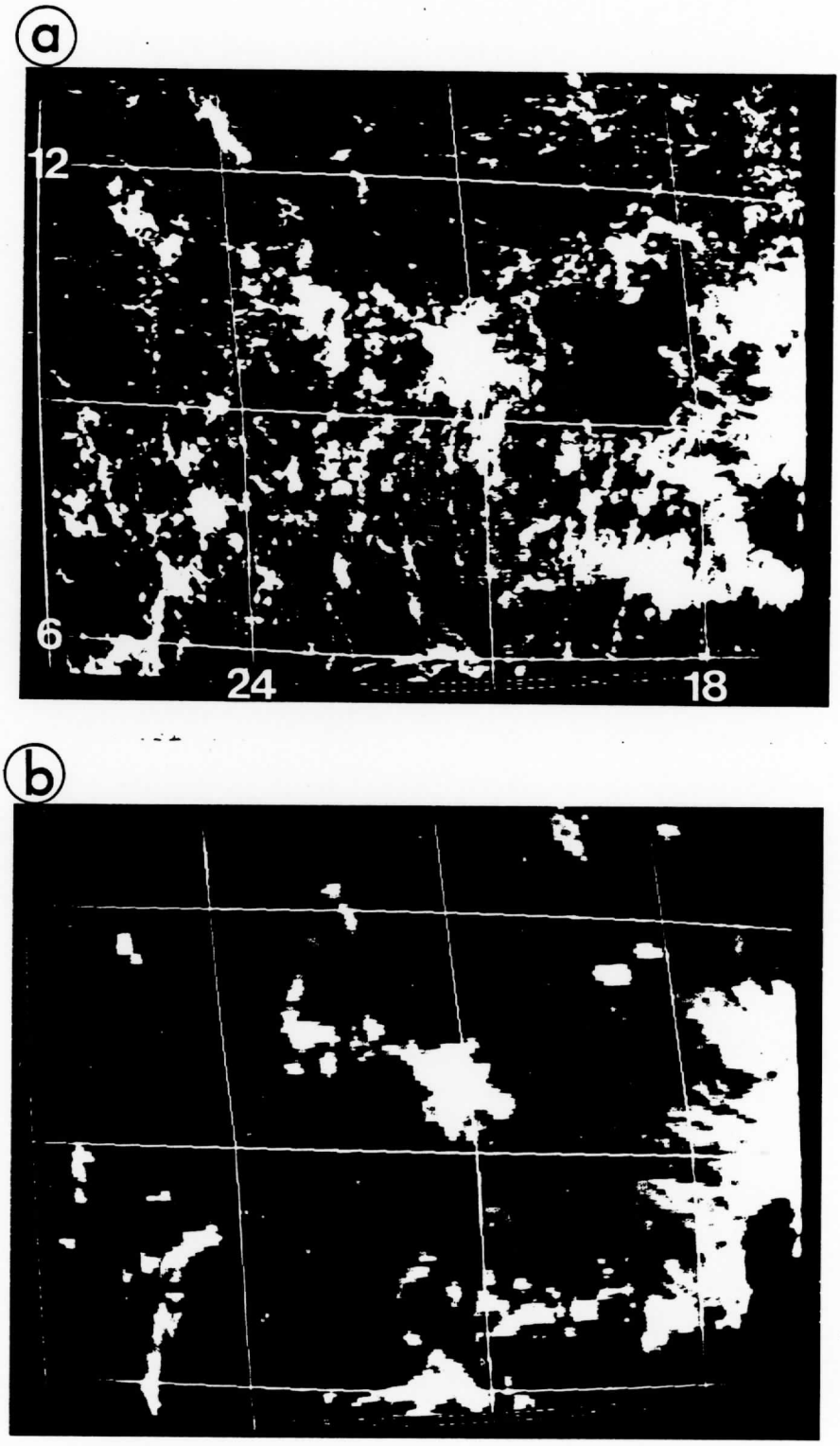

Fig. 5.C.4 SMS-I images for 1200 GMT, 18 September 1974. Grid interval is three degrees of latitude and longitude.
a. Visible.
b. Infrared.

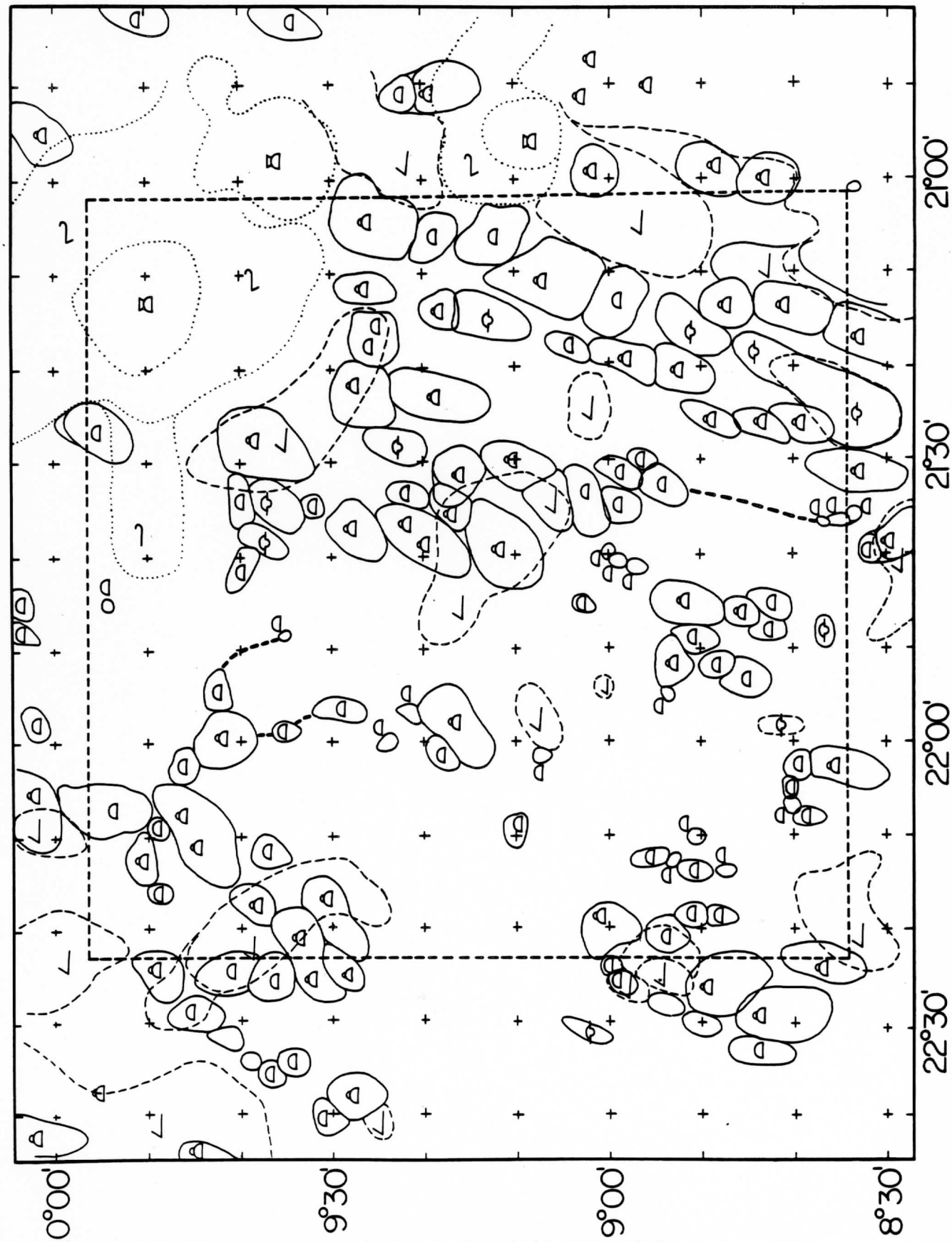

Fig. 5.C.5 Plan view map of clouds for 1345 GMT, 18 September 1974. (Satellite scan time was 1352 GMT.) The convention is the same as for Fig. 2. The heavy dashed lines represent arcs of tiny cumulus clouds. The aircraft flew a box pattern. This figure also appears in Warner et al. (1980).

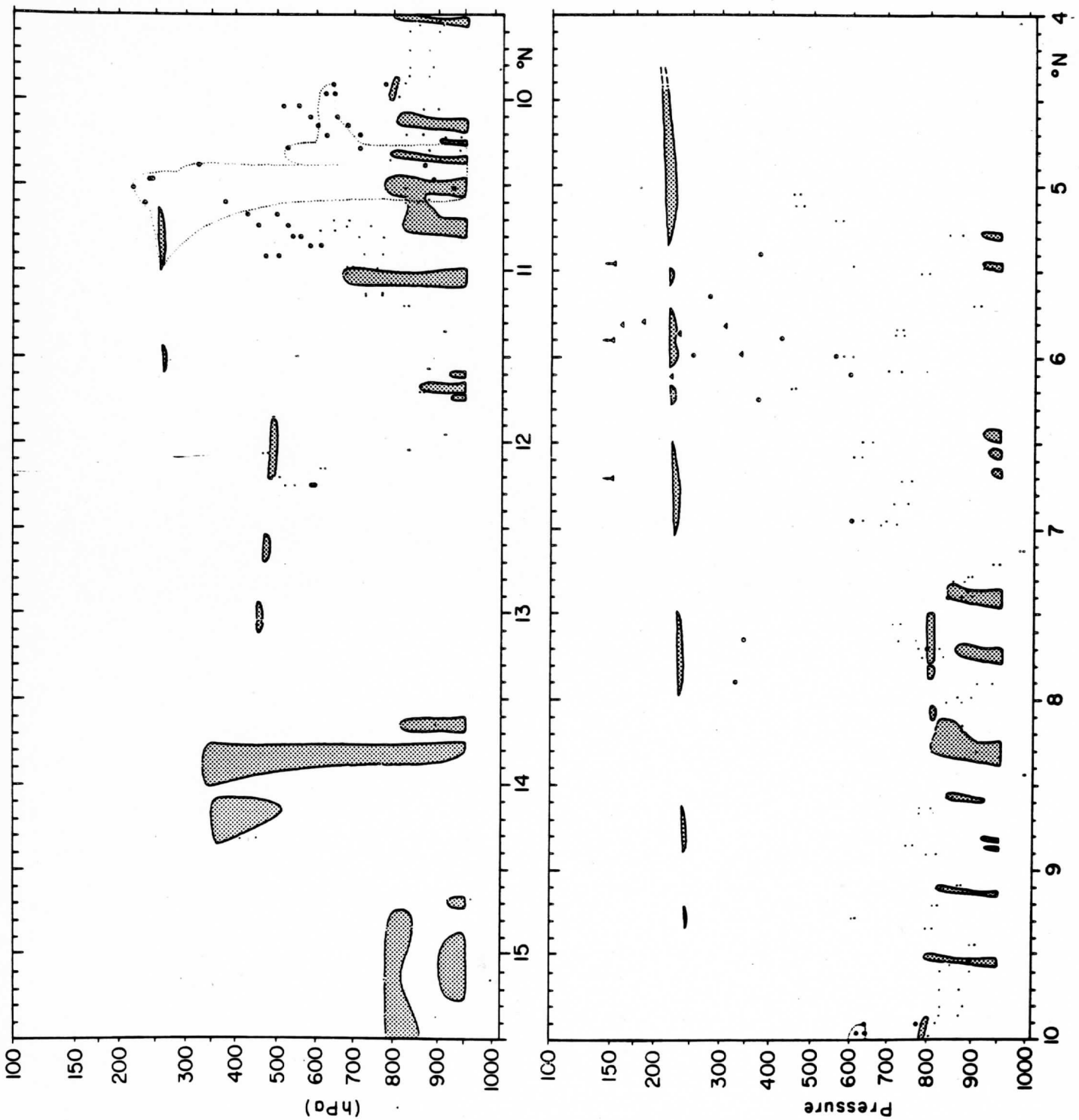

Fig. 5.C.6 Section view map of clouds for 1200 GMT, 18 September 1974 along the meridian of 23°30'W. The dotted lines show the cloud structure of a cumulonimbus ensemble located near 10.5°N, along the meridian of 23°00'W. Pairs of points represent heights of tops and bases of clouds calculated by Mosher's algorithm. The dots show calculations for the section line, the circles show calculations off the section line. Small triangles represent cloud heights calculated from shadows.

cumulonimbus between 10° and 11°N. Cumulus apparently were generating stratus cloud (through spreading of the tops of the towers) near 850 and 650 mb.

5.D Conclusions and Recommendations

There are two main weaknesses to this method of cloud mapping. First, the method is labor intensive. It demands much skill as well as effort to produce even one map. Second, the technology may not be easy to transfer, especially that part which deals with the calculation of cloud top height and cloud thickness.

The strengths of the technique are also twofold. First, it employs time changes to help spot and identify clouds. Second, at least potentially, it makes use of the full dynamic and spatial resolution of the data.

Several improvements suggest themselves. For plan view maps it may be helpful to adapt the technique of Shenk et al. (1976), for cloud typing by multi-spectral thresholding, to GOES infrared and visible images (also see Section 4.B). By this technique a first-pass map of cloud type could be generated (perhaps interactively), then revised as necessary according to cloud appearance, calculations, and behavior. For section view maps it might be useful to plot visible and infrared brightness along section lines as a way of increasing spatial resolution and location accuracy. In addition, as has been mentioned in Section 2, with two scan-synchronized satellites it would be possible to measure cloud heights by stereographic observation.

References

Anderson, R. K., E. W. Ferguson, and V. J. Oliver, 1966: The Use of Satellite Pictures in Weather Analysis and Forecasting. Tech. Note No. 75, World Meteorological Organization, Geneva, 184 pp.

_____, and N. F. Veltishchev, 1973: The Use of Satellite Pictures in Weather Analysis and Forecasting. Tech. Note No. 124, World Meteorological Organization, Geneva, 275 pp.

_____, J. P. Ashman, F. Bittner, G. R. Farr, E. W. Ferguson, V. J. Oliver, A. H. Smith, 1969: Application of Meteorological Satellite Data in Analysis and Forecasting. ESSA Tech. Rep. NESC 51, Nat. Oceanic and Atmospheric Administration, Washington.

Barrett, E. C., 1974: Climatology from Satellites. Methuen & Co., London. 418 pp.

Betts, A. K., 1978: Convection in the tropics. In Meteorology over the Tropical Oceans (D. B. Shaw, ed.), Royal Meteorological Society, Bracknell, Berkshire, pp. 105-132.

Brandli, H. W., 1979: Satellite Meteorology. AWS-TR-76-264, 188 pp., from NTIS.

Conover, J. H., 1962: Cloud Interpretation from Satellite Altitudes. Res. Note 81, Air Force Cambridge Research Laboratories, L. G. Hanscom Field, Mass., 77 pp.

_____, 1963: Cloud Interpretation from Satellite Altitudes. Supplement 1 to Research Note 81, Air Force Cambridge Research Laboratories, L. G. Hanscom Field, Mass., 17 pp.

Erickson, C. O. and L. F. Hubert, 1961: Indentification of Cloudforms from TIROS-I Pictures. Meteorol. Satellite Lab. Rep. No. 7, U. S. Weather Bureau, 68 pp.

Lo, R. C., and D. R. Johnson, 1971: An investigation of cloud distributions from satellite infrared radiation data. Mon. Wea. Rev., 99, 599-605.

Mower, R. N., G. L. Austin, A. K. Betts,, C. Gautier, R. Grossman, J. Kelley, F. Marks, and D. W. Martin, 1979: A case study of GATE convective activity. Atmosphere-Ocean, 17, 46-59.

Shenk, W. E., R. J. Holub and R. A. Neff, 1976: A multispectral cloud type identification method developed for tropical ocean areas with Nimbus-3 MRIR measurements. Mon. Wea. Rev., 104, 284-291.

Warner, C., J. Simpson, D. W. Martin, D. Suchman, F. R. Mosher and R. F. Reinking, 1979: Shallow convection on day 261 of GATE: Mesoscale arcs. Mon. Wea. Rev., 107, 1617-35.

_____, _____, G. Van Helvoirt, D. W. Martin, D. Suchman and G. L. Austin, 1980: Deep convection on day 261 of GATE. Mon. Wea. Rev., 108, 170-94.